CISTER

Research Center in
Real-Time & Embedded
Computing Systems

PhD Thesis

Computing Aggregate Quantities in Large-Scale and Dense Sensor Networks

Maryam Vahabi

Computing Aggregate Quantities in Large-Scale and Dense Sensor Networks

Maryam Vahabi

CISTER Research Center

Polytechnic Institute of Porto (ISEP-IPP)

Rua Dr. António Bernardino de Almeida, 431

4200-072 Porto

Portugal

Tel.: +351.22.8340509, Fax: +351.22.8321159

E-mail:

http://www.cister.isep.ipp.pt

Abstract

Although the information technology transformation of the 20th century appeared revolutionary, a bigger change is on the horizon. The term cyber-physical system (CPS)has come to describe the research and technological efforts that will ultimately allow theinterlinking of the real-world physical objects and the cyber-space efficiently.Technological advances in hardware design enable the emergence of low-cost singleembedded computer equipped with sensing, processing and communication capabilities.This makes it economically feasible to densely deploy networks with very large quantitiesof such nodes. Accordingly, it is possible to take a very large number of sensor readingsfrom the physical world, compute quantities and take decisions out of them.Very dense networks offer a better resolution of the physical world and therefore abetter capability of detecting the occurrence of an event; this is of paramount importancefor a number of foreseeable applications. Environmental monitoring and structural healthmonitoring (SHM) are two examples of such applications. In this Thesis, we considerdensely instrumented CPS applications.Considering the typical limited capabilities of sensor nodes (in terms of communication and processing), computing an estimate of the state of the physical world is challenging. In general, the main challenge of dense sensing networks is categorized into twodistinct classes: data transmission and data aggregation.Assume a large-scale dense networked sensor system, whose nodes have a commonsensing goal: to measure a physical phenomenon and also to compute different featuresfrom the distribution of sensor readings in order to trigger a set of control commands forthe actuators in a timely manner. Based on the aforementioned challenges, we formulatethe Thesis hypothesis as follows: we believe that it is possible to extract certain featuresof a physical phenomenon in a dense sensor network, in a reliable and timely way, andwith a time complexity that is essentially independent of the number of sensor nodes.Therefore, the primary objective of this Thesis is to devise technologies and methodologies that enable extracting certain features of a physical phenomenon monitored bya dense sensing network in a timely and reliable manner. To reach this primary objective, a set of scientific and technical objectives have been identified. The first objectiveis to devise an error recovery scheme for the slotted WiDOM protocol in a noisy wireless channel. This scheme should enable reliable data transmission in harsh environmentswhere sensor nodes are more prone to interference. The second objective is to devisean aggregation mechanism that captures the dynamics of the physical quantities and selfadapts according to the physical changes. This mechanism allows obtaining an accurateinterpolation for a dynamic physical quantity. The third objective is to devise algorithmsto identify various features in a distribution of a physical phenomenon. Feature extraction algorithms enable identifying the location and the boundaries of events in dense sensing applications.

FACULDADE DE ENGENHARIA DA UNIVERSIDADE DO PORTO

Computing Aggregate Quantities in Large-Scale and Dense Sensor Networks

Maryam Vahabi

DISSERTATION

U. PORTO

FEUP FACULDADE DE ENGENHARIA
UNIVERSIDADE DO PORTO

Doctoral Program in Electrical and Computer Engineering

Supervisor: Eduardo Manuel de Médicis Tovar

January 19, 2016

Computing Aggregate Quantities in Large-Scale and Dense Sensor Networks

Maryam Vahabi

Doctoral Program in Electrical and Computer Engineering

Approved by:

President: Prof. José Alfredo Ribeiro da Silva Matos

External Referee: Prof. Nicolas Navet

External Referee: Prof. Leandro Buss Becker

FEUP Referee: Prof. Manuel Alberto Pereira Ricardo

FEUP Referee: Prof. Paulo José Lopes Machado Portugal

Supervisor: Prof. Eduardo Manuel Médicis Tovar

January 19, 2016

Abstract

Although the information technology transformation of the 20th century appeared revolutionary, a bigger change is on the horizon. The term cyber-physical system (CPS) has come to describe the research and technological efforts that will ultimately allow the interlinking of the real-world physical objects and the cyber-space efficiently.

Technological advances in hardware design enable the emergence of low-cost single embedded computer equipped with sensing, processing and communication capabilities. This makes it economically feasible to densely deploy networks with very large quantities of such nodes. Accordingly, it is possible to take a very large number of sensor readings from the physical world, compute quantities and take decisions out of them.

Very dense networks offer a better resolution of the physical world and therefore a better capability of detecting the occurrence of an event; this is of paramount importance for a number of foreseeable applications. Environmental monitoring and structural health monitoring (SHM) are two examples of such applications. In this Thesis, we consider densely instrumented CPS applications.

Considering the typical limited capabilities of sensor nodes (in terms of communication and processing), computing an estimate of the state of the physical world is challenging. In general, the main challenge of dense sensing networks is categorized into two distinct classes: data transmission and data aggregation.

Assume a large-scale dense networked sensor system, whose nodes have a common sensing goal: to measure a physical phenomenon and also to compute different features from the distribution of sensor readings in order to trigger a set of control commands for the actuators in a timely manner. Based on the aforementioned challenges, we formulate the Thesis hypothesis as follows: we believe that it is possible to extract certain features of a physical phenomenon in a dense sensor network, in a reliable and timely way, and with a time complexity that is essentially independent of the number of sensor nodes.

Therefore, the primary objective of this Thesis is to devise technologies and methodologies that enable extracting certain features of a physical phenomenon monitored by a dense sensing network in a timely and reliable manner. To reach this primary objective, a set of scientific and technical objectives have been identified. The first objective is to devise an error recovery scheme for the slotted WiDOM protocol in a noisy wireless channel. This scheme should enable reliable data transmission in harsh environments where sensor nodes are more prone to interference. The second objective is to devise an aggregation mechanism that captures the dynamics of the physical quantities and self adapts according to the physical changes. This mechanism allows obtaining an accurate interpolation for a dynamic physical quantity. The third objective is to devise algorithms to identify various features in a distribution of a physical phenomenon. Feature extraction

algorithms enable identifying the location and the boundaries of events in dense sensing applications.

Resumo

Embora a transformação tecnológica da informação no século 20 pareceu revolucionária, uma mudança ainda maior está no horizonte. O termo cyber-physical system (CPS) chegou para descrever a investigação e os esforços tecnológicos que permitirão a interligação dos objetos físicos do mundo real ao ciber-espaço de forma eficiente.

Os avanços tecnológicos no design de hardware permitiram o surgimento de computadores embebidos únicos de baixo custo, equipado com capacidades de detecção, processamento e comunicação. Isto torna economicamente viável implantações densas de redes com grandes quantidades de tais nós. Deste modo, é possível fazer grande número de leituras dos sensores do mundo físico, calcular quantidades e tomar decisões locais.

Redes muito densas oferecem uma melhor resolução do mundo físico e, portanto, uma melhor capacidade de detectar a ocorrência de um evento; isso é de suma importância para um número de aplicações previstas. Monitoramento ambiental e monitoramento de integridade estrutural (SHM) são dois exemplos de tais aplicações. Nesta Tese, consideramos aplicações CPS densamente instrumentadas.

Considerando as capacidades limitadas típicas de nós sensores (em termos de comunicação e processamento), o cálculo de uma estimativa do estado do mundo físico é um desafio. Em geral, o principal desafio das redes densas de sensoriamento é dividida em duas classes distintas: transmissão de dados e de agregação de dados.

Suponha que um sistema de rede de sensores densa e de grande escala, cujos nós têm objetivo comum de sensoriamento: medir um fenômeno físico e calcular diferentes características da distribuição das leituras dos sensores, a fim de desencadear um conjunto de comandos de controle para atuadores de forma temporal. Com base nos desafios acima mencionados, formulamos a hipótese de Tese como se segue: acreditamos que é possível extrair certas características de um fenómeno físico de uma rede de sensores densa, de uma maneira fiável e atempada, e com uma complexidade de tempo que é essencialmente independente do número de nodos de sensores.

Portanto, o objetivo principal deste trabalho é desenvolver tecnologias e metodologias que permitam a extração de certas características de um fenômeno físico monitorado por uma rede densa de de sensores de forma temporal e confiável. Para alcançar este objectivo primordial, um conjunto de objectivos científicos e técnicos foram identificados. O primeiro objectivo é conceber um sistema de recuperação de erro para o protocolo WiDOM em um canal sem fio ruidoso. Este regime deve permitir a transmissão de dados confiável em ambientes ruidosos onde nós sensores estao mais propensos à interferência. O segundo objectivo é conceber um mecanismo de agregação que captura a dinâmica das quantidades físicas, que se auto adapta de acordo com as mudanças físicas. Este mecanismo permite a obtenção de uma interpolação rigorosa para a quantidade física dinâmica.

O terceiro objectivo é conceber algoritmos para identificar várias características em uma distribuição de um fenômeno físico. Algoritmos de extração de características permitem identificar a localização e os limites de eventos em aplicações de sensoriamento densas.

Acknowledgements

First and foremost, I would like to thank my supervisor, Eduardo Tovar for his continuous support during my PhD. His guidance helped me in all the time of research, during paper submissions and writing the Thesis. Despite his busy schedule as the director of CISTER/INESC-TEC, he was always very helpful. I feel fortunate for having had the opportunity to conduct research in such a supportive place.

I also like to thank Björn Andersson for his guidance during the first two years of my PhD when he was at CISTER/INESC-TEC. I enjoyed his immense knowledge and enthusiasm that inspired and motivated me.

I should express my gratitude to Stefano Tennina, who was always available with patience to discuss and find solutions. I think he is one of the most patient, respected mentors I have ever met. It was really a pleasant experience to work with him as he has deep knowledge in the sensor network area and real-world experiments.

Several contributions in this Thesis resulted from collaborations with other researchers in our lab. Vikram Gupta was always coming to meetings with nice ideas, and we were discussing on many interesting research problems. Michele Albano and Raghu Rangarajan were also very helpful in consolidating those ideas. Their deep knowledge helped me to provide efficient algorithms.

I also thank Patrick Meumeu Yomsi, Artem Burmyakov and João Loureiro for the stimulating discussions and the rest of my fellow students to make the lab environment at CISTER more alive and cheerful. I wish to acknowledge all who contributed in administrative and everyday bureaucracy: Sandra, Inês and Cristiana.

Finally, I would like to thank my beloved mother for always inspiring me to excel in academics. My father for encouraging me in my childhood and taught me to remain curious. He is not with us anymore, but I hope that I have made him proud. My father-and mother-in-law were always encouraging me to pursue my studies. I sincerely hope that I continue to meet their expectations. Finally, and most importantly, I would like to thank my dear husband and best friend, Hossein Fotouhi, for his support, encouragement, patience and unwavering love. He made these years the best years of my life.

Contents

List of Figures

List of Tables

List of Algorithms

Abbreviations

BB	Black Bursts
BIA	Basic Interpolation Algorithm
CAN	Controller Area Network
COTS	Commercial-Off-The-Shelf
CPS	Cyber-Physical System
CSMA	Carrier Sense Multiple Access
DB-MAC	Delay Bounded Medium Access Control
DIA	Differential Interpolation Algorithm
DSME	Deterministic and Synchronous Multi-channel Extension
EDF	Earliest Deadline First
GTS	Guaranteed Time Slots
HIPERLAN	High Performance Local Area Network
HNC	High Noisy Channel
ISM	Industrial, Scientific and Medical
LNC	Low Noisy Channel
MAC	Medium Access Control
MBD	Multiple Broadcast Domains
MCU	Micro-Controller Unit
MVDS	Minimum Virtual Dominating Set
PCF	Point Coordination Function
PIFS	PCF Inter-Frame Space
QoS	Quality-of-Service
RAM	Random-Access Memory
RF	Radio Frequency
RIG	Register Interfering Graph
RTOS	Real-Time Operating System
SBD	Single Broadcast Domain
SHM	Structural Health Monitoring
SPNC	Sporadic Noisy Channel
TDMA	Time Division Multiple Access
TFSS	Time For Signal Sensing
TTSMNG	Time To Start Managin
TTSRCV	Time To Start Receiving
WAI	Weighted-Average Interpolation
WCRT	Worst Case Response Time
WIA-PA	Wireless network for Industrial Automation - Process Automation

WiDOM	Wireless Dominance
WirelessHART	Wireless Highway Addressable Remote Transducer
WLAN	Wireless Local Area Networks
WSN	Wireless Sensor Network

Chapter 1

Introduction

Although the information technology transformation of the 20th century appeared revolutionary, a bigger change is on the horizon. The term cyber-physical system (CPS) has come to describe the research and technological efforts that will ultimately allow the interlinking of the real-world physical objects and the cyber-space efficiently [ECPS02, SLMR05].

The integration of physical processes and computing is not new. Embedded systems have been in place over the last few decades and these systems often combine physical processes with computing. The revolution is coming from the massively deploying networked embedded computing devices, allowing instrumenting the physical world with pervasive networks of sensor-rich embedded computation [SLMR05].

1.1   Research and Application Context

Technological advances in hardware design enable the emergence of low-cost single embedded computer equipped with sensing, processing and communication capabilities. This makes it economically feasible to densely deploy networks with very large quantities of such nodes. Accordingly, it is possible to take a very large number of sensor readings from the physical world, compute quantities and take decisions out of them. Very dense networks offer a better resolution of the physical world and therefore a better capability of detecting the occurrence of an event; this is of paramount importance for a number

of foreseeable applications. Environmental monitoring and structural health monitoring (SHM) are two examples of such applications.

In this Thesis, we consider densely instrumented CPS applications.

In [LDB+09], the authors report a densely deployment of sensor nodes for environmental monitoring with high data resolution and fidelity. Such a high resolution sensing enables a more precise understanding of the variability and the dynamics of the environmental parameters.

High spatial resolution is also used in structural health monitoring to accurately identify structural damages by analyzing the measured data through mathematical modeling [SCMSJ11]. SHM is relevant in aircraft, civil infrastructure (e.g. bridges and building) and laboratory specimens (e.g. beams and composite plates) [CGJ+04], just to provide a few examples.

In addition to detect the structural damage in a physical infrastructure, the aircraft industry is also considering the benefit of using dense sensing (and actuation), to minimize the carbon footprint. Active flow control [DM10, TPB+12] is one such technological developments that allows significant reduction of drag and therefore, related fuel consumption and pollution emissions [R+04]. One approach to achieve the flow control is to perform local adjustments of the skin surfaces using a very dense deployment of sensor, controller, and actuator nodes (smart skin patches) embedded in the aircraft wings and fuselage [DOBY14].

Many research projects (e.g. [LSBP02, LBP03, VLVS+03]) have considered dense deployment of sensing devices using substrate surface as a platform for power supply and communication bus. The Pushpin project [LSBP02] is a system with identical dense sensing devices, where sensor nodes have the form factor of pushpins. Employing these small sensor devices with such density is envisioned as an enabler for an electric skin.

The Tribble (Tactile Reactive Interface Built By Linked Elements) project [LBP03] is a dense sensing system consisting of 20 hexagonal and 12 pentagonal tiles connected as a sphere resembling a soccer ball. The tiles communicate neighbor to neighbor. Tribble was designed as a test-bed for dense sensing to investigate applications involving multi-modal electronic skins.

Pin & Play [VLVS⁺03] are networking objects that are used on surfaces such as walls and boards. The purpose of Pin & Play is to network objects in everyday environments by literally pinning them to a networked surface. The following section will address possible classes of applications which can benefit from dense sensing.

1.2 Research Challenges and Problem Statement

The scale of densely instrumented CPS poses huge challenges in terms of inter-connectivity and timely data processing. In this Thesis, we will look at efficient, scalable data acquisition methods for such dense CPS applications. CPS systems with high spatial resolution sensing must typically fulfill the following aggregation requirements (**R1** to **R5**):

R1. Computation (for estimating the state of the physical world) must be based on sensor readings from many sensor nodes, potentially all sensor nodes. The rationale for this requirement is that if the computation is based only on sensor readings from a single sensor node or a small subset of sensor nodes, we derive no benefit from the large and densely deployed number of sensor nodes available.

R2. Sensor nodes must be able to communicate. The rationale for **R2** follows from **R1**.

R3. Broadcast media (such as a shared wired bus or a wireless channel) must be used for communication. The rationale for **R3** follows from the fact that a point-to-point communication network is too expensive as the number of sensor nodes becomes large.

R4. The computation (for estimating the state of the physical world) must be performed within low and bounded delay. Note that the communication process is a part of this computation. The rationale for **R4** follows from the fact that control algorithms must obtain an estimate of the physical world that is not too old.

R5. The computation (for estimating the state of the physical world) must be scalable. The rationale for **R5** follows from the fact that unscalable computation leads to an outdated estimation of the physical world. Considering the communication cost,

for sensor networks of size m in a single broadcast domain, based on **R3**, any computation that fulfills **R1** will have a time-complexity that depends on the number of sensor nodes ($O(m)$).

Considering the limited capabilities of sensor nodes (in terms of communication and processing), computing an estimate of the state of the physical world, while fulfilling all the aforementioned requirements is challenging. In general, the main challenge of dense sensing networks is categorized into two distinct classes: data transmission and data aggregation.

Data Transmission in Dense Networks. Sensor nodes must communicate through a shared broadcast medium such as shared bus or a wireless channel. The medium access control (MAC) plays a key role in managing the data exchange in wired or wireless media. In this Thesis we focus on the wireless case since it simplifies inter-connectivity in dense deployments. However, the challenge is that wireless channels are much more error prone than wired cabling [CVV08]. Besides causing higher communication latency and jitters, transmission errors also directly affect the network reliability by increasing the packet drop rates. In dense networks, it is assumed that collecting data from all sensor nodes compensate the reading losses due to the high correlation of measurements among neighbor nodes. Nevertheless, collecting all the information from such networks is time consuming and less practical. It is therefore needed to devise techniques to reduce the number of packet exchanges.

There exists a class of MAC protocols based on dominance (also called binary countdown protocols) [MW79], which are used in the CAN bus (controller area network) [Bos91] and WiDOM [PAT07]. By assigning priority levels to different nodes' traffic, dominance-based protocols allow transmissions to the node that has the most constructive information (e.g. measuring the highest/lowest readings) for issuing proper control commands. In this way, dominance-based MAC protocols provide time-bounded guarantees for data transmission. However, employing this type of MAC protocols comes with a cost. Consider the case where a high priority packet drops due to an interference in an unreliable wireless

medium. Since there is no other packet with the same information, the control command is impaired due to the lack of information in the lost packet.

In general, real-time service guarantees are divided into two classes: hard real-time and soft real-time. In hard real-time systems, end-to-end delay upper-bounds must be guaranteed. The arrival of a message after its deadline (known as deadline miss) is considered as a system failure. Conversely, in soft real-time systems, a probabilistic guarantee is required and infrequent deadline misses are tolerable. In this Thesis, we aim at providing a deterministic end-to-end delay guarantee.

From a layered view, the MAC sub-layer should provide channel access delay (single-hop) guarantees. In this Thesis we consider dominance-based MAC protocols that also excel in the computation of complex aggregate quantities. There exists a valid upper-bound for message transmission delays in the CAN [DBBL07] and WiDOM [PAT07] MAC protocols. In this Thesis we provide a valid upper-bound on end-to-end delay for the slotted version of the WiDOM protocol, since slotted WiDOM provides a lower overhead as compared to the original WiDOM protocol. In this Thesis we also consider an error recovery scheme to improve the reliability of slotted WiDOM under noisy channel conditions. Timeliness analysis that considers these mechanisms is also an important contribution of this Thesis.

> **In this Thesis, we consider reliability and timeliness requirements in densely deployed CPS.**

Data Aggregation in Dense Networks. Collecting sensor readings from all sensor nodes in a densely deployed environment is quite costly, both in time and energy. Various sensor nodes may often detect common physical phenomena, thus increasing the chance of redundant correlated readings. Therefore, in-network filtering and processing techniques can definitely help to conserve time in real-time applications. Previous research [APT07] has made available algorithms for computing certain aggregate quantities such as `MIN`, `MAX` or `COUNT`, with a time-complexity that is independent of the number of nodes (as we will explain in Chapter 3). These algorithms are based on dominance protocols, and are used as the basic building blocks for computing other aggregated quantities [PGAT09,
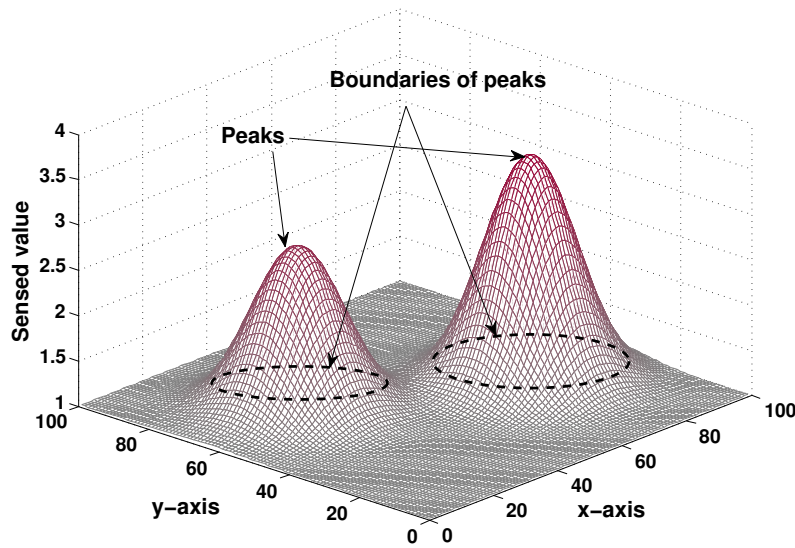
Figure 1.1: An example of a distribution of a physical quantity (*signal*) over a 2D deployment of dense sensor network.

TAP$^+$08]. Utilizing these dominance-based algorithms may enable fulfilling all the previously mentioned aggregation requirements (**R1**-**R5**).

Indeed scalable methods for computing aggregate quantities (such as `MIN`, `MAX` or `COUNT`) are useful in many applications. However, in many other cases the usefulness would come if it would be possible to produce an approximate representation of all sensor readings. In that way, it would be possible to compute any desired quantity based on that approximate representation, thus exploiting the fact that sensor readings are often spatially and temporally correlated with only a few abrupt changes in time or space. In fact, previous research works [APE$^+$08, ETPA11, PGAT09] have proposed algorithms for obtaining an approximate interpolation of sensor readings in dense sensor deployments. These algorithms exploit dominance-based MAC protocols, therefore presenting important scalability properties for densely instrumented CPS. We believe that it is possible to further improve the performance of these algorithms by (i) taking the knowledge of often-occurring spatial correlation of sensor readings and (ii) embedding the dynamics of the physical phenomenon in the algorithms.

In dense sensing CPS, obtaining an accurate and up-to-date status of the physical dynamics is critical for controlling tasks. Figure 1.1 presents an example of the distribution of sensor readings (for simplicity *signal*) over a two-dimensional deployment of a dense

sensor network. Each data point in the signal represents a value measured by a sensor node. Extracting features of the signal distribution, such as peaks and boundaries, is very challenging in terms of timeliness and scalability. The main concern is to collect a subset of readings with the most constructive information in a timely way. For instance, for very dynamic signals (like pressure in air flow control application), there must exist a functionality that detects the rate of change in the dynamics of the signal and embed the change into the algorithm. Dominance-based MAC protocols offer the potential to efficiently compute simple aggregate quantities (`MIN`, `MAX`). These protocols require an interference free medium for data transmission. However, this cannot be a valid assumption for wireless case.

We address the following challenges in this Thesis:

– How to devise a reliable data transmission for slotted WiDOM protocol that considers a more realistic channel model that encompass interference.

– How to devise efficient aggregation algorithms that self adapt according to the dynamics of the physical quantity and thus mitigating the accuracy problem (see Chapter 3) of previously proposed algorithms.

– How to extract more sophisticated features (such as peaks or boundaries) also in a scalable and efficient way.

1.3   Thesis Hypothesis

Consider a large-scale dense networked sensor system, whose nodes have a common sensing goal: to measure a physical phenomenon and also to compute different features from the distribution of sensor readings in order to trigger a set of control commands for the actuators in a timely manner. Based on the aforementioned reasoning and problem statement, we formulate the hypothesis as follows:

> *We believe that it is possible to extract certain features of a physical phenomenon (e.g., the location and the intensity of an event, and the area affected by the event) in a dense sensor network, in a reliable and timely way,*

and with a time complexity that is essentially independent of the number of sensor nodes.

1.4   Research Objectives and Approach

The primary objective of this Thesis is to devise technologies and methodologies that enable extracting certain features of a physical phenomenon monitored by a dense sensing network in a timely and reliable manner. To reach this primary objective, a set of scientific and technical *objectives* have been identified.

The first objective is to devise an error recovery scheme for the slotted WiDOM protocol in a noisy wireless channel. This scheme should enable reliable data transmission in harsh environments where sensor nodes are more prone to interference. Typically, wireless sensor nodes operate in the 2.4 GHz Industrial, Scientific and Medical (ISM) band, which is shared by IEEE 802.15.1 (Bluetooth) and the far more powerful IEEE 802.11b/WiFi. Moreover, most commodity wireless devices (e.g. baby monitors, walkie-talkies, and microwave ovens) use the same 2.4 GHz ISM band. Since all these systems coexist in the ISM wireless spectrum, providing an error recovery scheme is paramount. The approach we will follow will exploit an error recovery scheme by implementing data acknowledgment (Ack) in slotted WiDOM protocol. This approach is further explained in Chapter 4.

The second objective is to devise an aggregation mechanism that captures the dynamics of the physical quantities and self adapts according to the physical changes. This mechanism allows obtaining an accurate interpolation for a dynamic physical quantity. To do so, we design an add-on functionality for the existing interpolation algorithm that provides a set of change pattern metrics and updates these metrics in real-time. Further details on this approach is explained in Chapter 5.

The third objective is to devise algorithms to identify various features in a distribution of a physical phenomenon. Feature extraction algorithms enable identifying the location and the boundaries of events in dense sensing applications. To achieve this objective a set of functions were used for extracting various features from a distribution of physical

quantity. These functions take advantage of prioritized MAC design to compute `MIN/MAX` and employ them as the main element for the feature extraction purpose. we will describe this approach in Chapter 6.

1.5   Research Contributions

We outline the scientific and technological *contributions* of the Thesis in the next paragraph.

In the course of the work that led to this Thesis, we designed, implemented and validated a reliable data transmission mechanism for slotted WiDOM protocol. In that direction, in an initial phase of the work, we evaluated the schedulability analysis of slotted WiDOM [VA10]. We then further extended the initial schedulability analysis by considering the error recovery mechanism for the case where sensor nodes suffer from interference in the wireless channel. We devised the Ack-enabled slotted WiDOM in the Nano-RK operating system [ERR05] and evaluated this protocol in a noisy environment. The most important results are compiled and published as [VTTA15];

Another important set of results concerns the design and implementation of an adaptive aggregation algorithm that detects variations in the dynamics of the physical quantity in real-time [VTA13]. These dynamics are embedded into the interpolation mechanism to compensate the errors in the approximated representation of the physical quantity. The implementation details of this algorithm are provided in this Thesis in Chapter 5.

At last but not the least, we designed and implemented several feature extraction mechanisms suitable for dense sensor deployments. In particular, three distinct functions were proposed to provide the location of peaks and the boundaries around them in the distribution of a physical quantity (signal) [VGAT14]. An extension of the feature extraction mechanism to multi-hop dense network was then proposed [VGA$^+$15]. Two distinct approaches were used: (i) a classical clustering technique that extracts centrally the features of the corresponding cluster and then transmit the information to the destination; and (ii) a new technique (ripple-based) that employs flooding to find `MIN/MAX` globally. In the ripple-based approach the features are computed in the same way as in a single

broadcast domain. We compared these two approaches and showed their performance in various scenarios. The code for this implementation is also available on-line [Vah15].

1.6   Structure of the Thesis

The remainder of this Thesis is organized as follows. In Chapter 2 we provide the necessary background on dominance-based MAC protocols. Timeliness aspects are discussed and other real-time MAC protocols, and characteristics are briefly surveyed. In Chapter 3 we review previous relevant work that exploits dominance-based MAC protocols to efficiently compute aggregate quantities. We discuss relevant aggregate quantities such as MIN (the basic building block used in all algorithms aiming for computation other aggregation quantities) and the more complex one (that includes positioning information) and main focus of our work: complex feature extraction.

Chapters 4, 5 and 6 describe the main contributions attained in this research work. In Chapter 4, we detail a novel proposal to improve the reliability of slotted WiDOM under noisy channel conditions. Besides describing the implementation of the error detection mechanism, we propose a novel response-time formulation that enables computing the upper-bound on message transmission delay for slotted WiDOM. In Chapter 5, we present and discuss the results on a novel sophisticated adaptive method to compute approximate interpolation in densely-deployed sensor systems. In this method we present an add-on functionality that computes the change pattern metric of the physical signal in order to provide more accurate approximate representation of the physical signal. In Chapter 6 we propose a set of algorithms that identify the main features of a sensor reading distribution and extend the proposed functionality to a large multi-hop dense network in a fully distributed manner by leveraging the inherent properties of the dominance-based MAC protocols.

Finally, in Chapter 7, we conclude this Thesis by providing a summary of the research contributions and an outline of potential research challenges that build on the current results.

Chapter 2

Background and Related Work — Binary/Countdown MAC Protocols

In this chapter, we provide relevant background information regarding the family of medium access control protocols used as a basis throughout the research work described in this Thesis. First, a brief introduction to binary/countdown MAC protocol is provided. Then, the adaptation of that MAC protocol to the wireless case, dubbed WiDOM (wireless dominance), is described and important related research efforts surveyed.

2.1   Introduction

Real-time computing systems are those systems in which correctness of the system depends not only on the logical result of computation but also on the time at which the results are produced [SSH99]. This implies that, unlike more traditional information and communication systems, where there is a separation between correctness and performance, in real-time computing systems correctness and performance are tightly interrelated. Only a few decades ago, real-time computing systems were an important but narrow niche of computer systems, consisting mainly of military systems, air traffic control and embedded systems for manufacturing and process control. This association caused that real-time systems problems did not attract widespread interest from the computer community.

Meanwhile, the emergence of large-scale distributed systems, enabled by advances in networking technology, has broaden real-time concerns into a mainstream enterprise, with clients in a wide variety of industries and academic disciplines. Terms such as "Cooperating-Objects" [MM09], "Cyber-Physical Systems" or "Internet of Things" [AIM10, Kop11, SGLW09, COM09] have come to describe the research and technological efforts that will ultimately efficiently allow interlinking the real world physical objects and cyberspace.

The integration of physical processes and computing is however nothing dramatically new: embedded systems have been in place since a long time to denote systems that combine physical processes with computing. The revolution is coming from extensively networking embedded computing devices, in a blend that involves sensing, actuation, computation, networking, pervasiveness and physical processes. And interaction with the physical world always implies timeliness as a main concern in the design process. This tendency has been establishing real-time technology as a priority for commercial strategy and academic research for the foreseeable future and also for a wider number of applications.

Collecting data from high-density networks can make use of specific properties of the communication medium to collect aggregates in a fast and energy-efficient manner. WiDOM [PAT07] is such a medium access control protocol that can be employed to efficiently compute aggregates in a timely manner with significantly lesser message exchanges, as shown in [PAT07, ETPA11]. With that approach, the number of messages exchanged and time to gather an aggregate are not dependent on the number of nodes in a given broadcast domain, thus facilitating dense networks without correspondingly high-energy and temporal costs.

Acquiring the representation of the physical world must be done with a low (and bounded) delay. Due to the large number of devices, which potentially offers high spatial resolution, communication becomes challenging, and obtaining a representation of the physical world with a low (and bounded) delay can be a major obstacle. So, the desire for high spatial resolution may come at the cost of precluding high temporal resolution.

In [SAL$^+$03] the authors outline various challenges in real-time communication in

sensor networks. Quality-of-Service oriented approaches, like those described in [FLE06], provide probabilistic timing and reliability guarantees based on the application requirements. Such provisions are necessary in systems with real-time requirements, and especially in critical systems employed in for example, aeronautical applications. Reducing the radio power can help not only to achieve energy-savings, but can also limit the radio-coverage in dense networks, thereby reducing packet collisions. Low-power radio designs [SAL$^+$03, FLE06] have been proposed that can help on achieving the above goals.

Another approach to reduce the delay induced by wireless communication is the adoption of decentralized computation. The analysis of sensor data within a small cluster of nodes or locally on single nodes with the objective of extracting data features relevant for the application will contribute to the reduction of the communication traffic. However, it must be ensured that the energy and time saved on the communication is not lost with the additional processing. The computation capabilities of the node must be then adapted accordingly, using for example reconfigurable computing [HZG09].

2.2 Binary/Countdown MAC Protocols

Many emerging embedded applications are designed to respond to stimuli from the environment. Typically, these events are triggered sporadically; that is, the exact time of a transmission request is unknown but a lower bound on the time between two consecutive transmission requests from the same message stream is known. Such traffic is called sporadic message streams.

While many scheduling algorithms and analysis techniques for wireless communications are available for periodic messages, the case of sporadic messages is less studied. Most of the current wireless protocols cannot be analyzed to offer pre-run-time guarantees that sporadic messages meet deadlines, and the protocols that do offer such guarantees rely on polling, which is inefficient when the deadline is short and the minimum time between two consecutive requests is long.

In wired networks, sporadic messages can be efficiently scheduled using the controller area network (CAN) bus [Bos91], and this has already proven to be useful in
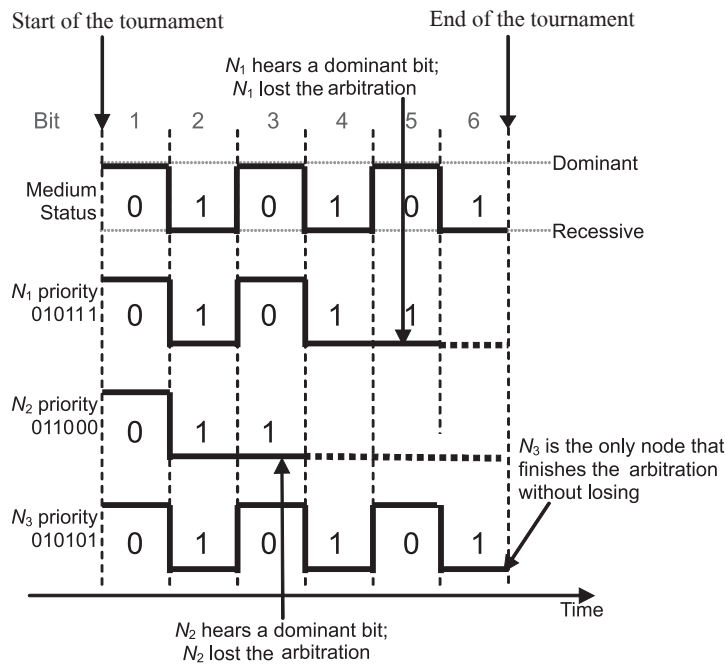
Figure 2.1: Arbitration in dominance/binary-countdown protocols.

industry, as witnessed by the pervasive use of the CAN bus. It has a medium access control (MAC) protocol which is collision-free and prioritized, and hence it is possible to schedule the bus such that if message characteristics (minimum inter-arrival times, transmission times, jitter, etc.) are known, then it is possible to compute upper-bounds on message delays [BLDB06, THW94].

This MAC protocol belongs to a family called dominance or binary countdown protocols [MW79]. In such protocols, messages are assigned unique priorities, and before nodes try to transmit, they perform a contention resolution phase named arbitration such that the node trying to transmit the highest-priority message succeeds.

During the arbitration (depicted in Figure 2.1), each node sends the message priority, bit-by-bit, starting with the most significant one, while simultaneously monitoring the medium. The medium must be devised in such a way that nodes will only detect a "1" value if no other node is transmitting a "0". Otherwise, every node detects a "0" value regardless of what the node itself is sending. For this reason, a "0" is said to be a dominant bit, while a "1" is said to be a recessive bit. Therefore, low numbers in the priority field of a message represent high priorities.

If a node contends with a recessive bit but hears a dominant bit, then it will refrain

from transmitting any further bits, and will proceed only monitoring the medium. Finally, exactly one node reaches the end of the arbitration phase, and this node (the winning node) proceeds with transmitting the data part of the message. As a result of the contention for the medium, all participating nodes will have knowledge of the winner's priority.

Besides its ability to handle efficiently sporadic message streams, binary/countdown MAC protocols can also be efficiently exploited to compute aggregate quantities. The following example illustrates this.

The problem of obtaining aggregated quantities (e.g., MIN) in a single broadcast domain can be solved with a naive algorithm: every node broadcasts its sensor reading sequentially. Hence, all nodes know all sensor readings and then they can obtain the aggregated quantity. This has the drawback that in a broadcast domain with m nodes, at least m broadcasts are required to be performed. Considering a network designed for $m \geq 100$, the naive approach can be inefficient; it causes a large delay.

Let us consider the simple application scenario as depicted in Figure 2.2 (a), where a node (node N_1) needs to know the minimum (MIN) temperature reading among its neighbors. Let us assume that no other node attempts to access the medium before this node. A naive approach would imply that N_1 broadcasts a request to all its neighbors and then N_1 would wait for the corresponding replies from all of them.

As a simplification, assume that nodes orderly access the medium in a time division multiple access (TDMA) fashion, and that the initiator node knows the number of neighbor nodes. Then, N_1 can derive a waiting timeout for replies based on this knowledge. Clearly, with this approach, the execution time depends on the number of neighbor nodes (m).

Figure 2.2 (c) depicts another naive approach, but using a CAN-like MAC protocol. Assume, in that case, that the priorities the nodes use to access the medium are ordered according to the nodes' *ID*, and are statically defined prior to runtime. Note that in order to send a message, nodes have to perform arbitration before accessing the medium. When a node wins, it sends its response and stops trying to access the medium. It is clear that using a naive approach with CAN brings no timing advantages as compared to the previous naive solution (Figure 2.2 (a)).

(a) Naïve algorithm (TDMA-like MAC)   (b) Novel algorithm (CAN-like MAC)

(c) Naïve algorithm (CAN-like MAC)
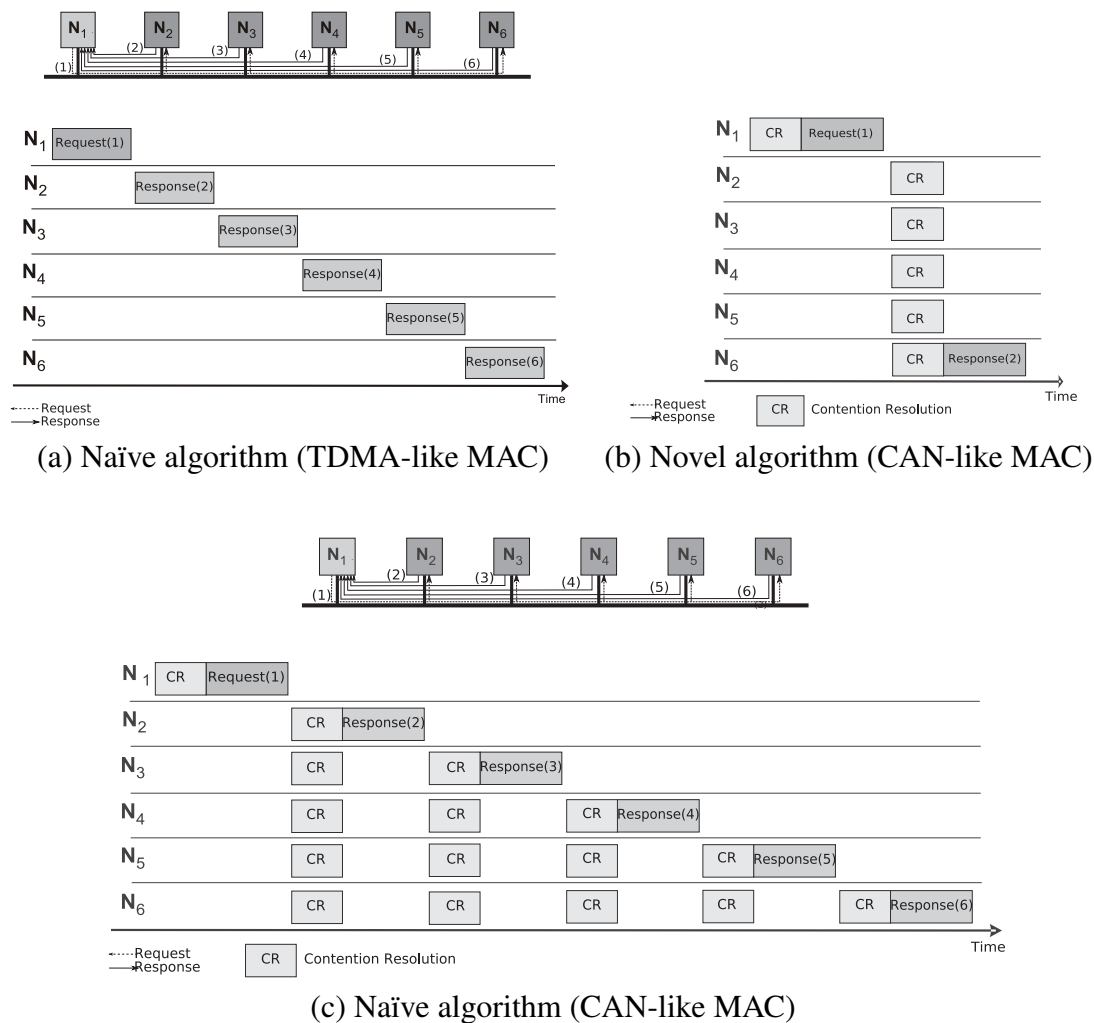
Figure 2.2: Dominance/Binary-countdown arbitration motivating examples. (a) Example application with TDMA-like MAC; (b) possible solution by exploiting the properties of a CAN-like MAC, where priorities are assigned at runtime according to the sensed values; (c) possible solution using a CAN-like MAC with fixed priorities for the messages.

With such an approach, to obtain the minimum temperature among its neighbors, node N_1 needs to perform a broadcast request that will trigger all its neighbors to contend for the medium using the prioritized MAC protocol. If neighbors access the medium using the value of their temperature reading as the priority, the priority winning the contention for the medium will be the minimum temperature reading.

With this scheme, more than one node can win the contention for the medium. But, considering that at the end of the arbitration the priority of the winner is known to all nodes, no more information needs to be transmitted by the winning node. In this scenario, the time to obtain the minimum temperature reading only depends on the time to perform

the contention for the medium, not on *m*. If, for example, one wishes that the winning node transmits information (such as its location) in the data packet, then one can code the priority of the nodes by adding a unique number (for example, the node *ID*) in the least significant bits, such that priorities will be unique. Such use, results in a time complexity of *log m*.

A similar approach can be used to obtain the maximum (MAX) temperature reading. In that case, instead of directly coding the priority with the temperature reading, nodes will use the bitwise negation of the temperature reading as the priority. Upon completion of the medium access contention, given the winning priority, nodes perform bitwise negation again to know the maximum temperature value.

MIN and MAX are just two simple and pretty much obvious examples of how aggregate quantities can be obtained with a minimum message complexity (and therefore time complexity) by exploiting binary/countdown MAC protocols, provided that message priorities are dynamically assigned at runtime upon the values of the sensed quantity.

2.3 Binary/Countdown MAC Protocols in Wireless

WiDOM was proposed [PAT07] to solve the problem of sporadic messages scheduled on a wireless channel, and it relies on adapting dominance/binary countdown protocols to the wireless channel.

This adaptation is non-trivial due to the following reasons: (i) implementations of dominance protocols for a wired medium are based on a wired-AND behavior of the bus, where the dominant signal overwrites the recessive signal; (ii) these implementations require that nodes are able to monitor the medium while transmitting—clearly this does not easily extend to the case of wireless channels— and (iii) due to non-idealistic of the used transceivers and nature of the wireless medium. In the following we explain the way WiDOM overcomes all the mentioned issues.

WiDOM is composed of three phases: *synchronization*; *contention resolution* or *tournament*; and *data exchange* —see Figure 2.3. In all dominance/binary countdown protocols, nodes need to agree on a common time before starting the contention resolution
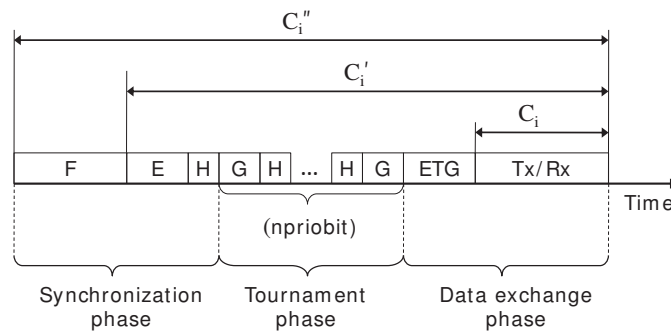
Figure 2.3: Timing order of the WiDOM protocol.

phase. This phase is of paramount importance since a small time drift in transmitting the priority bits may lead to an erroneous result. Hence, the synchronization is needed to provide a common reference point in time so that all nodes can start the competition at the same time and it should happen right before the tournament phase.

In the initial version of WiDOM, at the start of synchronization, nodes should wait for a long period of idle time "F" —see Figure 2.3, such that no node disrupts an ongoing tournament. Then nodes with a pending message wait for another time span "E" to compensate for the potential clock drift and also ensuring that all nodes have enough time to listen for "F" time units. Afterwards, nodes start sending a carrier pulse for a duration of "H" time units that signals the start of a tournament and establishes a common time reference. To do so, they have to switch from receive mode to send mode, which takes "SWX" units of time. By sending this signal, all nodes restart their timers and synchronization ends.

In the tournament phase, nodes transmit the priority of the message contending for the medium bit-by-bit. If a node loses the contention of a bit (i.e. it transmits a recessive bit and receives a dominant bit), it does not continue further bits and only proceed listening to the medium to find out the priority of the winner. If a node does not lose the contention during the current bit, it will proceed with the contention for the next bit.

The nodes that have a dominant bit, start transmitting a pulse of carrier for the duration of "H" units of time, while nodes with a recessive bit perform carrier sensing for the same time span. Also, note that the fact that wireless transceivers are not able to send and receive simultaneously poses no problem to WiDOM since when a node has a dominant

bit, there is no need for reception and when a node has a recessive bit, it sends nothing; it performs carrier sensing.

There is also a guarding time interval "G" to separate pulses of carrier waves. This guarding time interval makes the protocol robust against clock inaccuracies, and takes into account that signals need a non-zero time to propagate from one node to another. At the end of the tournament, the node that does not receive a pulse wins the competition and waits for "ETG" time units before starting data transmission.

2.4   Slotted WiDOM

The original implementation of WiDOM, explained in the previous section, is based on commercial off-the-shelf (COTS) wireless sensor network (WSN) platforms. That version of WiDOM implies a significant additional overhead. Part of that overhead is due to technological limitations, importantly the switching time between transmission and reception mode, that can be alleviated by carefully chosen hardware. Another part of that overhead is caused by the required synchronization in which nodes should wait for a long period of silence before any data transmission.

Slotted WiDOM is a more recent version of WiDOM aimed at reducing the overhead. To do so, the authors have developed an add-on platform (called WiFLEX [PGAT09, Gom08]) to perform the tournament phase more efficiently (lower overhead) and with lower energy consumption. A novel synchronization mechanism that exploits an out-of-band signaling technique was introduced in the design.

Most WSN platforms use the Chipcon CC2420 radio [T. 07], which does not offer the desirable characteristics needed for the WiDOM implementation. In terms of hardware, the WiFLEX approach consists of two small boards: the WiFLEX-main board (simply main board), illustrated in Figure 2.4-(a), and the WiFLEX-daughter board (daughter board), illustrated in Figure 2.4-(b). This platform can be plugged into common WSN platforms such as the MicaZ [I. 04] or FireFly [MRR07]—see Figure 2.4.

The main board sends and receives pulses during the tournament, while the daughter board, which is also known as WiFLEX-rxsync, is only responsible for receiving syn-

(a) WiFLEX_main board

(b) WiFLEX_daughter board

(c) WiFLEX_daughter board stacked
on the WiFLEX_main board

(d) WiFLEX platform stacked on
Firefly sensor

(e) WiFLEX platform stacked on
MicaZ sensor
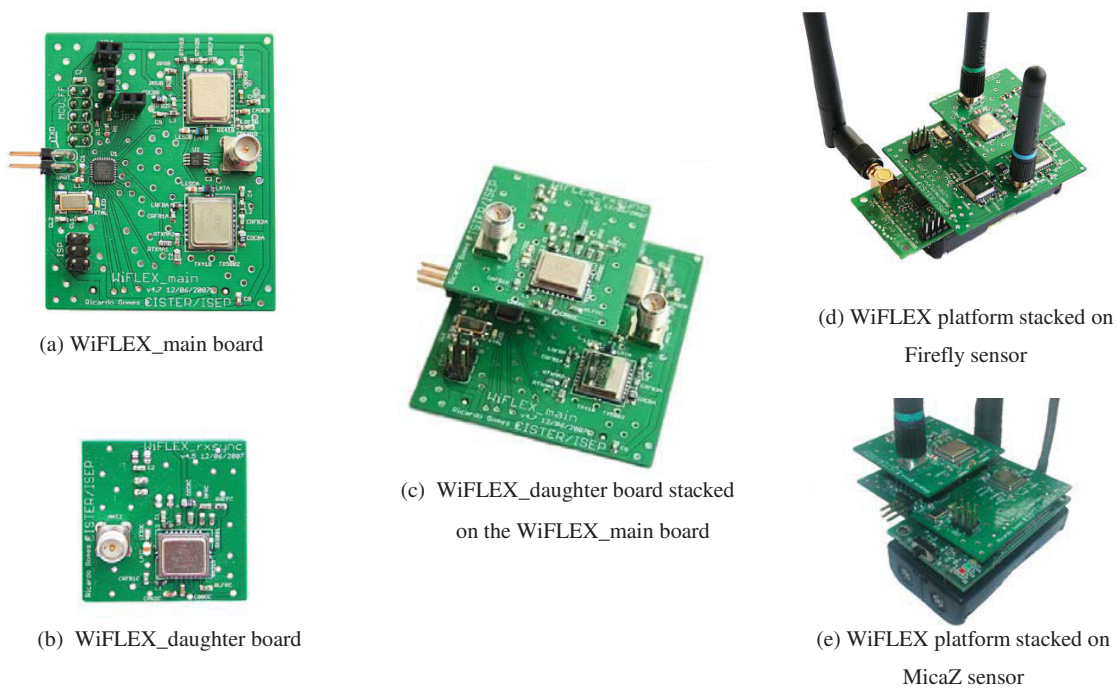
Figure 2.4: Hardware platform.

chronization pulses. Figure 2.4-(c) shows how these two boards are assembled. The main board is equipped with a low-power Micro-Controller Unit (MCU) in order to run the MAC protocol on both the WiFLEX and the host platforms concurrently, and to provide a mechanism for higher level communication between those two platforms. The MCU controls two independent radio modules embedded in the main board: (i) one transmitter and (ii) one receiver that share a single antenna. This antenna is assigned to each radio module through a high-frequency switch under the MCU supervision.

Another single receiver module has been used in the daughter board that is always ready to receive the synchronization signal. The advantage of using the separate receiver (daughter board) is the possibility of setting it perpetually in reception mode and eliminating the switch time and maintaining accurate synchronization. Furthermore, by utilizing out-of-band signaling for synchronization, nodes are not forced to wait for a long duration of "F" time units. This allows a major reduction of the protocol overhead.

Poor balanced data (large number of consecutive 1's or 0's) results in unreliable signal detection on the receivers. To avoid this problem it is best to use data that has equal number of 1's and 0's in a period of time. To provide such a balanced data on the receiver

Figure 2.5: Dominant and recessive signal sequence with bit stuffing.

of the main board, a bit stuffing technique is exploited during the tournament phase. The idea behind this technique is to introduce redundant information to maintain channel activity. To do so, a dominant bit is coded as a "1" + "0" signal sequence and a recessive bit as two consecutive "0" bits and then introducing a bit stuffing composed of a "1" + "0" signal sequence after each dominant or recessive bit. See Figure 2.5 for illustration of this principle.

In the tournament phase the radio module on the main board exchanges the data only during priority bit exchange and after that it stays idle until the next tournament phase. Since the radio activity is not maintained, the same problem may occur in the detection of the first priority bit. To solve this problem, a special start symbol or preamble has been introduced at the beginning of the tournament phase. Two consecutive dominant bits are sufficient to allow a correct detection between noise and the start of an incoming priority bit without imposing high overhead.

The same policy is also applied in the synchronization signal transmission. To maintain channel activity, a burst of consecutive sequence of "0" + "1" with the same pulse duration is used. A longer duration of "1" pulse (for a duration of time for signal sensing – TFSS) is then considered to signal the reception of a synchronization signal — see Figure 2.6.

Figure 2.6: Synchronization signal burst.

A*: (Prio_Tra); Transferring priority from WSN host platform to WiFLEX.
B*: (Win_Prio); Transferring winner priority from WiFLEX to WSN host platform.

Figure 2.7: Timing order of the slotted WiDOM protocol.

This synchronization signal is broadcast periodically with a period of P_S. Given the periodic nature of such synchronization signal, which creates timeslots, we call this version of WiDOM "slotted WiDOM".

Summing up all the implementation details, the "superframe" of the Slotted WiDOM protocol is as depicted in Figure 2.7. There are three important issues that deal with the add-on circuitry that is used in this implementation of WiDOM. These are outlined next.

(i) In the tournament phase, before going through the competition, the priority of the enqueued message should be notified to the WiFLEX board and at the end of the competition, the priority of the winner should be reported back to the WSN host platform. Thus, in the slotted WiDOM , we need to consider two time intervals (A and B) for internal communications between the two boards.

(ii) Only those nodes that have messages in their queues wait for receiving the synch signal; this means that if a node enqueues a message slightly after the synch signal broadcast, it will not participate in the currently on-going tournament, even if the tournament phase formally has not started, yet.

(iii) Due to hardware shortcomings, bit stuffing is used after each priority bit and due to the same reason two dominant bits instead of a single one should be sent as preamble, to indicate the start of the contention period.

Table 2.1: WiDOM parameters.

Parameter	Description	Implementation
P_S	Synchronization signal periodicity	slotted WiDOM
TFSS	Time needed to sense synchronization signal	slotted WiDOM
A (PRIO_TRA)	Priority transmission from WSN host to Wi-FLEX	slotted WiDOM
B (WIN_PRIO)	Winner priority reported by WiFLEX	slotted WiDOM
H	Carrier pulse duration	Both
G	Guarding time	Both
npriobits	Number of priority bits	Both
ETG	Guarding time at the end of tournament	Both
C_i	Time to transmit a message from message stream i	Both
E	Time to cope with synchronization imperfection	WiDOM
F	Initial idle period for synchronization	WiDOM

Table 2.1 summarizes all the parameters and their meaning for the two versions of WiDOM.

2.5   Other Prioritized Wireless MAC Protocols

Guaranteeing timely delivery of critical traffic is a major challenge in time critical applications. Many research works have focused on minimizing the energy consumption of these hardly resource-constrained networks. However, the real-time support to high priority traffic within such applications has started to be investigated only recently. Some attempts to support time guarantees in conventional protocols by assigning priorities to the network traffic are reported in [SZBG14, AC01, SK96].

The definition of the WLAN standard, IEEE 802.11 [CWKS97], stimulated the development of many prioritized carrier sense multiple access (CSMA) schemes. Some of these variants, [AC01, BCV01, JC99], propose to fine tune the parameters defined in the standard in order to guarantee that deadlines are met for each traffic flow. Some others, e.g., [TWTLB11], suggest to combine time division multiple access (TDMA) approaches with a traffic scheduler. Nevertheless, unless some additional scheduling features, such as those described in [WIA11], are used, these techniques suffer from two drawbacks: (i) they do not fully achieve a priority-based scheduling, since it may happen that a high

priority message has to wait in the transmission queue for a lower priority message to be sent; and (ii) collisions may still occur, as a result of using CSMA in the IEEE 802.11. Both problems certainly lead to deadline misses in real-time applications.

Due to collisions, nodes may suffer from long access delays before being able to transmit. A conventional method is to send jamming signals (called Black Bursts, BB) in order to win access for the transmission of higher priority messages [SK96, SK99]. Same approach is employed in the HIPERLAN protocol [JMMR97]. In BB-based protocols, a station with real-time traffic waits until a channel becomes idle for a PCF [1] Inter-Frame Space (PIFS) period and then contends for the channel by transmission of jamming signals. The collision interval between two or more pulses of energy is measured in order to resolve the contention. The longest jamming transmission wins the channel access. After transmitting the BB signal, a node waits for an observation time to check if any node is transmitting a longer BB. If the channel remains idle during this time, the node sends its data frame. A recent work [SZBG14] proposed the use of BB signals to distinguish the highest priority and critical control packets. The drawbacks of BB signals lie in (i) the inability to cope with the hidden terminal problem, and (ii) the unreliability in the presence of interference.

Strawman [ÖMV$^+$12] is designed for duty-cycled low-power networks. A Strawman round starts by receiving a `COLLISION REQUEST` packet. The senders interpret this packet as the beginning of a new round, and contend for the channel by sending a `COLLISION` packet of random length. Similar to the BB-based approach, the receiver estimates the length of the longest `COLLISION` packet and broadcasts a `DECISION` packet containing the longest measured length, implicitly informing the corresponding transmitter that it is granted access to the channel. Employing `DECISION` packets helps to alleviate the hidden terminal problem. However, emitting pulses of energy or dummy packets, a station wastes considerable channel bandwidth and energy to send each outgoing frame. Moreover, this overhead (the length of BB or `COLLISION` packet) will increase linearly with the number of priority levels since the maximum length of the black burst is proportional to the number of priority levels. Therefore, only a small number of priority levels

---

[1]Point Coordination Function

can be supported.

Another technique [YV06], not based on IEEE 802.11, implements prioritization by using two separate narrow band busy-tones to communicate that a node is backlogged with a high-priority message. This technique has the drawback of requiring very specialized hardware, requiring extra bandwidth (for the narrow band signals). Also, it only supports two priority levels.

MAC protocols have also been proposed from the real-time systems community with the goal of meeting deadlines [ZKI10, SRS12, KOK14]. Some protocols use tables (sometimes called TDMA templates) with explicit start times of message transmission. These tables are created at run-time either in a distributed fashion [CBBS03] or centrally by a leader [LSR04]. It is also conceivable to use a TDMA template designed before run-time [KG93] and use it to schedule wireless traffic. However, all these time-table driven approaches have the drawback of requiring that sporadic message streams are dealt with using polling, which, as previously stated, is inefficient.

Another approach, Implicit-EDF [CZSB02], is based on the assumption that all nodes know the traffic on the other nodes that compete for the medium, and all these nodes execute the EDF scheduling algorithm. Unfortunately, this algorithm is based on the assumption that a node knows the arrival time of messages on other nodes, and this implies that polling must be used to deal with sporadic message streams.

The standard IEEE 802.15.4 [80206] provides a Guaranteed Time Slots (GTS) mechanism to allocate specific duration within a superframe for soft real-time traffic. The IEEE 802.15.4e Working Group redesigned the existing IEEE 802.15.4 MAC standard to support emerging needs of embedded industrial applications. The Deterministic and Synchronous Multi-channel Extension (DSME) mechanism in IEEE 802.15.4e [80212] is one of the main extensions that provides prioritized channel access by reserving specific DSME guaranteed time slots for high priority traffic. Through the DSME prioritization method, the high priority messages are not transmitted immediately after their generation. Devices wait for dedicated slots to transmit the messages. Thus, whenever a high priority message is generated after the dedicated time slot is passed, the device must wait for the next assigned slots, thus the standard do not allow to resolve the priority inversion

problem.

Several industrial standards such as WirelessHART [wir10], ISA-100.11a [ISA09] and WIA-PA [WIA11] leverage IEEE 802.15.4 physical layer with a low rate of maximum 250 kbps and a low implementation complexity for resource-constrained devices. They mainly utilize TDMA approaches to provide guaranteed access to the wireless medium. An adaptive scheduling algorithm can effectively improve the timeliness support by means of delay optimization or mitigation [TLB12, LRY$^+$12]. The standards also adopt packet-level channel hopping to improve the reliability of individual wireless links by combating external interference and multi-path fading.

ISA-100.11a, WirelessHART and WIA-PA provide a limited service differentiation in MAC schemes. They support four traffic categories. High-priority packets are allowed to access the medium prior to low-priority packets. Hence, all data flows should be allocated into one of these four classes of traffic flow and then a polling-based mechanism resolves the competition among these traffic levels.

Another work called GinMAC [SBR10] is proposed to deliver data in a timely manner. This protocol encompasses three procedures: off-line network dimensioning, an exclusive TDMA schedule and delay conform reliability control to support timeliness requirements. In the implementation of GinMAC the traffic patterns and channel characteristics are known a-priori and all complex calculations including slot allocation is done offline. Due to off-line dimensioning, the protocol has a more predictable performance. Although GinMAC can support mission-critical data delivery, it has some limitations. For example, the protocol is tailored for a control loop setting in which sensor data must be forwarded to the sink, resulting in a convergecast traffic pattern. Some mission-critical applications, such as battlefield tracking, may create different traffic patterns and thus cannot be supported by GinMAC. Furthermore, as GinMAC is a TDMA-based protocol with exclusive slot usage, it is suitable for a dense albeit relatively small network. In order to remove this scalability restriction, additional work is required.

In [WUT05], a MAC protocol based on a binary countdown was proposed. However, the binary countdown arbitration was employed such that collisions can cause deadline misses.

2.6   Summary

This chapter provided background material on medium access control protocols relevant to the proposed research work. We briefly introduced the binary/countdown MAC protocol. The main advantages of this MAC design were defined in terms of (i) timeliness support for event-triggered messages and (ii) simultaneous non-destructive transmission of information in a single broadcast domain. These will be shown to be important characteristics to be exploited for efficient distributed computations in densely deployed sensor networks.

Both wired (CAN bus) and wireless (WiDOM) versions of this MAC design were described, including an add-on hardware to eliminate the shortcoming of the original WiDOM implementation: slotted WiDOM.

While the CAN bus implements error recovery schemes, no such mechanism have been devised for the WiDOM protocol. That would be relevant given the error prone nature of wireless channels. We will address this challenge in Chapter 4 and propose a novel solution to the problem.

Chapter 3

Background and Related Work –
In-network Data Aggregation

One of the key purposes of sensor network deployments is to collect data from the physical environment in order to obtain the desired information about the status of the phenomena of interest. Data aggregation is defined as the process of aggregating data from multiple sensor nodes to eliminate the redundant transmission and therefore to prolong network lifetime. In this chapter, we survey various techniques of data aggregation in sensor networks. A special focus is then given to the use of dominance-based technologies for computing aggregate quantities.

3.1 Data Aggregation Techniques

Data aggregation is used either to fuse data from different sensors to eliminate redundant transmissions [KEW02, WFS08] or to fuse data and apply signal processing for computing some properties such as MIN (MAX), AVERAGE or SUM [MSFC02].

   Data aggregation techniques are tightly coupled with how data is gathered at the sensor nodes (data-centric) as well as how packets are routed through the network (routing-centric) [FRWZ07]. There are two well-known categories for packet forwarding in the network: tree-based and cluster-based approaches.

29

According to the tree-based approach [IGE$^+$03, LRS02, XHE01], first there is the need to construct a spanning tree that is rooted at the sink node. Upon receiving a request from the sink, nodes start performing in-network aggregation along the aggregation tree by proceeding level by level from their leaves to their root. So, if two or more messages arrive to a given node, their aggregate can be easily computed. The main drawback of this approach is that due to channel impairments, it is possible to lose an aggregated data. In fact, a single message at a given level of the tree may aggregate the data coming from the whole related sub-tree. When a packet is lost at a given level of the tree, the data coming from the related sub-tree will be lost as well.

The cluster-based approaches [Hei00, MR04, YG02, ZNLF04] are also based on a hierarchical organization of the network. Initially, nodes are subdivided into clusters and a special node, called cluster-head, is selected in each cluster. The cluster-head nodes are elected in order to aggregate data locally and transmit the result of such an aggregation to the sink. If the sink node loses the packet coming from a cluster-head, it will lose all the information about the underlying cluster.

Several studies have been done on real-time data aggregation. Most of these studies couple the aggregation mechanism with the underlying routing or MAC approaches. Zhang et al. [ZJX10] investigated the problem of maximizing information collection under a delay bound constraint for CSMA/CA-based MAC protocols in sensor networks. They proposed an optimal algorithm and a distributed heuristic algorithm to allocate the maximal allowable transmission delay at each sensor node. Although, their approach does not guarantee the reception of all measurements; they have achieved the information collection ratio of 95% in the best case.

A different approach to route packets by performing data aggregation is presented in [DBMC04], where the routing and the MAC protocols are jointly designed. The primary objective of the Delay Bounded Medium Access Control (DB-MAC) [DBMC04] scheme is to minimize the latency for delay bounded applications while taking advantage of data aggregation mechanisms for increased energy efficiency.

However, considering a dense network, all the aforementioned protocols suffer from poor timeliness. The time complexity of finding a simple aggregate quantity (e.g. MIN)

depends on either the number of nodes in the same broadcast domain, if a TDMA MAC approach is used, or on the number of allowable retransmissions and some none deterministic factors, if a contention-based MAC protocol is used.

3.2   Boundary Detection Techniques

Boundary detection in sensor networks often aimed in various applications. There are different approaches to address the problem of boundary detection and determining the extent of an event in sensor networks [CG03, NM03, WGM06, SBP04, ATS14].

Chintalapudi and Govindan presented localized edge detection techniques based on statistics, image processing, and classification [CG03]. Nowak and Mitra described a method for hierarchical boundary estimation using recursive dyadic partitioning [NM03]. They developed an inverse proportionality relation between energy consumption and the mean-square error in boundary detection and showed that their method is near-optimal with respect to this fundamental trade-off. Another hierarchical boundary estimation is proposed in [ATS14], where a contiguous two-dimentional shape of an event is found with a threshold-based boundary detection.

Other schemes represent the boundary of an event or the signal landscape of a sensor network compactly using in-network aggregation [BGHS06, GSW09, HHMS03, DRK11, HR10]. Gandhi et al. studied the problem of monitoring the events of sensor networks using sparse sampling [GSW09]. However, their algorithm requires the prior knowledge of the event geometry (e.g. circle, ellipse, or rectangle) for computational efficiency. Similar method has been explored in [DRK11], which utilized a regression-based spatial estimation technique to determine discrete points on the boundary. Ham et al. present a distributed boundary detection based on in-network aggregation in which only sensor nodes that identify a boundary transmit their observation to the remote station [HR10]. To that end, they first applied a Delaunay triangulation to determine the neighbors of each node and then generate boundary segments between neighboring sensors. However, this algorithm cannot be known as a fully decentralized approach since the two steps mentioned above should be done centrally through a remote station.

There are also contour-based methods for deciding the type of an event [XLCL06, LL10]. In these works, the authors consider energy-efficient techniques to construct and incrementally update a number of two-dimentional contour maps in a sensor network. Another field of research involving detecting holes and topological features in a sensor network is presented in [Fun05, KFPF06]. In these approaches, local connectivity graphs are used to infer static features of an event but these approaches require the involvement of all the nodes in the network.

3.3   Scalablity Issues

Most of the techniques mentioned in Sections 3.1 and 3.2 exploit the opportunities for parallel transmission and of en-route aggregation of data. However, in densely instrumented systems where even a very small area may contain several hundreds of sensor nodes, the performance of the common data aggregation techniques is limited by the fact that nodes in the same broadcast domain cannot transmit in parallel. Thus, the time-complexity of those approaches also heavily depends on the number of sensor nodes. This results in long delays for collecting the information of all nodes and obtaining the required set of measurements.

In this context, dominance-based protocols have emerged as an enabler protocol for efficient aggregation techniques offering a much lower time complexity. The following subsections describe in detail techniques that exploit dominance-based MAC protocols to efficiently compute aggregate qualities with a time complexity that is independent of the number of nodes in a broadcast domain. Basic aggregate quantities such as `MIN` will be addressed, as well more complex ones such as approximate interpolation, which builds on the `MIN` "primitive".

3.4 Computing Aggregate Quantities by Exploiting Dominance

It is possible to devise algorithms for sensor data processing such that its time-complexity is independent of the number of nodes. In fact, if each node uses the value of its sensor reading instead of an arbitrary priority, the node winning the contention for the medium will be the one with the minimum (`MIN`) of the sensed values [APE$^+$08, ETPA11, PGAT09]. It is straight forward for the case where all measured values are non-negative. However, for the case where negative values are involved, sensor nodes should add an offset to their measurements before starting the arbitration, in order to be sure that all values are non-negative. In [APE$^+$08], it is demonstrated that CAN-enabled platforms can be used to compute various aggregate quantities. In [PGAT09] the authors show the same, but using slotted WiDOM.

In order to understand how a dominance-based MAC protocol can be used to efficiently compute an aggregate quantity, consider a simple example of how to compute the minimum of all sensor readings. One naïve approach as shown in Figure 2.2 (a) would be to use a time-division multiple-access (TDMA) scheme and assign one timeslot to each sensor node and let a sensor node transmit its sensor reading in its slot. After one TDMA cycle, a node knows all sensor readings and the `MIN` value can be computed but, unfortunately, the time-complexity is $O(m)$, where m is the number of sensor nodes. The same type of naïve scheme can be implemented with a prioritized MAC protocol. Figure 2.2 (c) shows this. Nodes contend with each other and each time the winner sends its measured value to the sink and similarly the `MIN` value is computed. Now consider a prioritized MAC protocol where a sensor node uses its sensed data as its priority. The MAC protocol will grant medium access to the sensor node with the minimum sensor reading —see Figure 2.2 (b). Since a dominance-based prioritized MAC protocol makes all sensor nodes know the priority of the sensor node which was granted the medium, it holds that all sensor nodes will know the minimum of the sensor reading. This makes it possible to compute `MIN`.

The importance of the above method is that its time-complexity is independent of

the number of nodes in the broadcast domain. Similarly, the maximum value (`MAX`) can be obtained by this method. The only difference is that for computing the `MAX` value nodes use the bitwise negation of their sensed values as their priorities and compete for channel. The computation time of this method has a time complexity of $O(npriobits)$, where *npriobits* is the number of bits used to represent the data (priority).

Other aggregate quantities (even if approximations) such as `COUNT`, `AVERAGE`, and `SUM` can be computed using same building block as explained in computing `MIN` and `MAX` [APT09]. It is also possible to track how a physical quantity varies over an area observed by a dense network with the time-complexity that does not depend on the number of sensor nodes.

In our work we are particularly interested in how to perform sensing in a densely deployed sensor network. Approximate interpolation is an approach we will exploit.

3.5 The Basic Interpolation Algorithm

Each node is assumed to be able to take sensor readings and to know its location. All nodes use the same function to interpolate the sensor data. Nodes start with the interpolation function being a flat surface. Then, at each round, one node, which is called control point, will be selected and broadcast its measured value together with its location. Upon receiving the message, other nodes re-compute the interpolation function and this procedure iterates for a predefined number of iterations (*k*). Since at each iteration one control point is selected, *k* also represents the number of control points used to obtain an interpolation.

In order to find the most effective subset of control points, the technique described previously for finding the `MIN` value is used. In the Basic Interpolation Algorithm (BIA) [APE$^+$08], the node with the highest interpolation error has the highest priority to send its value. For a node n_i, the interpolation error e_i is defined as the absolute difference of its sensor value, v_i, and its interpolated value, $f(x_i, y_i)$:

$$e_i = |v_i - f(x_i, y_i)| \tag{3.1}$$

where x_i and y_i are space coordinates and the function $f(x, y)$ approximates the sensor readings throughout the area of interest. The next step is to provide an interpolation function which is represented by a set of control points S. Each control point $p_i \in S$ has three attributes: x_i, y_i and v_i. The value of the approximate interpolation at the location (x_i, y_i) is given by v_i. In each iteration, the node with the highest interpolation error is found and is added to the set of control points, S. The interpolation function $f(x, y)$ —also called weighted-average interpolation (WAI) function [SS04, She, TOMO05]— is mathematically defined as follows:

$$f(x, y) = \begin{cases} 0 & \text{if } S = \emptyset \\ v_i & \exists P_i \in S : x_i = x \wedge y_i = y \\ \frac{\Sigma_{i \in s} v_i \cdot w_i(x,y)}{\Sigma_{i \in s} w_i(x,y)} & \text{otherwise} \end{cases} \tag{3.2}$$

where $w_i(x, y)$ is a weight that is inversely proportional to the distance between the ith control point and the point in the location (x, y), and is given by:

$$w_i(x, y) = \frac{1}{(x_i - x)^2 + (y_i - y)^2} \tag{3.3}$$

Algorithm 1 shows the pseudo code corresponding to BIA. It must be mentioned that this procedure is executed by all nodes so that all of them have the same approximation of the interpolation. This algorithm is valid for the case where we deal with a smooth physical signal that exhibits comparably (to the time the computation takes) slow variations over time. It is also assumed that there are no faulty sensors in the network.

Algorithm 1: Basic Interpolation Algorithm

    input : Number of iteration (k)
    output: Approximate interpolation of sensor readings

1   $S \leftarrow \emptyset$
2   **for** $i = 1 : k$ **do**
3   re-compute the interpolation value according to Equation 3.2
4   calculate e_i
5   select the sensor node n_i with maximum e_i
6   add the node n_i to the set of control points S
7   **end**

(a) Original Signal   (b) Interpolated Signal
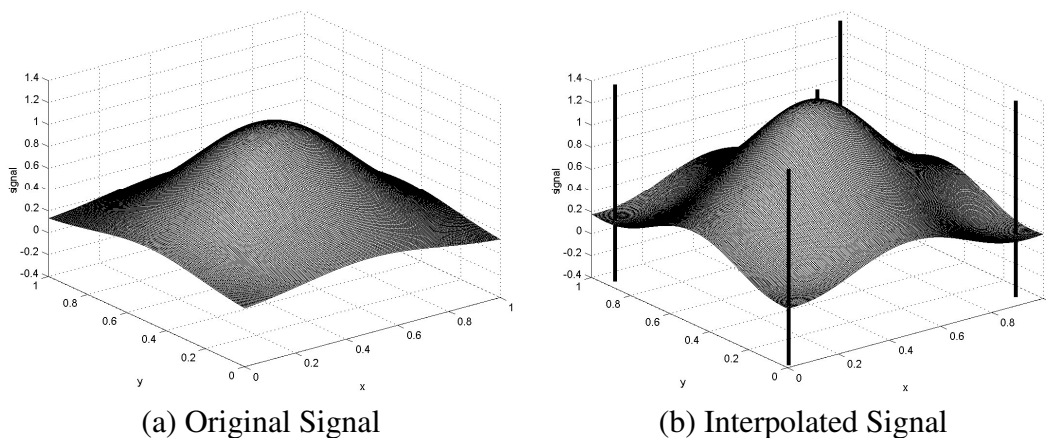
Figure 3.1: Interpolation example (taken from [APE$^+$08]).

Figure 3.1 illustrates the operation of the BIA scheme for a given example. Figure 3.1 (a) shows how a physical quantity varies as a function of space coordinates *x* and *y*. Figure 3.1 (b) shows an interpolation which is an approximate representation of this physical quantity; the lines indicate the location of control points in the set *S*.

In the following sub-sections we discuss variations of the algorithm that address the above mentioned shortcomings.

3.6   The Differential Interpolation Algorithm

BIA is good when the physical quantity changes very little during the execution of the interpolation algorithm. There are applications that track a low changing phenomenon such as temperature or humidity. However, this is not the case of some others such as active air flow control in aircraft [TPB$^+$12, LRT15]. Ignoring the dynamics of the physical quantities causes the interpolation represented by the set of control points *S* to significantly diverge from the real state of the physical quantity being monitored.

A possible solution to tackle this problem — the differential interpolation algorithm (DIA) proposal [ETPA11]— is to embed the physical change pattern into the interpolation algorithm. To do so, each time after adding a new control point to the set *S* (Line 6 in Algorithm 1), the previous selected control points in *S* should be updated based on a model that emulates the dynamics of the physical environment. The pseudo-code of the updated algorithm is shown in Algorithm 2. An application designer must define the

---

Algorithm 2: Differential Interpolation Algorithm

---

input : Number of iteration (k), and change pattern

output: Approximate interpolation of sensor readings

1   $S \leftarrow \emptyset$

2   **for** $i = 1 : k$ **do**

3   calculated the interpolation function $f(x,y)$ based on S

4   calculate e_i

5   select the sensor node n_i with maximum e_i

6   add the node n_i to the set of control points S

7   **for** each element $(x_i, y_i, v_i) \in S$ **do**

8   calculate the new value of (x_i, y_i, v_i) according to the given change pattern

9   replace the (x_i, y_i, v_i) value in S by $(xnew_i, ynew_i, vnew_i)$

10   **end**

11 **end**

---

change pattern parameters offline. It is obvious that the better the model of the dynamics of the physical world is, the smaller the error of computed interpolation will be.

The DIA approach helps to provide a more accurate representation of the physical signal, since the change pattern keeps updating the previous selected control points continuously. However, DIA is still unable to provide a system-dependent interpolation algorithm since the proper change pattern cannot be automatically detected by the system and needs to be assigned by the application designer.

In this Thesis (Chapter 5), we propose novel methodologies to overcome these limitations.

3.7   Basic Interpolation Algorithm with Fault Tolerance

BIA is obviously sensitive to faulty sensors; a single faulty sensor can have a significant impact on the computed interpolation and cause all sensor nodes to misperceive the physical environment. This risk increases as systems become larger and hence it could offset the performance of the algorithm.

Authors in [APT08] addressed this problem assuming that sensor readings might be faulty but it can be assumed that the correct sensor readings are always in majority within a set of neighbor nodes. Knowing that sensor readings exhibit spatial locality (nodes

---

Algorithm 3: Faulty Node Tolerant Algorithm

    input : Number of iteration (k), and `THRESHOLD` level
    output: Approximate interpolation of sensor readings

1 All nodes perform Algorithm 1
2 **for** $i = 1 : k$ **do**
3 | $SILENT_i \leftarrow$ FALSE
4 **end**
5 Let T to be a subset of nodes that contains all elements of the set S
6 T is the same on all nodes
7 **for** $\forall N_j \in T$ **do**
8 | **for** $\forall N_k \in T$ **do**
9 | | $sqrdv = (v_j - v_k)^2$
10 | | $sqrddist = (x_j - x_k)^2 + (y_j - y_k)^2$
11 | | **if** $SILENT_j ==$FALSE && $SILENT_k ==$FALSE && $sqrdv >$ `THRESHOLD`.$sqrddist$ **then**
12 | | | $SILENT_j ==$ TRUE
13 | | | $SILENT_k ==$ TRUE
14 | | **end**
15 | **end**
16 **end**
17 All nodes N_i with $SILENT_i ==$ FALSE perform Algorithm 1

---

that are close in space have similar sensor readings) [GBT$^+$04], the authors defined a parameter that bounds the gradient of the signal amongst non-faulty neighboring nodes.

In that approach, first an interpolation is obtained as in Algorithm 1. Then each pair of nodes in the set T are inspected and the square of the difference between the sensor readings (*sqrdv*) relative to the square of the distance between them (*sqrddist*) is computed — see Algorithm 3. If this value is greater than what is possible by the physical dynamics (this knowledge is specified by the designer, using the variable `THRESHOLD`) then both nodes are declared as *SILENT*; meaning that there must be at least one of the nodes in the pair that does not work correctly. After inspection (Lines 7 to 16), those nodes with *SILENT* attributes as FALSE run Algorithm 1 again.

Observe that the set of nodes that are selected in Line 1 of the algorithm is the same for all nodes, and all nodes agree on which nodes are silent. Also observe that during the inspection procedure, the algorithm may cause a small number of sensor nodes that are non-faulty to be *SILENT*. This is acceptable since we consider dense networks.
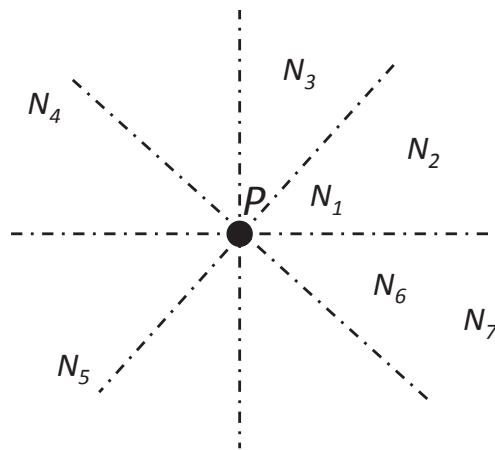
Figure 3.2: Interpolation at location P.

In Chapter 4, we propose novel mechanisms and response time analysis for an Ack-enabled slotted WiDOM, thus strongly contributing, improve the resilience (to communication faults) of our scalable algorithms.

3.8 Interpolation Algorithm for Non-smooth Signals

Recall the BIA where all nodes are aware of their locations. The WAI technique used in Algorithm 1 provides a fair representation of the sensor data if the physical signal is smoothly varying within the space. Consider the case where we are interested in finding the temperature in an area that is separated by a window. Imagine that these two areas have a very different temperature (a cool server room and an administrator office). Using the WAI technique (exactly as mentioned in Algorithm 1) results in an inaccurate interpolation that diverges severely from the real values of temperature.

A technique has been proposed in [TAP+08] to accommodate non-smooth signals. To compute the interpolation through Equation 3.2, instead of all control points in the set S, nodes must consider only a subset of them. Figure 3.2 shows an example of computing the interpolation at location $P(x,y)$. A node has to divide its surrounding region into eight identical sectors, and then during computation of Equation 3.2, it chooses the control points that are located closer to it.

Consider the region containing nodes N_1 and N_2 in Figure 3.2. To obtain an interpolation at P, the algorithm considers N_1's data only — irrespective of the difference in the

data values at N_1 and N_2. Intuitively, if the difference is significant, for example due to a wall in between the two nodes, then taking N_2's data into account will lead to interpolation inaccuracy. In other words, N_1's data "masks" N_2's. Following this argument, the nearest neighbor of P from each of the sectors constructs the subset $T \subset S$ that is used to compute interpolation. Therefore, in this example, $T = (N_1, N_3, N_4, N_5, N_6)$.

Although this method provides a viable solution for non-smooth signals, it increases the time-complexity of the algorithm and only offer a fair interpolation if it runs for a large number of iterations, which implies the use of a large number of control points.

3.9   Concluding Remarks

In this chapter, we surveyed previous relevant works on data aggregation and boundary detection. We showed that the related works are unable to efficiently satisfy the real-time requirements considering the nature of dense sensing systems. We stressed the importance of dominance-based MAC protocols to support aggregate quantity computations in such dense sensed environments.

We reviewed relevant work that has been exploiting dominance-based approach. We identified some limitations in those works, for which we propose solutions in Chapters 4, 5 and 6 of this Thesis

Chapter 4

Improving the Reliability of Slotted WiDOM

In this chapter, we focus on a new version of WiDOM (dubbed slotted WiDOM), which offers lower overhead as compared to the original version, and propose a new schedulability analysis for slotted WiDOM that considers message streams with release jitter. In order to provide a timing analysis with higher practical value, the effect of transmission faults must be taken into account. Therefore, in our novel analysis, we consider the case where messages are transmitted in more realistic wireless channels affected by noise and interference.

4.1 Introduction

In order to guarantee the timeliness of a message stream, there must exist a pre-run-time analysis to show whether it is feasible to accommodate this set of message streams such that no messages miss their deadlines. Indeed, the design of a real-time and reliable wireless MAC protocol that is able to efficiently handle event-driven (sporadic) messages needs the following requirements to be met:

R1 A prioritized MAC protocol should exist for a wireless channel. Among all computer nodes that request to transmit, this protocol grants the right to transmit on the channel to the computer node with the highest priority message;

R2 The overhead related to the arbitration of the prioritized MAC protocol should scale (grow slowly) with the number of priority levels;

R3 A schedulability analysis should exist for the prioritized MAC protocol;

R4 The schedulablity analysis should take into consideration the case where corrupted messages in a noisy channel impose the need for retransmission.

Finally, in order to obtain an efficient system, the following requirement should also be satisfied:

R5 The overhead related to the arbitration of the prioritized MAC protocol should be low.

Unfortunately, the current state of the art cannot fulfill all these requirements. The Controller Area Network (CAN) [Bos91], which is devised for a wired channel, offers many priority levels (hence fulfilling R2). For the wireless version of CAN, dubbed WiDOM [PAT07, AT06], there exists a corresponding schedulability analysis as well (hence fulfilling R1, R2 and R3), but the existing analysis is based on the assumption that no errors can happen during the message transmission (missing R4). Another problem with this protocol is that it imposes a large overhead (missing R5). On this account, the slotted WiDOM [13], already mentioned in Chapter 2, offers low overhead (hence fulfilling R1, R2 and R5) but no schedulability analysis is available for it. The development of a schedulability analysis for slotted WiDOM — with the capability of analyzing the responsiveness of message streams that suffer from release jitter and also experience noise on the channel — would, however, offer us the missing piece in fulfilling the five requirements listed above.

In this chapter, we also introduce a technique for error recovery in the slotted WiDOM such that the protocol is made more reliable under poor channel conditions. We develop a novel schedulability analysis for slotted WiDOM taking into account the erroneous transmissions of messages which may happen under noisy conditions. Previous work [PAT07] has already provided the schedulability analysis of WiDOM, but that analysis is only applicable to the basic implementation, not to the slotted version. It also considers that all messages are transmitted over an error-free channel.

In the following sections, we first explain the error recovery mechanism proposed for the slotted WiDOM and then we present a new schedulability analysis that takes into account the erroneous transmissions of message.

4.2 Ack-Enabled Slotted WiDOM

Besides physical aspects related to signal propagation, in a wireless channel a communication error may result from the interference due to various transmitters sharing the same frequency band, like Wi-Fi, Bluetooth and other sensor networks. It may also come from the presence, in the vicinity, of electromagnetic sources such as electric motors or microwave ovens.

To minimize the impact of external interferers on the reliability of the system, we implement an error recovery scheme based on acknowledgment (Ack) packet transmission after receiving any data packet. Through this scheme, if the sender does not receive back an Ack packet from the receiver during a predefined period of time, it will re-issue the data transmission. In other words, the sender retries to send the same packet in the next tournament and retransmit the data until it receives the Ack from the intended receiver. It should be mentioned that the retransmission of the corrupted packet may not happen immediately after the erroneous transmission, since a higher priority message may be enqueued while the sender is waiting for the Ack of the previous transmission.

Note that the error recovery method that we use for WiDOM is not exactly similar to the one that is used in the CAN bus. Unlike CAN, we do not need to globalize a detected error because in this version of WiDOM we are dealing with unicast transmissions, not multicast. To save more resources, we do not assign an individual timeslot for sending the Ack packet, since the Ack packet size is comparatively smaller than the data packet size and can be transmitted at the end of data transmission within the same timeslot. Figure 4.1 shows the "superframe" of the slotted WiDOM protocol. The ACK box in the figure is considered to accommodate the switching time (from send mode to the receive mode) and also the time duration a node needs to wait to receive the Ack message from the receiver. Accordingly, the periodicity of P_S should be chosen in a way that a message with the
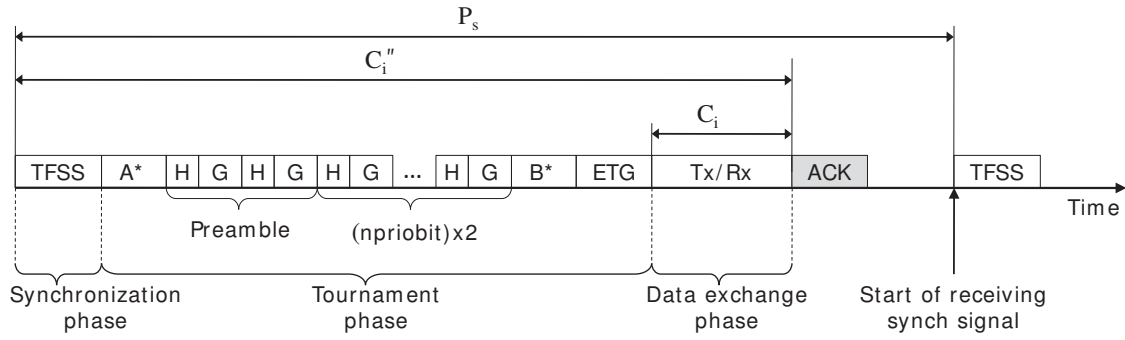
A*: (Prio_Tra); Transferring priority from WSN host platform to WiFLEX.
B*: (Win_Prio); Transferring winner priority from WiFLEX to WSN host platform.
ACK: Acknowledge packet transmission for error recovery scheme (optional).

Figure 4.1: Timing of slotted WiDOM with a master node including three phases of synchronization, tournament and data-exchange (time intervals are not drawn to scale).

longest transmission time (C_i) could be able to finish its transmission and receive its Ack packet before the start of the next synch signal.

This constraint is formulated as follows:

$$P_s \geq \text{TFSS} + \text{Prio\_Tra} + 2 \times (H + G) \times (\text{npriobits} + 1)$$
$$+ \text{ETG} + \text{Win\_Prio} + \max(C_i) + \text{SWX} + \text{ACK} \tag{4.1}$$

SWX is the time needed by the radio to switch from receive to transmit mode and vice versa. TFSS is the time needed to recognize the synch signal— see Table 2.1. Prio_Tra and Win_Prio are time spans needed for WiFLEX and host WSN platform communications. G is the guard time to let discrimination between two H-length priority bits. ETG is a gap at the end of the tournament to let nodes set their radio according to the result of the tournament, and ACK is the time for transmitting an acknowledgement packet.

A random noise burst can cause a transmission error on either a data or an Ack packet. If such a transmission error occurs, packet retransmission is required, leading to an increase in the message transmission time. We estimate the time overhead imposed by such transmission errors.

Let δ denote the duration of a noise burst. The number of slots affected by a δ-duration noise burst is at most $1 + \lceil \frac{\delta}{P_s} \rceil$. Then the new message transmission time is
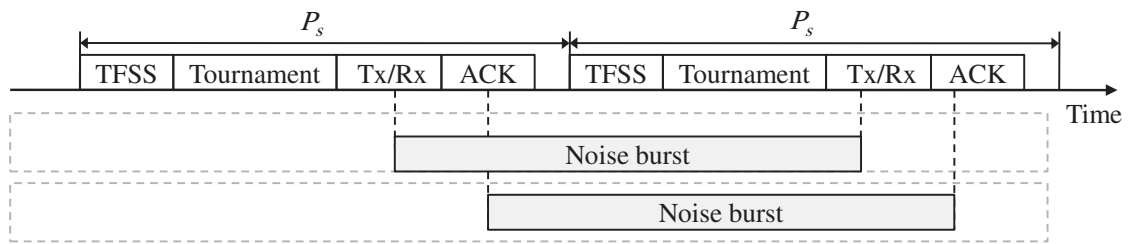
Figure 4.2: Error caused by a noise burst with length of one timeslot.

delayed by $(D(\delta))$, computed as follows:

$$D(\delta) = P_s \times \left(1 + \left\lceil \frac{\delta}{P_s} \right\rceil \right). \tag{4.2}$$

Figure 4.2 shows an example of a noise burst with duration of one timeslot ($\delta = P_s$) that can add a delay of up to $2P_s$ on the message transmission time.

Given $F(\Delta t)$, an error function modeling the interference in a wireless channel during an interval Δt, the maximum incremental delay due to the error recovery scheme is:

$$E(\Delta t) = D(\delta) \times F(\Delta t). \tag{4.3}$$

Similarly to the technique proposed by the authors in [BVN+11], we consider two different types of noise sources: (*i*) a periodic noise burst with the period of T_p and the burst duration of δ_p; and (*ii*) a sporadic noise burst with a minimum inter-arrival time of T_s and a burst duration of δ_s. The sporadic noise models the interference caused by packet-based radios (e.g., Wi-Fi, Bluetooth) while the periodic noise models the interference induced by other electromagnetic noise sources. So, being K the number of periodic noise sources and J the sporadic ones, the overall delay within the interval Δt due to the error recovery process is given by [BVN+11]:

$$E(\Delta t) = \sum_{n=1}^{K} \left(\left\lceil \frac{\Delta t}{(T_p)_n} \right\rceil \times D((\delta_p)_n) \right) + \sum_{n=1}^{J} \left(\left\lceil \frac{\Delta t}{(T_s)_n} \right\rceil \times D((\delta_s)_n) \right). \tag{4.4}$$

The choice of using the deterministic noise patterns allows deriving the response time analysis of message streams in a closed form. This is obviously in some cases a simplification, but it also reproduces some realistic noise conditions as described in [BVN+11].

In this Thesis, we validate our findings with a real experimental testbed. Certainly, some other realistic scenarios would require the consideration of non-deterministic noise models. Although not in the scope of this work, the consideration of those non-deterministic noise models would require adapting our response time analytical framework using stochastic approaches, such as those described in [MCG13].

4.3   Calculating Response Time for Ack-Enabled WiDOM

The schedulability analysis presented in this section borrows the ideas from previously published CAN analysis [DBBL07]. It provides feasibility tests based on Worst Case Response Time (WCRT) computation. However, our analysis is non-trivial and slightly different from [DBBL07] since it deals with:

- the slotted nature of the protocol;

- the error detection approach, by including acknowledgment (Ack)-based mechanism and packet retransmissions, rather than redundancy through the repetition of (six) consecutive identical symbols [DBBL07], i.e., assuming more realistic wireless channel models; and

- the release jitter that generally occurs when messages are being queued.

The WCRT of a message stream (m_i) is known to be the longest response time among all message instances q that enter the ready queue for a period of time called *level-i busy period*. A level-i busy period is a time interval $[t_0, t_1)$ such that both t_0 and t_1 are beginning of a non-faulty superframe (i.e., superframes where all the three phases perform normally without any error occurrence). For each superframe in $[t_0, t_1)$ it holds that either (i) all transmitted packets have higher priority than m_i, or (ii) at most one transmitted packet with lower priority than m_i is transmitted in the first superframe (started at t_0). Figure 4.3 shows an example of a level-i busy period.

The preliminary WiDOM analysis, presented in [PAT07], is simplistic in the following aspects:
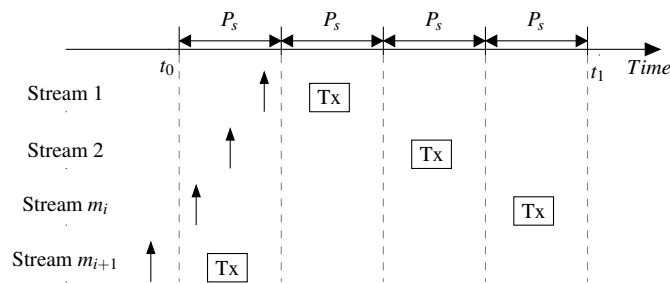
Figure 4.3: level-*i* busy period; lower index shows higher priority. The upward arrow indicates the release time of the message.

- It assumes that no transmission error can happen. It is not realistic to ignore the transmission errors, especially for error-prone wireless channels, when providing pre-run-time guarantees for mission-critical applications.

- It does not consider the release jitter that generally occurs while messages are being queued.

Consequently, following the analysis in [DBBL07], we observe that the WCRT of an instance *q* of a message stream m_i can be divided into four components as follows.

1. The queuing delay $w_{i,q}$, which corresponds to the longest time interval from the start of the busy period until when the instance *q* starts a successful transmission (see Figure 4.4). In general, $w_{i,q}$ comprises two elements: (i) blocking imposed by the messages of lower priority set $lp(i)$ and (ii) interference caused by set of higher priority messages $hp(i)$.

2. The transmission time C_i'', as the time span needed to finish a transmission, which includes the tournament duration and the time needed to detect the synch signal —see Figure 4.1.

3. The release jitter (or queuing jitter [PGAT09]) J_i, which is defined as the largest difference between the initiating time of an event and the time at which the message, triggered by the event, has been enqueued.

4. The error overheads E_i, including the time for receiving Ack packets, the retransmission time and the duration of a noise burst, which is provoked by an interference source.
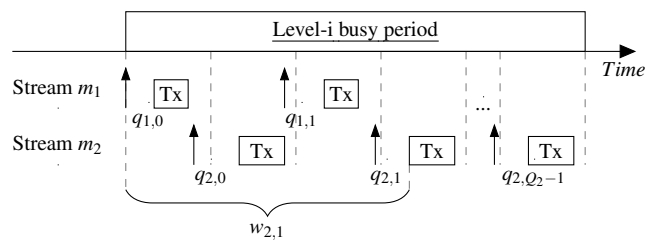
Figure 4.4: An example of queuing delay $\mathbf{w}_{i,q}$; lower index shows higher priority and upward arrows indicate the release time of the message.

To compute the response time of a message stream m_i in slotted WiDOM, we consider a busy period $[t_0, t_1)$. According to the definition, there should be a packet transmission in all non-faulty timeslots during the $[t_0, t_1)$ interval. We observe that, according to the release time of messages in high or low priority sets, eight distinct cases can occur, as summarized in Table 4.1. In order to reduce the level of pessimism in the computation we investigate each case individually and then derive the appropriate response time equations for each of them. Finally, the maximum of the response times over all these cases will correspond to the upper-bound on the WCRT for a set of message streams.

Table 4.2 summarizes all the symbols used in the following analysis.

Case 1.

There is no message released in the $[t_0 - P_s, t_0)$ interval, which is the last superframe immediately before the level-i busy period begins. This is the simplest case where there is neither blocking from the $lp(i)$ set nor further interference from the $hp(i)$ set. We can

Table 4.1: Different cases of WCRT computation. *lp(i)* / *hp(i)* corresponds to the set of message streams with priority lower / higher than message stream m_i.

Cases	Message in *lp(i)* arrived in $[t_0 - P_s, t_0)$?	Message m_i arrived in $[t_0 - P_s, t_0)$?	Message in *hp(i)* arrived in $[t_0 - P_s, t_0)$?
Case 1	✗	✗	✗
Case 2	✗	✗	✓
Case 3	✗	✓	✗
Case 4	✗	✓	✓
Case 5	✓	✗	✗
Case 6	✓	✗	✓
Case 7	✓	✓	✗
Case 8	✓	✓	✓

Table 4.2: List of symbols used in the computation of WCRT of a set of message streams.

Symbol	Description
R_i	WCRT for message stream i
L_i	The length of level-i busy period
Q_i	Number of instances in message stream i that become ready for transmission during L_i period
$W_{i,q}$	Time span from start of busy period until instance q start transmission
J_i	Release jitter of message stream i
C_i''	Time needed to finish the transmission of a message in message stream i
T_i	The periodicity of message stream i
P_s	The periodicity of synchronization signal
$P(L_e)$	The penalty of an L_e-length error occurring
$E_i(\Delta t)$	Extra time overhead imposed by the error recovery mechanism during a time interval Δt

compute the WCRT for the message stream m_i as follows:

$$R_i^{Case\ 1} = \max_{q=0,\dots,Q_i^{Case\ 1}-1} \left(w_{i,q}^{Case\ 1} + J_i + C''_i - q \times T_i \right) \tag{4.5}$$

where C_i'' is the time span needed to finish the transmission and can be obtained as follows:

$$C_i'' = \text{TFSS} + \text{Prio\_Tra} + 2(H+G)(\text{npriobits}+1)$$
$$+ \text{ETG} + \text{Win\_Prio} + C_i \tag{4.6}$$

In Equation (4.5), $w_{i,q}$ represents the longest time from the beginning of the busy period until when the instance q of the message stream m_i begins a successful transmission. T_i is the periodicity of message stream m_i. It is obvious that the erroneous transmission can lead to a longer delay. Therefore, the overhead of an error recovery mechanism must be considered and is formulated by the following recursive equation:

$$w_{i,q}^{Case\ 1} = \left(q + \sum_{j \in hp(i)} \left\lceil \frac{w_{i,q}^{Case\ 1} + J_j + Q_{bit}}{T_j} \right\rceil \right) \times P_s + E_i \left(w_{i,q}^{Case\ 1} + C''_i \right) \tag{4.7}$$

$E_i(\Delta t)$ is the maximum time required for the error signaling and recovery scheme in any time interval of length Δt —see Equation (4.4). Q_{bit} is the time granularity ($Q_{bit} =$

$4/250000 = 16\mu s$) [PAT07].

The number of message requests Q_i of the message stream m_i that become ready for transmission before the end of the busy period is given by:

$$Q_i = \left\lfloor \frac{L_i^{Case\ 1} + J_i}{T_i} \right\rfloor + 1 \tag{4.8}$$

where L_i is the length of the longest level-i busy period and can be computed recursively by:

$$L_i^{Case\ 1} = \sum_{j \in hp(i) \cup i} \left\lceil \frac{L_i^{Case\ 1} + J_j}{T_j} \right\rceil \times P_s + E_i\left(L_i^{Case\ 1}\right). \tag{4.9}$$

To investigate the remaining cases, we follow the same reasoning as above and adapt the analytical formulations as needed. Note that in each case we should replace the appropriate superscript in the response time equations.

Case 2.

There is an instance of the $hp(i)$ message stream released in the $[t_0 - P_s, t_0)$ interval. This case is rather similar to Case 1 except that we need to consider more interference imposed by the $hp(i)$ message stream. Therefore, R_i and Q_i can be calculated similarly as Case 1 (Equation (4.5) and Equation (4.8)), but we must consider the following changes in the computation of $w_{i,q}$ and L_i:

$$w_{i,q}^{Case\ 2} = (q + \sum_{j \in hp(i)} \lceil \frac{w_{i,q}^{Case\ 2} + P_s + J_j + Q_{bit}}{T_j} \rceil) \times P_s + E_i(w_{i,q}^{Case\ 2} + C_i'') \tag{4.10}$$

$$L_i^{Case\ 2} = \sum_{j \in hp(i) \cup i} \left\lceil \frac{L_i^{Case\ 2} + P_s + J_j}{T_j} \right\rceil \times P_s + E_i\left(L_i^{Case\ 2}\right). \tag{4.11}$$

Case 3.

In this case, neither $hp(i)$ nor $lp(i)$ messages occur in the $[t_0 - P_s, t_0)$ interval, but an instance q of the message stream m_i is released in $[t_0 - P_s, t_0)$ slightly after the synch

signal's broadcast. As described in Chapter 2, only nodes with non-empty ready queue wait to receive the synch signal. Thus, the instance q misses participating in the current tournament phase and should wait for the next superframe. As a consequence, this case is similar to Case 1, but the duration of an extra superframe must be added into Equation (4.5), resulting in:

$$R_i^{Case\ 3} = P_s + \max_{q=0,\dots,Q_i^{Case\ 3}-1} \left(w_{i,q}^{Case\ 3} + J_i + C''_i - q \times T_i \right). \tag{4.12}$$

Case 4.

There is no $lp(i)$ message released in the $[t_0 - P_s, t_0)$ interval, but both $hp(i)$ and an instance q of the message stream m_i are released during such interval. With the same reasoning stated in Case 2, Equation (4.7) and Equation (4.9) are rewritten as follows:

$$w_{i,q}^{Case\ 4} = \left(q + \sum_{j \in hp(i)} \left\lceil \frac{w_{i,q}^{Case\ 4} + P_s + J_j + Q_{bit}}{T_j} \right\rceil \right) \times P_s + E_i \left(w_{i,q}^{Case\ 4} + C''_i \right) \tag{4.13}$$

$$L_i^{Case\ 4} = \sum_{j \in hp(i) \cup i} \left\lceil \frac{L_i^{Case\ 4} + P_s + J_j}{T_j} \right\rceil \times P_s + E_i \left(L_i^{Case\ 4} \right). \tag{4.14}$$

Then R_i is expressed as follows:

$$R_i^{Case\ 4} = P_s + \max_{q=0,\dots,Q_i^{Case\ 4}-1} \left(w_{i,q}^{Case\ 4} + J_i + C''_i - q \times T_i \right). \tag{4.15}$$

Case 5.

There is an instance of $lp(i)$ released in the $[t_0 - P_s, t_0)$ interval but no other messages, neither m_i nor $hp(i)$ are released in the same period. Following the same reasoning as in Case 1, we should revise the computation of $w_{i,q}$ and L_i with a blocking term, obtaining:

$$w_{i,q}^{Case\ 5} = \left(q + \sum_{j \in hp(i)} \left\lceil \frac{w_{i,q}^{Case\ 5} + J_j + Q_{bit}}{T_j} \right\rceil + 1 \right) \times P_s + E_i \left(w_{i,q}^{Case\ 5} + C''_i \right) \quad (4.16)$$

$$L_i^{Case\ 5} = \left(1 + \sum_{j \in hp(i) \cup i} \left\lceil \frac{L_i^{Case\ 5} + J_j}{T_j} \right\rceil \right) \times P_s + E_i \left(L_i^{Case\ 5} \right). \quad (4.17)$$

Case 6.

In this case, both $hp(i)$ and $lp(i)$ messages are released within the $[t_0 - P_s, t_0)$ interval. Knowing that the low priority message is suppressed by the higher priority one, we can consider this case exactly the same as Case 2 where there is no $lp(i)$ message instance released.

Case 7.

There is no $hp(i)$ message in the $[t_0 - P_s, t_0)$ interval, but both $lp(i)$ message and an instance q from message stream m_i are released during this interval. It is clear that the $lp(i)$ message cannot impose any blocking to the response time computations; thus this case is equivalent to Case 3.

Case 8.

An instance of $hp(i)$, $lp(i)$ and the message stream m_i are released within the $[t_0 - P_s, t_0)$ interval. Following the same rationale as in the last two cases, $lp(i)$ message is suppressed by higher priority messages, which results in similar equations as in Case 4.

Finally, by looking at all the possible scenarios, and observing that the response time in Case 4 is greater than or equal to the response times of Case 1, Case 2 and Case 3, the WCRT of a message stream m_i is given by:

$$R_i = \max \left(R_i^{Case\ 4}, R_i^{Case\ 5} \right). \quad (4.18)$$

4.4   Implementation and Practical Aspects

We implemented the Ack-enabled WiDOM in the Nano-RK operating system [ERR05]. To the best of our knowledge, this is the first reported implementation of WiDOM (either slotted or unslotted) with an acknowledgement mechanism.

Nano-RK is a Real-Time Operating System (RTOS) designed for wireless sensor networks. It employs an energy-efficient time management scheme using one-shot timer interrupts, instead of polling interrupts. Due to that policy, the scheduler executes with the periodicity of such timer, i.e., approximately every 1 ms. Consequently, every time-related events, such as task periods and event wake-ups, will experience at most a 1 ms jitter with respect to their targeted time. Nevertheless, to enhance the accuracy of our estimations, jitter has been taken into account into our analytical computations.

Each sender node has three periodic tasks running on Nano-RK: Send-Task; Receive-Task and Management-Task. The pseudo-code for those tasks are presented as Algorithm 4, Algorithm 5 and Algorithm 6, respectively. At each request of Send-Task the variable *Gnt_N* is incremented by one. That variable is used to record the number of requests for packet transmission generated during an experiment. The arrival time of each

---

Algorithm 4: Send-Task

---

1 **while** <u>TRUE</u> **do**
2   *Gnt_T* ← keep the current time
3   *Gnt_N++*
4   *LockSend* ← TRUE
5   *SendPkt()*
6   *SSentFlag* ← 0
7   *LockSend* ← FALSE
8   Wait until next period
9 **end**

10 **Procedure** <u>SendPkt()</u>
11 **if** <u>successful access to hardware=1</u> **and** <u>my_ID=winner_ID</u> **then**
12   **if** <u>Transmission=original</u> **then**
13   Txed_N++
14   **end**
15   Transmit the packet over radio
16   *TTSRCV* ← TRUE
17 **end**

---

request is stored in the variable *Gnt_T*, in order to check the possibility of retransmissions in case of an unsuccessful data exchange.

Since the tournament phase is performed by a WiFLEX board, which is shared by two tasks (Send-Task and Management-Task), the access to that resource needs arbitration. This has been implemented by regulating the way tasks call a *SendPkt()* function, through a global flag (*LockSend*), which is set by the Send-Task only.

Through the *SendPkt()* function the nodes start contending for the channel. Based on the WiDOM protocol, each node uses its given *ID* number as its packet priority, and if two or more nodes access the channel at the same time, the collision will be resolved by the given priorities. As a result, if a node wins the tournament, it sends its packet and then "activates" the Receive-Task in order to wait for the reception of the corresponding acknowledgment packet. To do so, it sets a global flag (*TTSRCV*, time to start receiving) to TRUE — see Algorithm 4, line 16.

When the Receive-Task executes, one of the following conditions might hold: (i) the global flag *TTSRCV* has not been set, so the task suddenly exits, or (ii) the flag has been set by the Send-Task. In the latter case, the node switches to receive mode and waits to receive an Ack packet. If the received Ack packet is the expected one, i.e., it contains the correct information including the source ID and the sequence number of the recent data transmission, then the global flag "*SSentFlag*" (i.e., successful sent) will be set to TRUE.

Algorithm 5: Receive-Task

```
 1  while TRUE do
 2      if TTSRCV = FALSE then
 3          Wait until next period
 4      else
 5          Wait to receive the Ack packet
 6          if received Ack is correct then
 7              SSentFlag ← 1
 8          end
 9          TTSRCV ← FALSE
10          TTSMNG ← TRUE
11          Wait until next period
12      end
13  end
```

Algorithm 6: Management-Task

1	**while** TRUE **do**
2	**if** *TTSMNG* = FALSE **then**
3	Wait until next period
4	**else**
5	Now ← current time
6	*Elapsed_T* ← Now − *Gnt_T*
7	**if** *Elapsed_T* >(Send_Task_period −P_s) **and** *SSentFlag* = 0 **and** *LockSend* = FALSE **then**
8	*SendPkt()*
9	**end**
10	*TTSMNG* ← FALSE
11	Wait until next period
12	**end**
13	**end**

Either the Ack has been received or not, the Receive-Task ends up by "activating" the Management-Task to execute — see Algorithm 5, line 10.

Similarly, the Management-Task encounters one of these two situations when it requests to be executed: (i) the first situation occurs when the "*TTSMNG*" flag (time to start managing) is FALSE; in this case the task is released to the scheduler and waits for the next activation — see Algorithm 6, and (ii) the second situation occurs when the *TTSMNG* is TRUE, which usually happens after an unsuccessful transmission of data packet (i.e. not receiving an Ack packet). Then, if the *TTSMNG* is TRUE, a retransmission is needed. The first step for retransmission is to get the current time and check if there is enough time to perform a retransmission. To do so, it is needed to compute the elapsed time by subtracting the current time to the *Gnt_T* time, recorded at the beginning of the Send-Task. If there is enough time for a slot with duration P_s before the next activation of Send-Task (which is defined by the Send-Task period), then it is possible to retransmit the packet. However, the retransmission should be performed if the *SSentFlag* is still FALSE. In this case, the task calls the *SendPkt()* function, ensuring that the shared resource is currently available. Taking advantage of locks and flags, we are able to target an efficient way to control the execution of each task at the appropriate time instant. Table 4.3 shows the values Nano-RK allows to set for each task's configuration. A small number in *Task_prio* implies higher priority and the period of the Send-Task defines the

data rate of the nodes in each experiment.

Table 4.3: Tasks' configuration.

Parameter	Value
Send_Task_prio	2
Send_Task_period	MSG-Period
Send_Task.SchType	NON-PREEMPTIVE
Receive_Task_prio	3
Receive_Task_period	15 ms
Receive_Task.SchType	PREEMPTIVE
Managemant_Task_prio	4
Managemant_Task_period	15 ms
Managemant _Task.SchType	PREEMPTIVE

When a packet has no chance to be transmitted within its deadline, it is said that a deadline miss event occurred. In order to estimate how often this happens, at the end of each experiment, the difference between the number of generated packets (*Gnt_N*) and the number of actually transmitted packets (*Txed_N*) is computed. Similarly, to measure the response time, each node measures the delay between the instant of the Send-Task execution until the actual packet transmission. Then, this delay (W_i) piggybacks within the packet payload. Since we have used a hardware-timer with a time resolution of 1 μs, all the measured values have the accuracy of 1 μs. Upon receiving a packet, the receiver extracts the W_i and computes the response time (R_i) according to the following expression:

$$R_i = W_i + C_i \qquad (4.19)$$

where C_i is the duration of the data exchange phase (refer to Figure 4.1).

With the help of sniffer devices [KCG$^+$11] and a custom-designed log file's parser, built in C and bash programming, we were able to measure the packet loss ratio and the WCRT-miss ratio. Furthermore, to enrich the comparison of the performance between the original WiDOM and the novel Ack-based protocol, the energy consumed by the nodes at different data rates is also shown. Finally, to better appreciate the trade-offs between the performance indices, the behavior of the packet loss ratio against the energy consumption is presented.
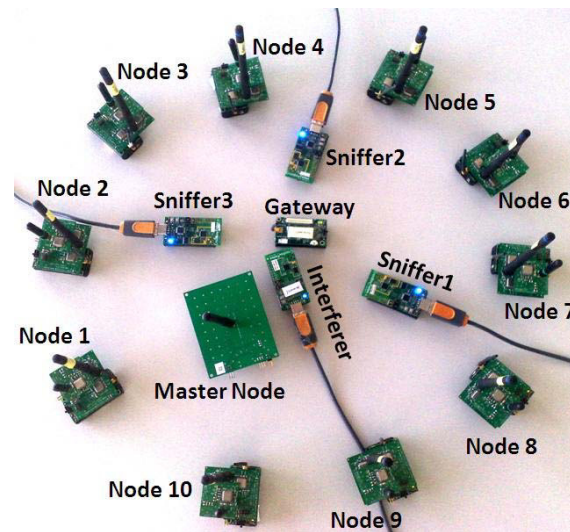
Figure 4.5: Experimental setup including 10 MicaZ sensor nodes that generates periodic traffic, one master node to signal the start of tournament, one gateway to collect sensor measurements and an interferer to generate noise and 3 sniffers to log data.

4.4.1 Experimental Setup

We have conducted several experiments by varying the interference level in the environment. Our testbed consisted of 10 MicaZ motes [CRO04] (featuring an Atmel ATmega128L 8-bit microcontroller with 128 kB in-system programmable memory and 4 kB available RAM memory) equipped with the WiFLEX add-on board [PGAT09]. An extra MicaZ mote acts as a gateway: this node is always waiting to receive data from the other nodes and never participates in the tournament phase to send back the Ack packets, so it does not need to be equipped with any extra hardware. Figure 4.5 illustrates the experimental set-up and the roles of the used hardware.

Each one of the 10 MicaZ equipped with the WiFLEX board is configured to run at a different data rate (i.e., *MSG-Period* as in Table 4.3) or a different priority. For instance, Node1's *MSG-Period* is $T_1 = 70$ ms, Node 2's *MSG-Period* is $T_2 = 180$ ms and so on, while for the last three nodes it holds that $T_8 = T_9 = T_{10} = 5.4$ s (refer to Tables 4.5 and 4.8). Note that, for the last three nodes, only the priority (given by the node's ID) is different.

The data packet length is set to 128 bytes (including PHY, MAC headers, CRC and payload). This is the maximum packet length supported by the CC2420 radio [T. 07] on the MicaZ platform. The length of Ack packets is 17 bytes. Given these values and

Table 4.4: Timeout values experimentally measured on MicaZ platform.

Parameter	Value
$H+G$	110 μs
$TFSS$	300 μs
$Prio\_Tra$	238 μs
Win_Prio	449 μs
ETG	555 μs
SWX	35 μs

considering the maximum data rate over the wireless medium (250 Kb/s in the ISM band of 2.4 GHz [T. 07]), the time needed to transmit a data packet is:

$$\forall i \in \{1,\ldots,n\} : C_i = 128 \times 8 \times \frac{1}{250000} = 4096 \ \mu s \qquad (4.20)$$

In the same way, the time needed to transmit an Ack packet is 554 μs. Applying Equation (4.6), we have:

$$\forall i \in \{1,\ldots,n\} : C_i'' = 9158 \ \mu s \qquad (4.21)$$

This value is computed with the timeouts as given in Table 4.4, experimentally measured from the real platform. Considering *npriobits*=15 and all the mentioned timeout values and the constraint in Equation (4.1), the periodicity of the *synch* signal P_s should be larger than 9747 μs. We choose P_s=15 *ms*, i.e., the master node sends a 300 μs-long synch signal every 15 *ms*. We relaxed this choice to allocate to the gateway some time to accomplish the data extraction from the received packet and to format the customized Ack packet. Consequently, the nodes were configured with different transmission rates, ranging from 190 bps to 14 kbps. Interestingly, these choices give analytical system utilization values ranging from 39% up to 61%.

4.4.2 Interference Pattern

We create two types of interference to test the WiDOM protocol: (i) periodic interference and (ii) sporadic interference. The periodic interference is usually spatially localized and follows a regular duty cycle pattern. The best example of this category is the interference produced by microwave ovens. To create this noise pattern, we utilize the Jamlab
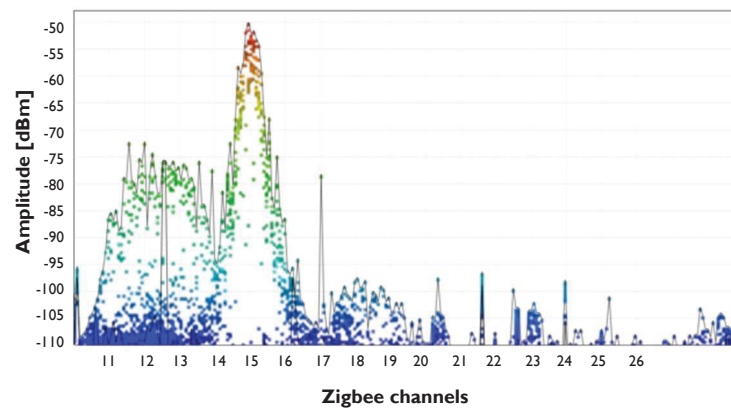
(a) Periodic interferer with duty cycle of 70 ms
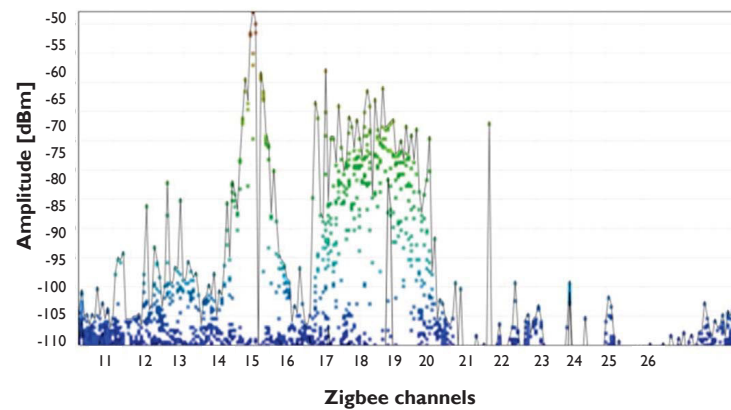
(b) Periodic interferer with duty cycle of 200 ms.
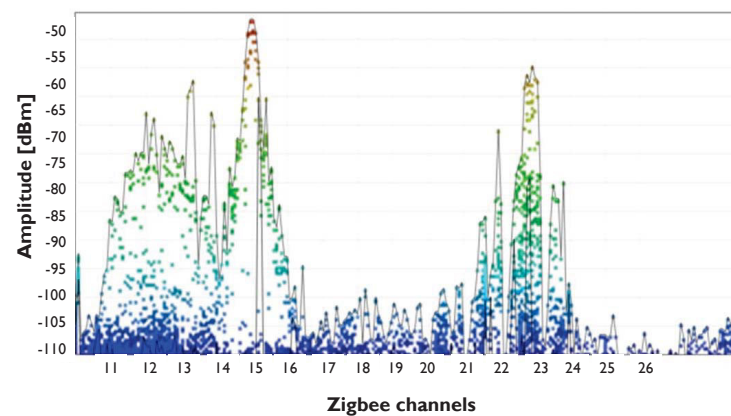
(c) Sporadic interferer with minimum inter-arrival time of 70 ms.

Figure 4.6: Spectrum occupancy in presence of interference. The spectrum analyzer also shows the effect of nearby IEEE 802.11 wireless routers.
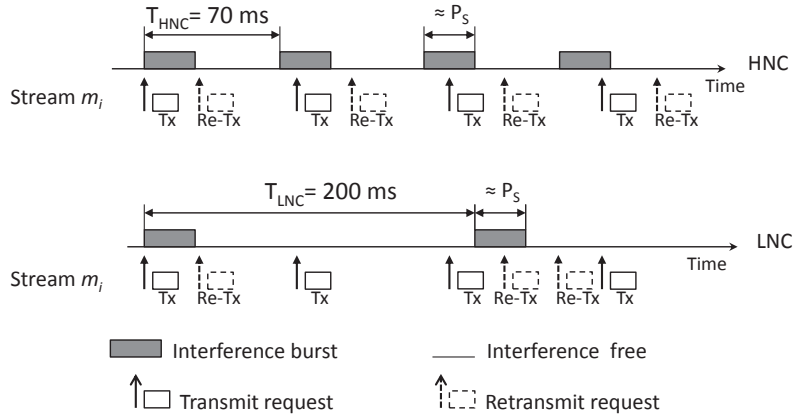
Figure 4.7: Example of data transmission under HNC and LNC interference.

tool [BVN$^+$11] running on an extra MicaZ node ("interferer" node in Figure 4.5). We set the interferer's duty cycle to 70 ms and 200 ms to compare the performance of the WiDOM protocol under different noise densities. We refer to the environment with higher noise burst rate as the High Noisy Channel (HNC) scenario —see Figure 4.6 (a), and the one with with lower noise burst rate as the Low Noisy Channel (LNC) scenario —see Figure 4.6 (b). Both periodic interferers send three packets with length of 128 bytes in burst to occupy the channel for the duration of one slot, P_s=15 ms —considering data rate of 250 Kb/s.

Figure 4.7 aims at clarifying, with an example, how the HNC and LNC channel conditions impact on the message stream transmissions. The message streams have the same data rate in both scenarios, i.e., the transmit requests generation time is the same. Clearly, the HNC scenario leads to more collisions than the LNC one, thus more frequent retransmissions.

The sporadic noise model emulates in a fully controlled way the interference generated by heavily loaded Wi-Fi access points. To generate this type of interference traffic, we used a simple model, inspired by the Markov model presented in [BVT$^+$10], consisting of two states: "clear channel" and "interference". Differently from the Jamlab tool [BVT$^+$10], in our model, instead of considering fully random and irregular interference pattern, we generate a fixed duration of "interference" to keep the burst length equal to one P_s period. In this state, the interferer broadcasts unmodulated signals. The duration of the "clear channel" state is defined through a constant slot 5 ms duration multiplied by

a random variable $\mathscr{R}$, uniformly distributed over the interval $[14, 200]$ ms. Hence, the time duration of staying on the clear channel state will be a random time period from 70 ms up to 1 s. In other words, the minimum inter-arrival time between two consecutive noise bursts is set to 70 ms. We refer to this scenario as the Sporadic Noisy Channel (SPNC) scenario —see Figure 4.6 (c).

All interferers generate noise in the Channel 15 of the IEEE 802.15.4 spectrum. In all scenarios, interferers are generating packets and transmitting them with the highest power level (0 dBm). As it is shown by the spectrum analyzer (Figure 4.6), the radiation power in all situations is the same, but the density of noise bursts is quite high in the Figure 4.6 (a) as compared to that in Figure 4.6 (b). It can be also observed that in the presence of a sporadic noise source, the channel spends more time in clear channel state as compared to the periodic noise source with duty cycle of 70 ms. Note that the spectrum analyzer visualizes the status of the entire ZigBee bandwidth, including the noise coming from WiFi/IEEE 802.11 wireless routers on the adjacent channels.

4.4.3 Evaluation

We utilize different interference patterns to evaluate the reliability and the robustness of the WiDOM protocol against noise, while having a predictable response time for message streams. Our evaluation focuses on five network performance indices as indicated next.

Packet loss ratio: the ratio of the data (measurements) missed in the gateway over total number of the generated data by sender nodes.

Deadline miss ratio: the ratio of messages that missed their deadlines over the total number of generated messages. In all scenarios, the deadline is considered to be implicit which is equal to the message periodicity.

WCRT miss ratio: the ratio of messages that have been sent after their calculated WCRT over the total number of generated messages.

Average response time: the average of all received messages response time in the gateway from any sender.

Energy consumption: the average energy consumption of each node, expressed as a function of the number of packets sent and received.

We run the experiment for both the original and the Ack-enabled versions of WiDOM in different noisy environments. All experiments were run for about 40 minutes, which corresponds to more than 40000 message transmission requests.

4.4.3.1 Packet Loss Ratio

Figure 4.8 depicts the packet loss ratio for both versions of the WiDOM protocol, under different noise conditions. According to the results, two observations can be made. First, the packet loss ratio for the Ack-enabled WiDOM is much smaller than that of the original version of the WiDOM protocol in all scenarios. This is due to the implementation of Ack packets, which provide a legitimate feedback on transmission status for the sender nodes, giving them a chance for retransmitting the lost packets.

Second, the high noisy channel (HNC) jeopardizes the network performance much more than the low noisy channel or the SPNC case. As it is illustrated in Figure 4.8, SPNC is less destructive, since the packet loss ratio under SPNC is lower than the one under HNC for both WiDOM versions. Two reasons contribute to this: (i) in heavy noisy channels there is a higher risk of collision for both data and Ack packets; and (ii) a higher collision rate inherently leads to more retransmission requests in the case of Ack-enabled WiDOM, which increases the traffic load.

Moreover, in each scenario the packet loss ratio is almost flat against the data rate. One could think that for higher transmission rates there ought to be higher amounts of packet loss. Indeed, this happens in absolute terms, but in terms of packet loss ratio (i.e., percentage), the effect is minimal.
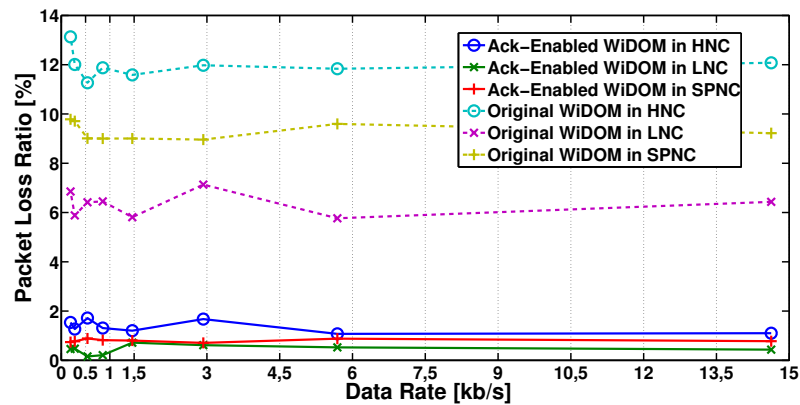
Figure 4.8: Packet loss ratio of Ack-enabled WiDOM and original WiDOM.

4.4.3.2 Timing Behavior

Tables 4.5- 4.7 show the response times achieved by the experimental setup of Ack-enabled WiDOM under HNC, LNC and SPNC interference environments, respectively. In particular, three distinct metrics are investigated in the time domain. The first metric is the deadline miss ratio, which corresponds to the number of generated packets that did not have the chance to be transmitted. It has been observed that for all scenarios there is no deadline miss for any message stream – the two variables *Gnt_N* and *Txed_N* were always equal.

The WCRT miss ratio is the second time metric considered. It indicates the number of messages that have been sent with a response time higher than their analytically computed WCRT. It has been computed by applying the response time analysis to calculate the upper-bound of response time for each message stream according to the analytical formulation detailed in the Section 4.3. We have used the timeouts as given in Table 4.4 and the upper-bound for the jitter has been estimated as 1 *ms*. We remind that Nano-RK uses a policy of scheduling the tasks and interrupts with a one-shot timer whose accuracy is 1 *ms*. So, all tasks might experience a jitter of around 1 *ms* for any execution.

Figure 4.9, illustrates the results given in Tables 4.5- 4.7, The analytically computed response time is shown by $Calc.R_i$ and the maximum and average values of response time observed in the tests for each message stream are given by $Exp.Max.R_i$ and $Exp.Avg.R_i$, respectively. These notation is used in tables and figures as well.

Table 4.5: Response time in HNC.

i	1		2		3		4		5	
Protocol	Ack-enabled WiDOM	Original WiDOM	Ack-enabled WiDOM	Original WiDOM	Ack-enabled WiDOM	Original WiDOM	Ack-enabled WiDOM	Original WiDOM	Ack-enabled WiDOM	Original WiDOM
$T_i(\mu s)$	70000		180000		350000		700000		1200000	
$Datarate(bps)$	14629		5689		2926		1463		853	
$Calc.R_i(\mu s)$	55158	25158	70158	40158	130158	55158	145158	70158	265158	100158
$Exp.Avg.R_i(\mu s)$	21389	14370	19729	16648	27887	18675	27835	20269	38450	24067
$Exp.Max.R_i(\mu s)$	53289	23163	56228	33835	91558	46490	109865	59157	169607	82223
i	6		7		8		9		10	
$T_i(\mu s)$	1900000		3700000		5400000		5400000		5400000	
$Datarate(bps)$	539		277		190		190		190	
$Calc.R_i(\mu s)$	280158	115158	340158	130158	355158	145158	490158	175158	565158	205158
$Exp.Avg.R_i(\mu s)$	35849	30499	39827	29554	54920	40113	52907	41039	58839	41063
$Exp.Max.R_i(\mu s)$	202986	94846	236513	108986	262178	76108	290555	77645	308128	149384

Table 4.6: Response time in LNC.

i	1		2		3		4		5	
Protocol	Ack-enabled WiDOM	Original WiDOM	Ack-enabled WiDOM	Original WiDOM	Ack-enabled WiDOM	Original WiDOM	Ack-enabled WiDOM	Original WiDOM	Ack-enabled WiDOM	Original WiDOM
$T_i(\mu s)$	70000		180000		350000		700000		1200000	
$Datarate(bps)$	14629		5689		2926		1463		853	
$Calc.R_i(\mu s)$	55158	25158	70158	40158	100158	55158	115158	70158	130158	100158
$Exp.Avg.R_i(\mu s)$	17769	13932	20020	16061	19342	18994	26118	20187	33916	22956
$Exp.Max.R_i(\mu s)$	53122	23159	59232	33809	80596	44296	94604	55271	108183	73483
i	6		7		8		9		10	
$T_i(\mu s)$	1900000		3700000		5400000		5400000		5400000	
$Datarate(bps)$	539		277		190		190		190	
$Calc.R_i(\mu s)$	145158	115158	175158	130158	205158	145158	265158	175158	280158	205158
$Exp.Avg.R_i(\mu s)$	35303	29103	38711	29801	37509	37001	40080	40127	45397	40741
$Exp.Max.R_i(\mu s)$	118599	94601	142268	104367	163848	96682	168064	105221	184175	82168

Table 4.7: Response time in SPNC.

i	1		2		3		4		5	
Protocol	Ack-enabled WiDOM	Original WiDOM	Ack-enabled WiDOM	Original WiDOM	Ack-enabled WiDOM	Original WiDOM	Ack-enabled WiDOM	Original WiDOM	Ack-enabled WiDOM	Original WiDOM
$T_i(\mu s)$	70000		180000		350000		700000		1200000	
$Datarate(bps)$	14629		5689		2926		1463		853	
$Calc.R_i(\mu s)$	55158	25158	70158	40158	130158	55158	145158	70158	265158	100158
$Exp.Avg.R_i(\mu s)$	19218	14122	19627	16201	19703	16962	26012	19961	35627	23108
$Exp.Max.R_i(\mu s)$	52942	23240	60124	35556	98219	44215	91240	56294	122419	73947
i	6		7		8		9		10	
$T_i(\mu s)$	1900000		3700000		5400000		5400000		5400000	
$Datarate(bps)$	539		277		190		190		190	
$Calc.R_i(\mu s)$	280158	115158	340158	130158	355158	145158	490158	175158	565158	205158
$Exp.Avg.R_i(\mu s)$	35604	29014	38868	29462	42191	39218	46713	40793	47508	41921
$Exp.Max.R_i(\mu s)$	132047	93261	153510	102286	185420	82490	181506	83912	181241	85122

Table 4.8: Response time for original WiDOM in non-lossy environment.

i	1		2		3		4		5	
$P_s(\mu s)$	10000	15000	10000	15000	10000	15000	10000	15000	10000	15000
$T_i(\mu s)$	30000	70000	70000	180000	120000	350000	300000	700000	900000	1200000
$Datarate(bps)$	34133	14629	14629	5689	8533	2926	3413	1463	1138	853
$Calc.R_i(\mu s)$	20158	25158	30158	40158	50158	55158	60158	70158	90158	100158
$Exp.Avg.R_i(\mu s)$	10936	14035	13417	16025	14512	18731	16204	19970	18301	23281
$Exp.Max.R_i(\mu s)$	17316	22901	27305	33914	36827	44260	50113	54218	54961	79540
i	6		7		8		9		10	
$T_i(\mu s)$	1900000		3700000		5400000		5400000		5400000	
$Datarate(bps)$	539	539	277	277	190	190	190	190	190	190
$Calc.R_i(\mu s)$	110158	115158	120158	130158	170158	145158	180158	175158	200158	205158
$Exp.Avg.R_i(\mu s)$	21743	26916	25047	29427	32184	36849	33927	39085	36265	40110
$Exp.Max.R_i(\mu s)$	61227	89301	75203	102546	69416	98113	76439	86343	80116	109754

(a) Ack-enabled WiDOM in HNC environment.

(b) Original WiDOM in HNC environment.

(c) Ack-enabled WiDOM in LNC environment.

(d) Original WiDOM in LNC environment.

(e) Ack-enabled WiDOM in SPNC environment.

(f) Original WiDOM in SPNC environment.
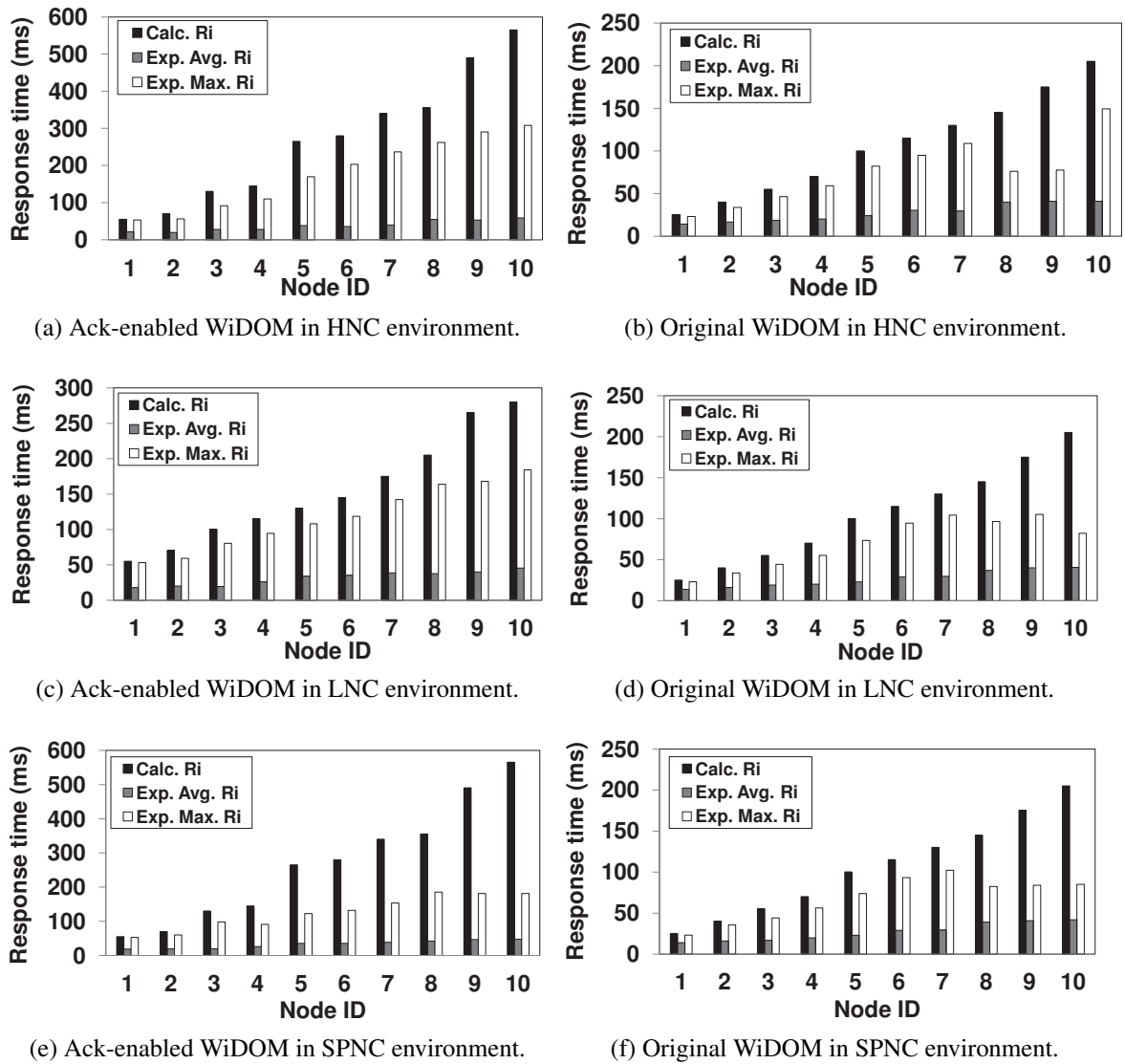
Figure 4.9: Response time comparison of Ack-enabled WiDOM and original WiDOM under different noise conditions.

Figure 4.9, clearly shows that no message experiences a response time higher than the calculated WCRT in all the considered scenarios, which substantiates the fact that the analytical model for the WCRT provides a fairly good upper-bound to the expected response time.

The average value of response time, $Exp.Avg.R_i$, is the third and last metric considered in the timing category. It clearly shows how the Ack-enabled mechanism slightly increases the response time for all the message streams.

As expected, this is what the system pays to achieve the good results in terms of packet
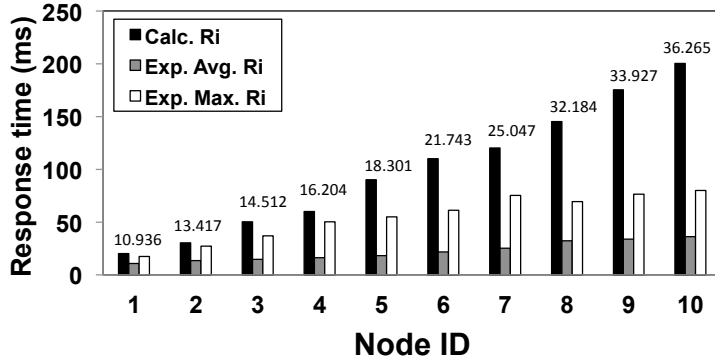
(a) Original WiDOM with $P_s = 10\ ms$.
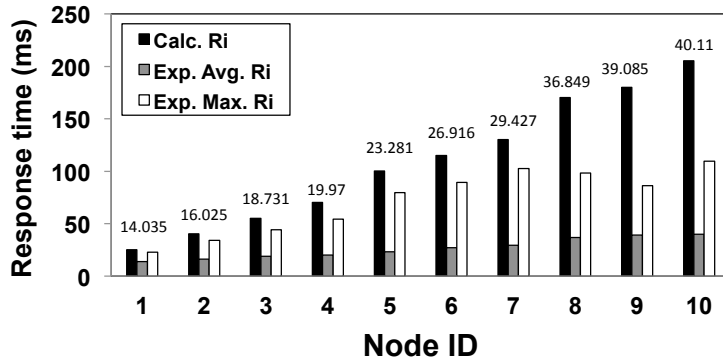
(b) Original WiDOM with $P_s = 15\ ms$.

Figure 4.10: Response time comparison of original WiDOM with different P_s in a non-lossy environment. The numbers indicate the value of the average response time.

loss ratio (as shown in Figure 4.8). Moreover, while the original WiDOM is almost indifferent to the various noise patterns, from the experimental results shown in the tables it can be observed that heavier noise leads to larger response times for the Ack-enabled slotted WiDOM. These results are not surprising since, as the noise density increases more packet collisions occur and consequently a higher number of retransmissions. Accordingly, for the original WiDOM, the average response time of message streams does not vary significantly with the channel conditions. The reason is that there is no mechanism devised in original WiDOM that takes into account the noise of the channel. Nodes send their packet only once according to their arrival schedules and there is no feedback to let them know about their transmission status.

The last observation led us to run another experiment for the original WiDOM in a non-lossy environment, in order to push the system to its limits. Since we are using the

original WiDOM there is no need to consider extra time for the gateway to process the received data packet and to issue an Ack packet, the synchronization period can be safely decreased from $P_s = 15$ ms to $P_s = 10$ ms; that is, a value closer to the theoretical limit as computed in Section 4.3. Accordingly, the data rate of the first five message streams can be increased.

Figure 4.10 shows the timing behavior of protocol in such a non-lossy environment, with a noise floor of -96 dBm. Once again, no packet loss has been observed nor deadline miss and no WCRT misses were reported. Observing the values in Table 4.8, it is also evident that by reducing the synchronization period, we could slightly achieve a better timing behavior, while accommodating nodes with higher data rates. This leads to the conclusion that in a non-lossy environment (interference probability reduced to 0) or for non-loss sensitive applications, it is preferable to opt for the original WiDOM approach, since it can provide better timing behavior.

Figures 4.11 to 4.14 summarize the previous findings by showing the average response time as a function of data rate in all considered interference scenarios. As confirmed by the above analysis of experimental results, the average response time in the Ack-enabled WiDOM is larger than that of the original WiDOM protocol in all scenarios. It appears clear that a heavier noisy channel deteriorates more the average response time as compared to a lighter noisy channel for the Ack-enabled WiDOM protocol, while the average response time for the original WiDOM protocol does not change significantly under different noise conditions. Finally, when the environment is non-lossy, it is possible to get smaller average response time values by implementing the original WiDOM protocol. The reason is that utilizing the original WiDOM it would be possible to reduce the synchronization period, P_s, which leads to faster packet transmission.

4.4.3.3   Energy Cost

As we have discussed earlier, implementing the Ack mechanism increases the reliability of the WiDOM protocol and makes it more robust in noisy environments, albeit at the cost of less responsiveness. Nevertheless, we should also consider the cost of extra energy consumption due to the exchange of extra packets. In particular, there are two major
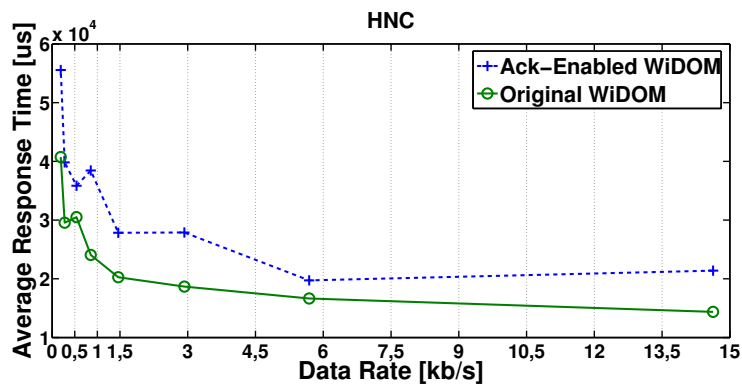
Figure 4.11: Average response time for Ack-enabled and original WiDOM in HNC.
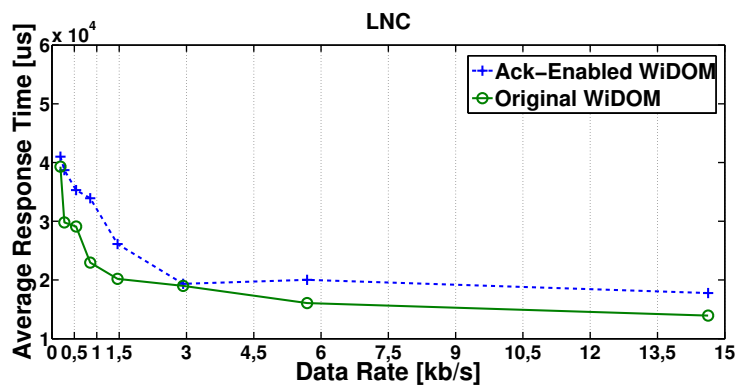
Figure 4.12: Average response time for Ack-enabled and original WiDOM in LNC.
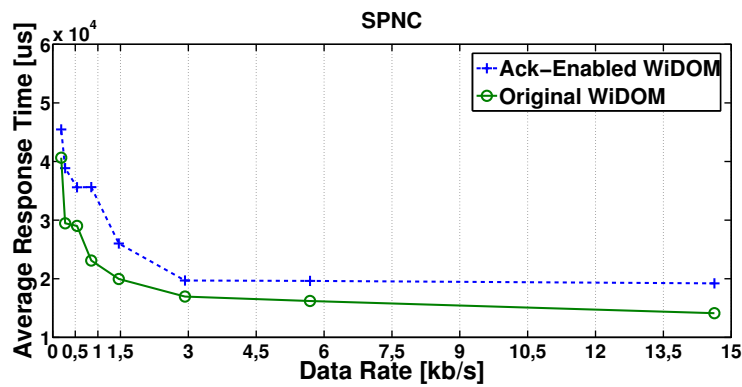
Figure 4.13: Average response time for Ack-enabled and original WiDOM in SPNC.
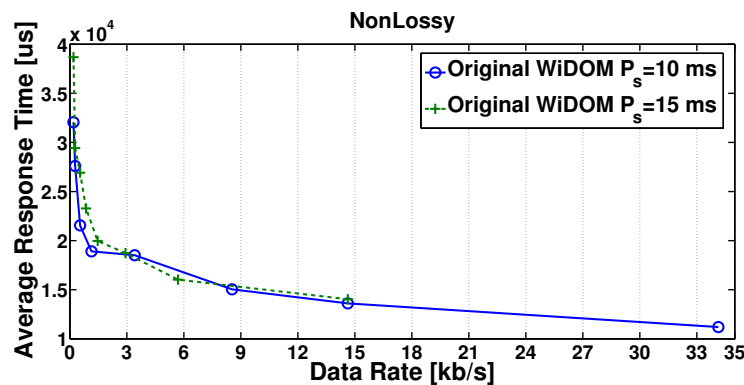
Figure 4.14: Average response time for original WiDOM in non-lossy environment with $P_s = 15$ ms and $P_s = 10$ ms and different data rates.

sources of energy consumption in the Ack-enabled WiDOM as compared to the original WiDOM: (i) the amount of energy for receiving the Ack packet and (ii) the extra cost for retransmitting after an unsuccessful transmission.

Cosidering the current draw of 19.7 mA in the receive mode and 14 mA in the transmit mode (transmission power level 19) of a MicaZ mote [CRO04], the normalized energy consumption for the Ack-enabled WiDOM is estimated as follows:

$$E(\text{Ack-enabled WiDOM}) =$$
$$3 \times \Big((\text{No\_TxPkt} + \text{No\_ReTxPkt}) \times 128$$
$$+ (\text{No\_AckPkt}) \times 17 \times \frac{19.7}{14} \Big) \quad (4.22)$$

where the factor 3 takes into account the voltage supply of the node, which is powered by two regular AA batteries. No_ReTxPkt represents the number of retransmitted 128 bytes-long packets, No_AckPkt indicates the number of 17 bytes-long Ack packets received by the nodes and No_TxPkt is the number of transmitted packets. Similarly, the normalized energy consumption of the original WiDOM can be estimated as follows:

$$E(\text{Original-WiDOM}) = 3 \times (\text{No\_TxPkt}) \times 128 \quad (4.23)$$

Thus, the extra energy we pay for implementing the Ack-enabled WiDOM against the original WiDOM for the same number of transmission request is:

$$\text{Energylossratio}[\%] =$$

$$100 \times \frac{E(\text{Ack-enabled WiDOM}) - E(\text{Original-WiDOM})}{E(\text{Original-WiDOM})} =$$

$$100 \times \frac{\text{No\_ReTxPkt} \times 128 + \text{No\_AckPkt} \times 17 \times \frac{19.7}{14}}{128 \times \text{No\_TxPkt}} \qquad (4.24)$$

We do not consider the extra cost paid by the gateway node to receive retransmissions and to send back the Ack packets. This makes sense under the common assumption that the gateway is provided with a continuous energy supply.

As it is shown in Figure 4.15, the extra energy cost of using the Ack-enabled mechanism as compared to the original WiDOM roughly ranges between 25% and 35%, for any data rate. In particular, the energy loss shows some fluctuations at a lower data rates and tends to stabilize as the data rate increases. The reason is that nodes at lower data rates may have the opportunity to experience disruptive bursts of interference more often than the others, and therefore they might need to retransmit more frequently to successfully deliver their messages.

In terms of interference impact, it is evident that the higher noise density conditions impose higher energy consumptions due to the higher number of retransmissions. The energy loss rate is about 10% higher for the HNC scenario as compared to that in LNC environment, while the SPNC case shows a performance similar to that with the LNC
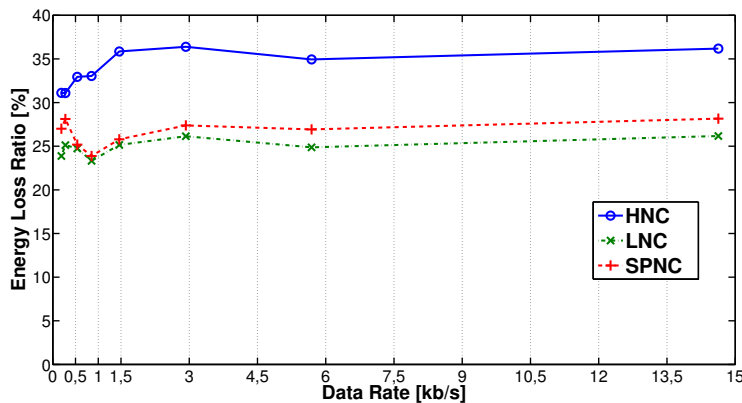
Figure 4.15: Energy loss ratio for Ack-enabled WiDOM vs. original WiDOM in HNC, LNC and SPNC environments.
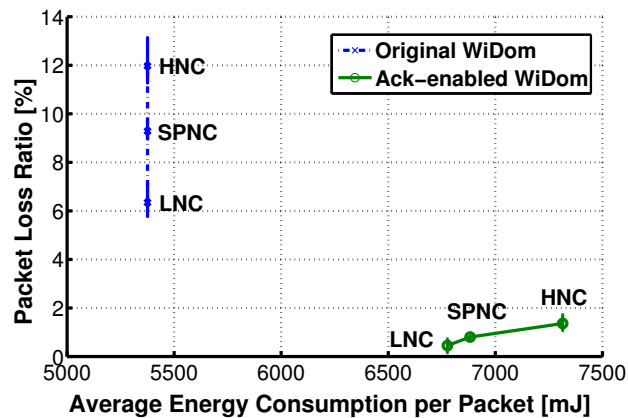
Figure 4.16: Packet loss ratio vs. average energy cost per packet for Ack-enabled WiDOM and original WiDOM under HNC, LNC and SPNC environments.

interference pattern.

Finally, to further examine the impact of the Ack-based mechanism, the packet loss ratio is plotted against the energy consumption per packet (see Figure 4.16). The energy consumption has been computed using the expressions for E(Ack-enabled WiDOM) and E(Original-WiDOM) as previously defined, normalized with respect to the number of transmitted packets, instead of the transmission current. As expected, the energy consumption of WiDOM is not affected by the interference level, while in the case of the Ack-enabled WiDOM is. This supports our claim that at the cost of roughly 30% more energy, it is possible to achieve a reduction of 90% in the packet loss ratio, i.e., keep it below (2%), regardless of the considered interference.

4.5 Concluding Remarks

In this section, we focused on the reliability of the WiDOM protocol. Our primary contribution was to offer an error recovery scheme to make the protocol more robust and reliable under noisy conditions. Another contribution of this section was to provide a novel response time analysis for the slotted WiDOM with message streams that suffer from release jitter and experience noisy channel conditions. We have shown that our analysis is non-trivial due to the slotted nature of the protocol. In order to reduce the level of pessimism in the calculated upper-bound, we individually explored all the possible cases that may happen according to the arrival pattern of message streams and then

picked the maximum upper-bound among all the possible cases.

To validate our calculated upper-bounds, we conducted a set of experiments under different noisy channel conditions. The experimental results have shown that implementing the Ack-enabled WiDOM reduces remarkably the packet loss rate to less than 2% even under high noisy channel as compared to the original WiDOM protocol. The experimental results also confirmed our analytical findings that the theoretical analysis offer valid upper-bound for each message streams.

Chapter 5

Self-Adaptive Approximate Interpolation scheme

In this chapter, we will propose a more efficient scalable data acquisition method for densely instrumented cyber-physical systems (CPS). Previous research works have proposed approaches for obtaining an approximate interpolation of sensor readings that are based on dominance protocols. Considering the dominance-based protocol, we design a new approach that offers a more accurate approximate interpolation by integrating the dynamics of the monitored signals into the computational process. We show that through a self-assessment functionality the algorithm detects sudden changes in the physical model and adapts itself accordingly.

5.1 Motivation

Recent advances in technology make it feasible to mass produce small sensor devices with sensing, computation and communication capabilities. These low-power wireless devices can also be powered by the energy scavenged from ambient radio waves [TRNA14]. These capabilities have enabled the integration of physical processes and computing, and spurred a new direction of research that envisioned massive deployments of networked embedded computing devices.

Dense networks offer a better resolution of the physical world and therefore a better capability of detecting the occurrence of an event; this is of paramount importance for a number of industrial applications. However, the scale of such systems poses huge challenges in terms of interconnectivity and timely data processing.

In this chapter, we focus on efficient and scalable data acquisition methods for such densely instrumented cyber-physical systems. As we discussed in Chapter 3, previous research works from our research group, have proposed approaches for obtaining an interpolation of sensor readings from different sensor nodes [APE$^+$08, ETPA11, APT08]. Those approaches are based on dominance protocols, presenting therefore excellent scalability properties for densely instrumented systems.

In fact, in Chapter 3, we discussed the role of dominance-based MAC protocols for computing relevant aggregate quantities. We mentioned that the basic interpolation algorithm (BIA) [APE$^+$08] offers an efficient approach to obtain an approximate interpolation of a physical phenomenon. However, the inability of the BIA algorithm in accommodating the dynamics of the monitored signals is identified as one of the main drawbacks of this approach. This is an important issue, specially when the speed of change of the monitored signal is much faster than the speed of the execution of the interpolation algorithm.

Recall from Section 3.5, where S is defined as a set of control points that incorporates in building the approximate interpolation. In a highly dynamic environment, the initial points that are taken into the set S become "outdated" fast, and as a result the approximate interpolation becomes inaccurate. This problem is more acute when the monitored signal is more complex (the one shown in Figure 3.1 is relatively simple) and therefore requiring more control points to be added to the set S.

A solution to this problem was attempted in [ETPA11]. In that work, the authors proposed a differential interpolation algorithm (DIA) that embeds a model of the dynamics of the physical signal into the algorithm. The DIA algorithm is summarized as follows: after selecting a new control point, all previously selected control points in the set S update their three attributes ((x, y) coordinates and v value) according to the defined change model. However, the approach has some limitations, as listed next.

1. There is no provision on how to obtain the physical model parameters to be incorporated into the algorithm (potentially without having any prior knowledge about the signal behavior).

2. There is no provision on any feedback control of the quality of the approximate interpolation, thus enabling the periodic re-computation of the physical model parameters that are embedded in the approximate interpolation algorithm.

In this correspondence, we consider a new physical change pattern monitoring technique that is added to DIA algorithm to enable that the approximate interpolation algorithm self adapts according to the dynamics of the physical signal. Doing so, our algorithm requires no a-priori knowledge of the parameters related to the temporal change model matrix, those elements of the matrix are estimated during the execution of the interpolation algorithm. Therefore, this chapter offers an important advancement to the state-of-the-art. Our novel approach not only incorporates a physical model to enable more accurate approximate interpolations, but also detects and self-adapts to changes in the physical model.

In the remainder of this chapter, we first present the general overview and detailed information of the proposed solution followed by evaluating the new approach.

5.2 Novel Approximate Interpolation Scheme

The novel algorithm to compute approximate interpolation functionality incorporates compensation in the control points to accommodate the dynamics of the physical signal. The proposed algorithm also includes *Learning* capabilities. Learning is performed at the beginning of the algorithm and every time that there is a need for re-computing the physical model parameters. These time instants are determined by a third functionality that is called *Assessment*. Figure 5.1 shows each of the mentioned functionalities, and the sequence of their executions. For simplicity, we use the term "sample" to denote an approximate interpolation.

Learning is needed at the beginning of the algorithm to determine the current dynamics of the physical signal. In this way, the first approximate interpolation is computed
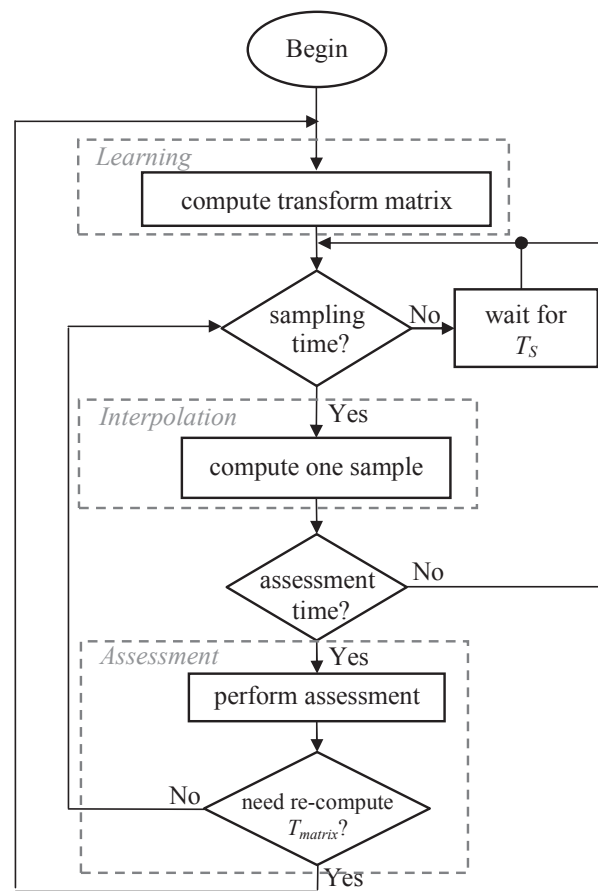
Figure 5.1: The proposed self-adaptive algorithm with *Learning* and *Assessment* functionalities.
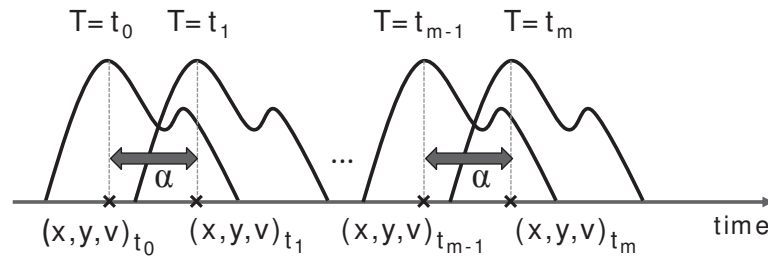
Figure 5.2: Signal translation during the execution of interpolation algorithm.

and then re-computed after a time interval T_S. In fact the time between two consecutive samples is denoted by T_S and the value of T_S is set by the application designer based on the application requirements. The *Assessment* phase is performed to investigate the correctness of the change pattern model given by the *Learning* functionality.

5.2.1   The *Learning* Phase

As mentioned earlier, during *Learning*, a matrix that models the change pattern of the physical signal is computed; we call this matrix the *transformation matrix* (T_{matrix}). To define the matrix parameters, $T_{i,j}$, the trend of the signal change is observed and a system of equations based on this observation is solved. To do so, we define a time window during which the tracking is performed. The term "round" represents the time it takes to execute an iteration in the approximate interpolation algorithm. As explained in Chapter 3, one round of interpolation involves the process of taking one control point and re-computing $f(x, y)$. The node with the highest error e_i can be found and added to the set S during one round.

Algorithm 7: *Learning* functionality

1 **for** $j = 1 : 5$ **do**
2 $\quad$ $S \leftarrow \emptyset$
3 $\quad$ calculate the interpolation function $f(x_i, y_i)$ based on S (as in Equation 3.2)
4 $\quad$ calculate e_j
5 $\quad$ select a sensor node N_k with the maximum e_k that is $e_k = e$
6 $\quad$ save the location (x, y) and the sensor reading (v) of the control point and form a system of equations
7 **end**
8 solve the system of equations to define parameters of T_{matrix}, $T_{i,j}$

Algorithm 7 summarizes the *Learning* functionality. It is assumed that there is a monotonous change in a physical quantity, which implies that the overall shape of the signal is preserved during the observation time. With this assumption, it can be claimed that by nullifying the set S (Line 2 in Algorithm 7) at the beginning of each iteration, it is possible to determine the location of the node with the highest error, which will correspond to the peak in the observed physical signal. Figure 5.2 shows an example of a dynamic signal that is translating with the rate of α in a specific direction. We found that tracking the location of a specific point on the physical signal for five consecutive rounds provides sufficient information to solve a system of equations through which the T_{matrix} is computed. We will justify this claim later, after explaining the procedure of updating set S.

5.2.2   The *Interpolation* Phase

While performing the *Interpolation*, our algorithm uses the T_{matrix} to update the data collected in the previous iteration. In particular, the algorithm selects a new control point at each round, and before computing the approximate interpolation $f(x,y)$, all the previously selected points in set S update their three attributes (x, y, v) by applying the affine transformation expressed by the T_{matrix} (see Equation 5.1). $xnew_i$, $ynew_i$ and $vnew_i$ are the new (updated) versions of the x coordinate, the y coordinate and the value of the control point p_i in the current round.

$$\begin{cases} xnew_i \leftarrow T_{1,1} \times x_i + T_{1,2} \times y_i + T_{1,3} \times v_i + T_{1,4} \\ ynew_i \leftarrow T_{2,1} \times x_i + T_{2,2} \times y_i + T_{2,3} \times v_i + T_{2,4} \\ vnew_i \leftarrow T_{3,1} \times x_i + T_{3,2} \times y_i + T_{3,3} \times v_i + T_{3,4} \end{cases} \tag{5.1}$$

5.2.3   Defining The Parameters of T_{matrix}

One approach to define the model parameters, $T_{i,j} : \{i \in \{1,2,3\}, j \in \{1,2,3,4\}\}$ in Equation 5.1, is to observe the trend of signal dynamics and then solve a system of equations based on that observation. To this end, as shown in Algorithm 7, we need to run the interpolation algorithm consecutively five times just for one round. The reason is that

the system equation given in Equation 5.1 includes 15 unknowns/variables (twelve $T_{i,j}$ variables and three new variables ($xnew_i, ynew_i, vnew_i$)), therefore, we need to resolve 15 equations to define $T_{i,j}$s. We know that within one round of interpolation the information of the node with the highest error (winner node) is found. This information includes values for the x and y coordinates and the value, v, of the winner node. Hence, with five times collecting the information of the winner node, we would be able to construct 15 distinct equations and finally define all parameters of the T_{matrix}. Accordingly, the model parameters $T_{i,j}$ are computed by solving the following equations:

$$
\begin{pmatrix}
x_1 & y_1 & v_1 & 1 \\
x_2 & y_2 & v_2 & 1 \\
x_3 & y_3 & v_3 & 1 \\
x_4 & y_4 & v_4 & 1
\end{pmatrix}
\times
\begin{pmatrix}
T_{1,1} \\
T_{1,2} \\
T_{1,3} \\
T_{1,4}
\end{pmatrix}
=
\begin{pmatrix}
x_2 \\
x_3 \\
x_4 \\
x_5
\end{pmatrix}
\tag{5.2}
$$

$$
\begin{pmatrix}
x_1 & y_1 & v_1 & 1 \\
x_2 & y_2 & v_2 & 1 \\
x_3 & y_3 & v_3 & 1 \\
x_4 & y_4 & v_4 & 1
\end{pmatrix}
\times
\begin{pmatrix}
T_{2,1} \\
T_{2,2} \\
T_{2,3} \\
T_{2,4}
\end{pmatrix}
=
\begin{pmatrix}
y_2 \\
y_3 \\
y_4 \\
y_5
\end{pmatrix}
\tag{5.3}
$$

$$
\begin{pmatrix}
x_1 & y_1 & v_1 & 1 \\
x_2 & y_2 & v_2 & 1 \\
x_3 & y_3 & v_3 & 1 \\
x_4 & y_4 & v_4 & 1
\end{pmatrix}
\times
\begin{pmatrix}
T_{3,1} \\
T_{3,2} \\
T_{3,3} \\
T_{3,4}
\end{pmatrix}
=
\begin{pmatrix}
v_2 \\
v_3 \\
v_4 \\
v_5
\end{pmatrix}
\tag{5.4}
$$

where (x_1, y_1, v_1) corresponds to the first set of information given by the winner node and (x_2, y_2, v_2) corresponds to the second set of information, and so forth.

Each node should perform this computation individually. This computation imposes more complexity to our algorithm. However, this additional computational cost promotes the new algorithm to be more generic as compared to the simple DIA algorithm. We show that by applying this self-adaptive mechanism to the interpolation algorithm, it provides a smaller average error as compared to the existing algorithms.

5.2.4   The *Assessment* Phase

It is important to keep the model parameters up-to-date after computing the elements of T_{matrix}. The algorithm needs to be able to detect the occurrence of a sudden change in the dynamics of the signal and adjust itself with the new change pattern. Applying feedback from the sensor field is helpful. To do so, we use a subset of the control points, let's say the first ξ numbers taken into the previous sample, and broadcast their observed error value as a feedback message to assess the quality of the T_{matrix}. The observed error of a control point is the difference between the measured value and the value of the interpolated signal in its location. Therefore, the observed error computed during *Assessment* is used to indicate the need for re-computing the transformation matrix. If the average observed error is larger than a threshold value ε, the currently used parameters of T_{matrix} are deemed as not valid anymore, and *Learning* will execute. Algorithm 8 illustrates the *Assessment* functionality.

Algorithm 8: *Assessment* functionality

---

1   **Requirements:**
2   (i) all nodes are aware of the start of the *Assessment*;
3   (ii) latest set S is preserved: $S = q_1, q_2, \ldots, q_k$;
4   **for** $j = 1 : \xi$ **do**
5   **if** $id == q_i.id$ **then**
6 | compute the error and broadcast it
7   **else**
8 | wait to receive a packet and store the observed error value
9   **end**
10 **end**
11 re-compute_$T_{matrix} \leftarrow FALSE$
12 **if** average observed error $> \varepsilon$ **then**
13   re-compute_$T_{matrix} \leftarrow TRUE$
14 **end**

During *Assessment*, in order to collect feedback messages, we assume a TDMA-based communication. The first requirement listed in Algorithm 8 is satisfied by utilizing the same synchronization technique applied to the prioritized MAC protocol [Bos91, PAT07, PGAT09], since all nodes agree on a common reference time to start either a round of interpolation or a TDMA-slot.

The Assessment functionality is performed with a periodicity T_A that is a multiple of T_S. The exact value of the self-assessment periodicity is defined by the application designer according to the required accuracy level. Intuitively, the smaller the *Assessment* frequency, the more accurate representation of the signal will be achieved.

5.3 Algorithm Evaluation

To evaluate the self-adaptive interpolation scheme, we developed several simulations in MATLAB, first to assess the efficiency of the transformation matrix, T_{matrix}, in computing only one sample of the physical signal and compare it against the basic approach. Then we examined the execution of the self-adaptive approach in an application simulated by MATLAB, where we aim at performing a continuous monitoring of a signal with a given pattern change.

5.3.1 The Efficiency of T_{matrix}

As discussed in Chapter 3, the approximate representation of the physical signal can be obtained by executing the interpolation algorithm for a number of rounds (defined by k in Algorithm 1). Through extensive simulations, we studied the average error of a sample of a physical signal computed by the basic interpolation approach and the new self-adaptive approach. We consider a dense network with 2500 nodes, deployed in a square grid fashion. We also consider having an input physical signal that can be modeled by a single peak middle shape signal (similar to the one given in Figure 3.1(a)) with the following Gaussian function:

$$p(x,y) = e^{-7((x-0.5)^2 + (y-0.5)^2)} + 0.1 \tag{5.5}$$

Three types of linear signal changes are considered : (i) scaling, (ii) increment and (iii) translation. Figure 5.3 compares the average error of a sample computed by the BIA and the self-adaptive algorithm as a function of the number of considered interpolation rounds. Simulation results show a remarkable improvement in the average error of a sample computed by the novel self-adaptive approach independently of the considered

(a) Scale (10%) (b) Increment (10%) (c) Translate (2%)
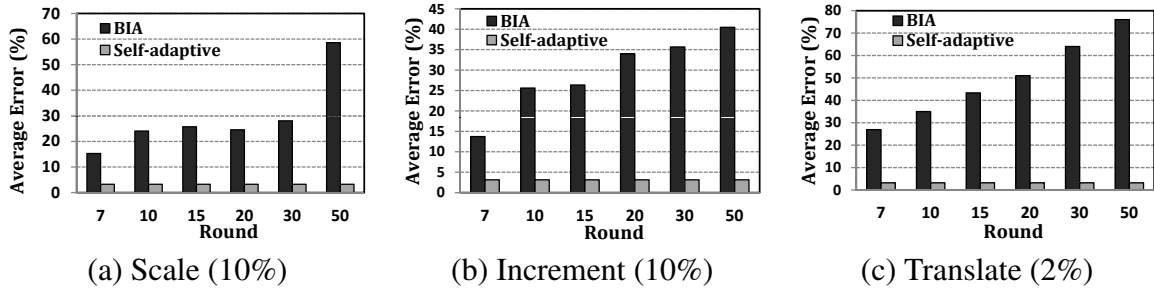
Figure 5.3: Average error in a sample computed by the BIA and the novel self-adaptive approach.

signal change model. While the novel approach provides a fair estimation of the physical signal (with an average error of about 3%), the BIA presents much poorer results. The average error of a sample computed by BIA keeps rising when the number of interpolation rounds increases. The reason is that dislike the self-adaptive approach that updates the value of the previously selected control points q_i in the set S before computing the $f(x,y)$, in the BIA approach, the value of the selected control points in S remains unchanged. This leads to a major deviation between the computed approximate interpolation and the real physical signal. In fact, longer execution of the interpolation deteriorates the accuracy of the sample computed by the BIA approach.

5.3.2   Performance Evaluation of Self-Adaptive Scheme

We consider the same simulation set up as in the previous subsection and the same input signal as defined by the Equation (5.5). The aim of this set of simulations is to assess the self-adaptive approach for the "continues" monitoring of a dynamic signal. In the experiments, we consider abrupt change patterns in the signal, applied by the displacement of the whole signal up and down. We express the displacement in terms of relative speed as compared to the duration of a round.

Figure 5.4 shows the speed of the change during the simulation time (4000 rounds). The positive values and negative values represent "movements" up and down, respectively. Note that the values change equally in all points (x_i, y_i) of the grid.

We run the simulation for 4000 rounds and set T_S to 25 rounds and T_A to $3 \times T_S$, which means that a new sample is computed every 25 rounds and the *Assessment* runs every
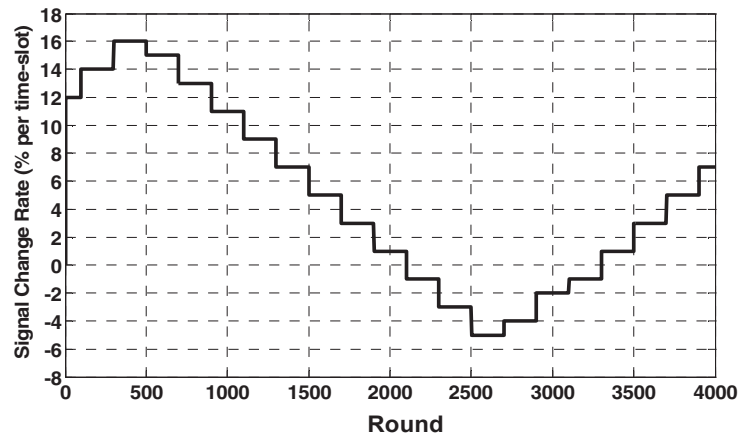
(a) Change pattern scenario.
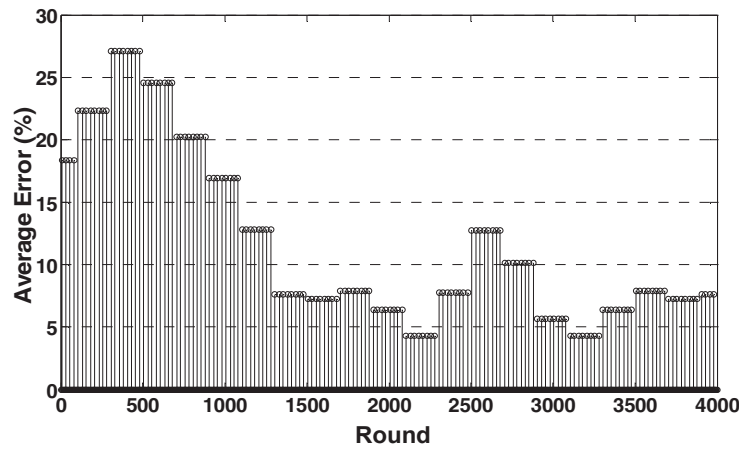
(b) The BIA approach.
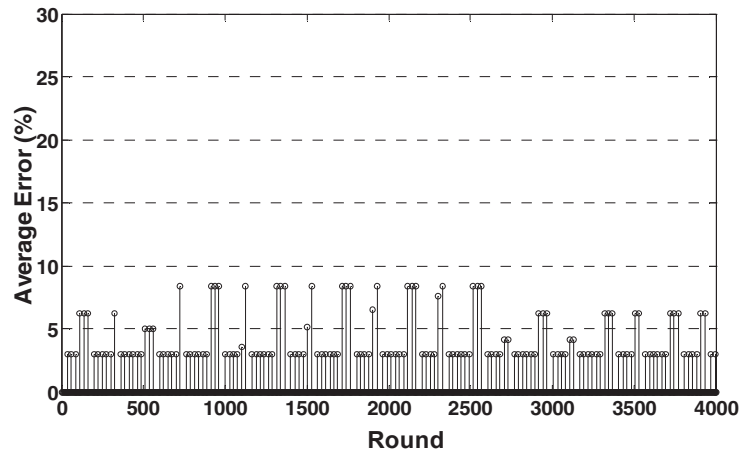
(c) The self-adaptive approach.

Figure 5.4: The average error of samples computed by the BIA and the self-adaptive approaches with $T_S = 25$ rounds and $T_A = 3 \times T_S$.

75 rounds. The number of control points is set to 6, which indicates that a new sample is computed during 6 rounds. In *Assessment*, we chose the first five control points that
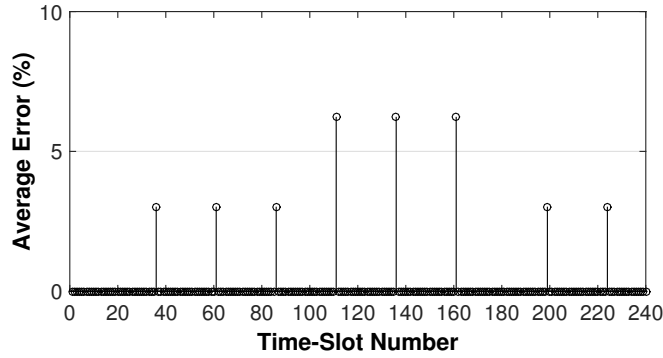
Figure 5.5: The zoom in view of the average error of samples computed by self-adaptive approach with $T_S = 25$ rounds and $T_A = 3 \times T_S$.

contributed in computing the latest interpolation sample ($\xi = 5$).

Since we set T_A to $3 \times T_S$, in the worst case, we may observe three samples with lower quality. In our described scenario, this happens for instance after round 100, when the change rate increases from 12% to 14%. Figure 5.5 shows the zoom-in view of Figure 5.4(c). Since the last assessment has occurred at round 86, and the next assessment occurs at round 161 (75 rounds later), the samples taken in rounds 111, 136 and 161 are computed with an outdated T_{matrix}, hence we see three low quality samples in a row. After the assessment in round 167, since the average observed error is not small enough (ε is chosen 0.01), all nodes prepare to execute the *Learning* phase to recompute the T_{matrix}.

The self-adaptive approach provides more accurate results (average error of about 3%) as compared to the BIA approach. For the simple physical signal with low change rate, the performance of the BIA approach is roughly the same as that of our novel algorithm, but for more complex signals, where there is a need to have more points in the set S for computing one sample, the novel algorithm outperforms BIA, even for slow change rates.

Besides, in worst case and for the described experiment, the novel algorithm provides samples with 9% as the largest average error, while with BIA, samples with an average error of 27% may result, especially when the signal change rate is high.

5.4 Summary

In Chapter 3, we described how the BIA approach enables to efficiently compute an approximate interpolation of a physical signal. The BIA approach works well for the case where a smooth physical signal is monitored and with the assumption that the signal remains steady over the time it takes to obtain an approximate sample. The DIA algorithm is also described as an attempt to provide a more accurate interpolation by embedding the physical dynamics into the interpolation algorithm. However, the DIA is unable to provide a system-dependent interpolation algorithm, since the proper change pattern parameters cannot be detected at run-time; they must be defined a-priori by the application designer. This chapter discussed and described a solution to tackle the above mentioned problem. Our novel algorithm provides an accurate approximate interpolation even if the signal and change patterns alter during the execution of the interpolation algorithm. More importantly, the algorithm self-adapts to incorporate variations in the change pattern.

Possible future work would involve synthesizing such an algorithm from a model of the physical world by incorporating changes in the *Assessment* rate as part of the feedback control as well as a more sophisticated technique to model more complex change patterns (not monotonous in the area of observation).

Chapter 6

Feature Extraction in Densely Sensed Environments

In this chapter, we present a novel feature extraction mechanism for dense sensor networks, where all nodes are located in one single broadcast domain (SBD). Then, we extend our SBD algorithm for a large dense network with multiple broadcast domains (MBD), where all nodes may not reside within the communication range of each other. This feature extraction mechanism employs the prioritized channel access mechanism of dominance-based protocols (i) to efficiently obtain global extrema of sensed quantities, (ii) to extract local extrema and (iii) to detect boundaries of events.

6.1   Feature Extraction

With the reduction in size and cost of sensor nodes, dense sensor networks are becoming more popular in a wide-range of applications. Some of these applications aim at providing an approximate interpolation of the monitored physical quantities, as discussed in Chapter 5. Some other applications with dense deployments are geared towards finding various *patterns* or *features* in the spread of sensed physical quantities over an area. In this Thesis, we define feature extraction as the process of determining certain features such as *peaks*, *boundaries* and *shapes* in the distribution of a physical quantity. Based on

the application requirements, it might be important to extract these features by performing in-network processing.

While feature extraction may not be an issue for a small density network (for example, tens of sensor nodes), it is still a challenging problem for a high density network. In applications where measurement constraints are required to have a high spatial granularity, covering even a small area (e.g., one square meter), may require hundreds to thousands of sensor nodes. Some examples of densely deployed sensing applications where features of physical quantity need to be monitored frequently are sleep monitoring for health [LXH+13], smart-surfaces for space and aviation [PLB04] and food industry [CO05]. In this chapter, we tackle the problem of feature extraction in applications that require such dense deployments.

6.2   Motivation

Figure 6.1 presents an example of the distribution of a physical quantity (e.g., temperature or pressure values) known as a *field*. In this example, the distribution has three regions of activity that require detection and evaluation. A dense sensor network for measuring such a physical quantity would involve deploying sensor nodes to measure each data point in the distribution. The regions of activity, called active regions, are defined as the regions, where the deployed sensor nodes sense some values of interest. One way to define these active regions is by estimating the boundaries of these regions. A naive approach to obtain this information would be to collect readings from all sensor nodes and process them centrally. This is usually inefficient, since typical channel access techniques do not scale with an increase in number of nodes. Therefore, it becomes advantageous to devise techniques that perform feature extraction irrespective of the density of the network.

Computing even simple aggregate quantities such as extrema (minimum or maximum) is not trivial for a dense network as it may require collecting data, in the worst case, from all nodes [PGAT09] (even if some sort of spatial sub-sampling is employed [NM03]). Dominance-based or binary-countdown MAC protocols, as discussed in Chapter 2, help in finding the minimum value in constant time [MW79, Bos91, PAT07]. Furthermore,
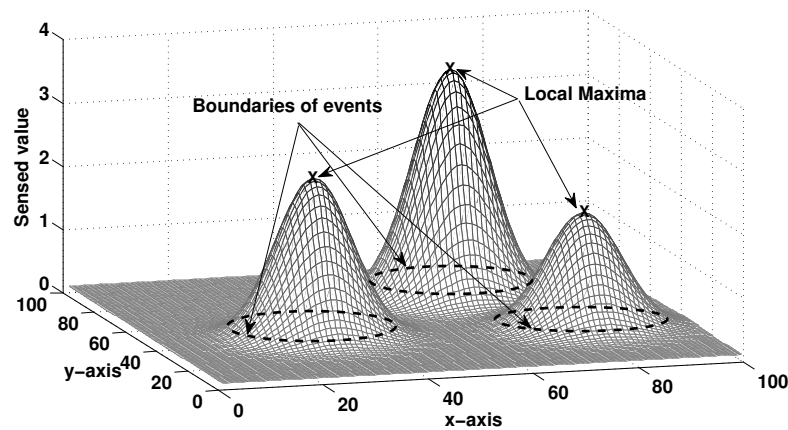
Figure 6.1: An example of a 2-D physical quantity *field* with $10,000$ sensor nodes. Each data point corresponds to a value sensed by an individual node.

finding peaks and their boundaries in a distributed network, where each data point is measured by individual sensor nodes, is computationally expensive, time consuming and typically does not linearly scale with an increase in network size.

In this chapter, we first establish that finding the local extrema is a challenge even after the global maximum is known. Once the global maximum is identified in constant time, we propose a few transforms that nodes employ on local data, which helps in identifying other peaks (local maxima) and their boundaries in the spread of the physical quantity being measured. Our proposed transforms, referred to as *augmenting functions*, allow the identification of local extrema in constant time. Moreover, instead of collecting all data as in the naive case, these augmenting functions result in fewer number of measurements being collected.

6.3 System Model

We consider a sensor network where each sensor node has a unique *identifier*, i, and measures a particular physical quantity, s_i, using a sensing unit. Each sensor node knows its 2-D coordinates (x, y) in the plane of deployment. We assume that the feature extraction mechanism can either be carried out periodically, as a part of a *sense-process-actuate* control-loop, or sporadically initiated by an external controller, like a data sink or a master node.

As stated earlier in this chapter, the collection of all sensor values across the total sensed area is referred to as a *field* (shown in Figure 6.1). Each data point in the *field* corresponds to a true (or non-faulty) sensor reading value, sensed by an individual sensor node at its physical location. The spatial granularity and the size of the *field* is directly correlated to the distribution of the nodes and their spread. We also define *active region* as a physical area populated by sensor nodes that sense some *activity*. The overarching goal of our technique is to find location, boundaries and shape of an *active region*, which we referred to as *features*, in the physical environment. To illustrate and evaluate our approach, we generate various sample *fields* by a summation of 2-D Gaussian functions.

Function $\mathcal{M}(v_i)$ represents the process of finding the MIN over values v_i published by independent sensor nodes in a broadcast medium, where $i \in \{1, 2, ...N\}$ and N is the number of sensor nodes in a broadcast domain. In fact, $\mathcal{M}(v_i)$ represents one execution of interpolation *round*, as discussed in Chapter 5, for an SBD domain (later on, in Section 6.5.2 we will discuss the details of function $\mathcal{M}$ for MBD, where several number of *rounds* need to be run). We exploit the property of simultaneous transmissions in dominance-based protocols to devise this function. v_i is the scaled value that each sensor node computes based on its measured value s_i and the global maximum s_{max} measured in the *field*.

After each *round*, all the other sensor nodes know the *identifier* and the location of the sensor node with the MIN value. This sensor node is known as the winner of the *round*. We use $\hat{i}$ to denote the *identifier* of the winner. Hence, the function $\mathcal{M}$ can be formally represented as:

$$\{\hat{v}, \hat{i}, \hat{x}, \hat{y}\} = \mathcal{M}(v_i) \quad \forall i \in \{1, 2, ...N\}$$

where $\hat{x}$ and $\hat{y}$ are the x and y coordinates of the sensor node with the global minimum value $\hat{v}$.

The choice of the v_i values used by an ith sensor node in the application of function $\mathcal{M}$ depends on the requirements of the application. It should be noted that a sensor node can only use its local information (such as *identifier*, sensor value and physical location) and other global data available from the previous iterations of $\mathcal{M}$. For our goal of identifying various features, we augment (or transform) these input values such that the

Table 6.1: Summary of the symbols and notations used in this chapter.

Symbol	Description
s_i	sensor value measured by sensor node i
s_{max}	maximum value collected by sensor nodes
$v_i = \frac{1+s_i}{s_{max}}$	scaled sensor value with respect to the maximum value over all sensor nodes
$A_\beta, A_\gamma, A_\delta$	*augmenting functions* used for different feature extraction techniques
$\mathcal{M}(v_i)$	finding the `MIN` over all v_i values
$\mathcal{M}(-v_i)$	finding the `MAX` over all v_i values
$\phi(v_i, x_i, y_i)$	function computed by sensor nodes
π_s	termination condition

global minimum returned by $\mathcal{M}$ corresponds to one of the local minima or an edge of an active region.

The function $\mathcal{M}$ can be applied to the value computed by ϕ_i, which is a function of the sensor values and their location. The codomain of the function ϕ_i denotes a set of values it can take. We assume that the cardinality of the codomain of ϕ_i is large enough that the probability of computing the same ϕ_i by two sensor nodes is negligible and thus an unique sensor node $\hat{i}$ is chosen. The time-complexity of $\mathcal{M}$ is proportional to the number of bits used to encode ϕ_i, and hence, it is proportional to the logarithm of the cardinality of the codomain. However, as all sensor nodes transmit simultaneously in a dominance-based MAC protocol, the time required for the application of $\mathcal{M}$ over a network is independent of the number of sensor nodes. Table 6.1 summarizes the notations and symbols that we use in the following sections, where we define a set of functions to extract different features of the *field*.

6.4   Feature Extraction Using Augmenting Functions

In this section, we describe in detail a set of augmenting functions that can extract an approximate but faithful representation of various features in the field by applying simple transforms on the sensor values. We show that this process can be done with a limited number of broadcast messages or floodings in the cases of SBD or MBD, respectively.
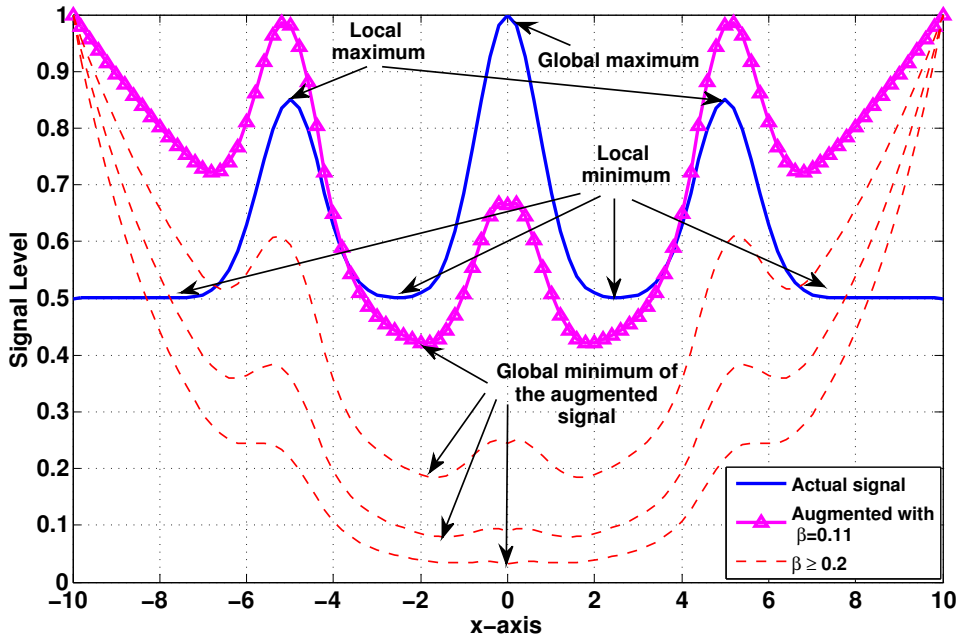
Figure 6.2: An example of *augmented function* $\mathscr{A}_\beta$ of the normalized input signal with various β in the range of [0.11, 0.5) in 1-D domain.

6.4.1 $\mathscr{A}_\beta$ Distance Augmenting Function

As described earlier, a global maximum value in a sensor *field* can be easily found by applying function $\mathscr{M}$. However, finding the spread or boundaries of this peak (local maximum) is not trivial. If we modify the MAC protocol such that the sensor node with the global maximum does not participate in the next *round*, there is still a high chance that one of the adjacent sensor nodes to the peak will become the next local maximum. On the other hand, we might have to predefine a neighborhood range around the peak that should be excluded in the next cycle to make sure that another local maximum be the new global maximum. In this case, choosing the size and shape of the neighborhood is also a challenge.

We demonstrate the process of finding an adjacent local minimum with a simple 1-D Gaussian *field* example, shown in Figure 6.2. Using this example we show that, by utilizing the augmenting function over the input signal, the adjacent local minimum becomes the global minimum.

In this example, the *field* consists of three peaks and the highest peak (the global maximum) lies in the center. Finding the spread of the peak with the global maximum is

not trivial as the global minimum point can be one of those sensor nodes near the borders of the *field*. It is important to suitably modify the process of identifying the extrema such that a local minimum adjacent to a peak (*adjacent valley*) can be found. For this purpose, we observe that an *adjacent valley* should have a low value and its distance from the peak should also be small. Hence, each value in the *field* is transformed (multiplied) with the distance from the peak. With this transformation, the points located farther from the peak are associated with higher values (compared with its sensed value) and only points with the lowest sensed value and the smallest distance from the peak can become the global minimum in the augmented *field*. It is possible that this global minimum is a point in an *adjacent valley*. The boundary of this peak is found with just two *rounds* of executing $\mathcal{M}$ function: (i) finding the global maximum in the original *field*; and (ii) identifying the global minimum in the augmented *field*.

For 2-D Gaussian *fields*, the 1-D approach described above can be directly applied. Different active regions of the *field* are found by excluding the sensor nodes lying inside the identified active region from participating in the next *rounds*. The process of finding active regions is shown in Algorithm 9. Initially, function $\mathcal{M}$ is used to find the global maximum (s_{max}), then a circular area around the identified peak is filtered out. The radius of this filtering circle is set as the distance of an *adjacent valley* from the peak. The value and the location of the *adjacent valley* ($S_{adj-valley}$ and $d_{adj-valley}$) are found by one application of $\mathcal{M}$ function (line 9 in Algorithm 9).

Each sensor node uses a function ϕ_β as an input to $\mathcal{M}$. The function ϕ_β takes into account two properties of the *field*: (i) sensed value s; and (ii) sensor's proximity to the peak d. That function is defined as follows:

$$\phi_\beta = v \times \mathcal{A}_\beta(d) \tag{6.1}$$

v is the scaled value and is defined as:

$$v = \frac{1+s}{1+s_{max}} \tag{6.2}$$

and s_{max} is the value of the global maximum, found at the beginning of the algorithm.

Algorithm 9: *Distance augmenting function ($\mathscr{A}_\beta$) executed on each sensor node n_i*

---

1 **begin**
2      $Silent \leftarrow 0$
3      $s_{max} \leftarrow \mathscr{M}(-\phi_s)$ `// find global MAX`
4      $\pi_s \leftarrow$ a fraction of s_{max} `// termination condition setting`
5   **while** $\underline{s_{new-peak} > \pi_s}$ **do**
6   **if** $\underline{Silent \neq 1}$ **then** `// if the node is not filtered out`
7              $s_{new-peak} \leftarrow \mathscr{M}(-\phi_s)$ `// find the new peak`
8   compute ϕ based on Equation 6.1
9              $< s_{adj-valley}, d_{adj-valley} > \leftarrow \mathscr{M}(\phi_\beta)$
10              $R_f \leftarrow d_{adj-valley}$
11              $d_i \leftarrow$ distance between *new-peak* and node n_i
12   **if** $\underline{d_i < R_f}$ **then**
13                  $Silent \leftarrow 1$
14   **end**
15   **end**
16   **end**
17 **end**

$\mathscr{A}_\beta(d)$ is the augmenting function, which is formulated as follows:

$$\mathscr{A}_\beta(d) = e^{\beta\left(\frac{d}{d_{max}}\right)^2} \tag{6.3}$$

where d_{max} is the diameter of the monitored area, and it is used to normalize the distance from the peak. β is a parameter to control the impact of distance on the augmented *field* with respect to the scaled value ν. To ensure that the winning sensor node is located at the adjacent local minimum of the *field*, the priority function ϕ_β is computed so that the distance is exponentially penalized.

Finally, by finding the global minimum over ϕ_β values at all the sensor nodes, we are able to find a point that lies in the *adjacent valley* with a high probability. The distance between the *adjacent valley* point and the peak determines the filtering radius, R_f (line 10 in Algorithm 9). Sensor nodes that are located within the filtering circle refrain from participating in the next iterations. Repeating this procedure conducts to finding all the peaks in the region. The algorithm stops when the value of the new peak ($s_{new-peak}$) is lower than a certain user defined threshold π_s, which is a fraction of the global maximum. By finding the peaks and their spread, this approach helps in identifying the location and the number of circular active regions in a *field*.

6.4.2 $\mathscr{A}_\gamma$ Vector Augmenting Function

Our second *augmenting function* is used for cases where we are interested in finding a boundary around all active regions. This approach can be used for a range of applications such as crowd monitoring for smart cities or sleep monitoring for health-care. In this approach, if we assign larger values of ϕ to sensor nodes that lie on the boundary of an active region, then the result of applying the $\mathscr{M}$ function over the negation of the ϕ value corresponds to the boundary of active regions. This is implemented by augmenting the sensor values with a function that grows in a particular direction.

The *vector augmenting function* $\mathscr{A}_\gamma$ is designed to work with binary *fields*, where the input signal is not smoothly distributed, and two neighboring sensor nodes may have very close or very different measurements. By applying $\mathscr{A}_\gamma$, each sensor node multiplies its measurement with a vector $\vec{u}$. The rationale behind using a direction is to find the sensor nodes that sense a high value and are located as far as possible in the direction given by $\vec{u}$, which corresponds to the edge of an active region in that direction. To compute the function ϕ, sensor nodes transform their locations with a direction as follows:

$$\phi_\gamma = v_p \times \mathscr{A}_\gamma(x, y, \theta) \tag{6.4}$$

where v_p is a *participation value*, which is either 0 or 1, depending on the sensed value being below or above a threshold. Sensor nodes with $v_p = 1$ are part of the active region. The *augmenting function* is defined as follows:

$$\mathscr{A}_\gamma(x, y, \theta) = e^{\gamma(x.\cos(\theta) + y.\sin(\theta))} \tag{6.5}$$

x and y are the coordinates of the sensor location and θ is the direction given by vector $\vec{u}$.

By using $\mathscr{A}_\gamma$, the value is "projected" in a direction given by the vector $\vec{u}$. The sensor node that has the largest value has a high probability of being located on the border of an active region in the direction of $\vec{u}$.

The way this approach works is outlined in Algorithm 10. The algorithm explores the region by choosing random directions defined in a set $\{\bar{v}_\theta\}$. We assume that the seed for generating this pseudo-random directions is generated by the initiator of the boundary

---

Algorithm 10: *Vector augmenting function $\mathscr{A}_\gamma$, executed on each sensor node n_i*

---

1 **begin**
2      $s_{max} \leftarrow \mathscr{M}(-\phi_s)$ `// find global MAX`
3      $\pi_s \leftarrow$ a fraction of s_{max} `// termination condition setting`
4      $\{f_\theta\} \leftarrow \varnothing$ `// the set of filtered directions`
5   **if** $\underline{s < \pi_s}$ **then**
6          $v_p \leftarrow 1$
7   **else**
8          $v_p \leftarrow 0$
9   **end**
10     $\{\bar{v}_\theta\} \leftarrow$ a set of θ directions
11   **foreach** $\underline{\theta \in \{\bar{v}_\theta\}}$ **do**
12   **if** $\underline{\theta \notin \{f_\theta\}}$ **then**
13   compute ϕ_γ based on Equation 6.4
14             $< s_{edge}, (x,y)_{edge}, \theta_{edge} > \leftarrow \mathscr{M}(-\phi_\gamma)$
15   **if** $\underline{(x,y)_{edge}}$ was found with other direction θ_x **then**
16                 $\{f_\theta\} \leftarrow \{f_\theta\} \cup \theta_x \theta + 2\varepsilon$
17   **end**
18   **end**
19   **end**
20 **end**

---

detection process. Thus, all the sensor nodes will use the same $\{\bar{v}_\theta\}$ in each iteration. Repeating this procedure in different directions makes it possible to find the boundary of an active region by computing the convex hull of the collected locations.

If two angles lead to a same point, it means that any angle over the arc confined by these two angles would result in that point. Thus, this arc can be filtered out from further investigation. Figure 6.3 shows an example where two angles of $\theta_1 = 31°$ and $\theta_2 = 89°$ lead to find the same location P_2. In this case, there is no need to examine more directions in the region of $31° \leq \theta \leq 89°$. We also use *marginal extension* ε to limit further the redundant directions in the arc denoted by $\theta_i \pm \varepsilon$. We discuss the impact of ε in Section 6.6.

More iterations of the algorithm leads to more accurate boundaries, but at the cost of more resource consumption. We show in Section 6.6 that with the above filtering strategy, we are able to reduce the number of dominance *rounds*, while still building a valid description of the active region. The worst case for our algorithm happens when the event boundary looks like a perfect circle where each new direction will give a new point (assume having a very dense deployment of sensors and consider a marginal extension of
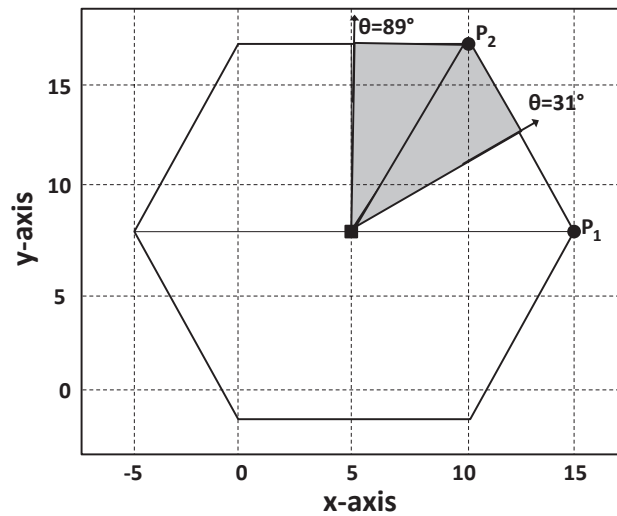
Figure 6.3: An example of boundary detection for a hexagonal-shape event.

$\varepsilon = 1^\circ$; in this case, up to 359 individual readings will be collected). However, the results show that the number of readings is usually much less in practice.

6.4.3 $\mathscr{A}_\delta$ Joint Augmenting Function

As described earlier, the *distance augmenting function* $\mathscr{A}_\beta$ identifies circular active regions. For complex *fields*, $\mathscr{A}_\beta$ may need several circular active regions to cover a non-circular shape. On the other hand, *vector augmenting function* $\mathscr{A}_\gamma$ only provides a convex hull of all the active regions. So, a *field* with several isolated active regions is identified as one large shape, which may not provide enough insights regarding the structure of the active regions.
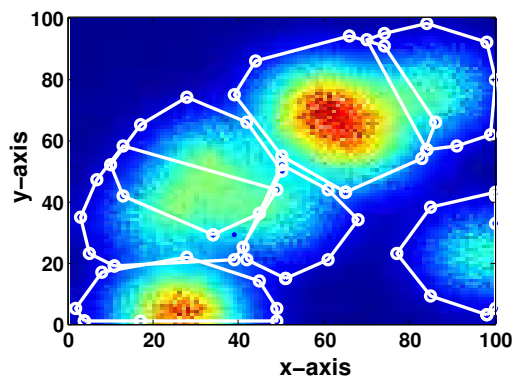
Figure 6.4: An example of boundary detection around the peaks with a non-uniform distribution.

To find the boundary of an active region with a non-circular distribution, we devised a new augmenting function $\mathscr{A}_\delta$, that is a composition of $\mathscr{A}_\beta$ and $\mathscr{A}_\gamma$. By applying $\mathscr{A}_\delta$, sensor nodes that were identified with the $\mathscr{M}$ function should have the following properties: (i) lie close to the peak; and (ii) locate on the edge of the local boundary in a given direction. The value used by each sensor node is then defined as follows:

$$\phi_\delta = \mathscr{A}_\delta \times \frac{\mathscr{A}_\beta(d)}{\mathscr{A}_\gamma(x,y,\theta)} \tag{6.6}$$

where $\mathscr{A}_\delta$ is given by:

$$\mathscr{A}_\delta = v^{-\delta}$$

$\mathscr{A}_\delta$ is an inverse polynomial of degree δ of the scaled sensed value v, and δ is a parameter to guarantee that the low values lying far away from a peak bring a stronger contribution to the ϕ values. As a consequence, for a given value of θ, the point that has the minimum value of ϕ_δ is more likely to lie on the boundary in the θ direction. We sweep the area around a peak with different values of θ. In our evaluation, for θ, we used equal intervals of $\pi/4$ ($\theta \in \{0, \pi/4, ...2\pi\}$). Smaller intervals will result in better accuracy of boundary at the cost of higher number of broadcast messages. Thus, after finding a new peak, the locations of the nearest *adjacent valleys* in eight directions are found, and the convex hull of all these readings represents the area around that active region. This enables us to find complex geometric shapes according to the shape of active regions instead of only circles, as shown with an example in Figure 6.4.

6.5   Computing Global Extrema in MBD Networks

In this section, we address the challenge of computing MIN in a dense network, where nodes are not necessarily confined to an SBD. We consider two different approaches to extend the functionality of $\mathscr{M}$ function for MBD dense networks: (i) clustering the network into several SBDs as proposed in [APT07], and (ii) a novel approach using concurrent transmissions by taking advantage of the dominance-based protocol.
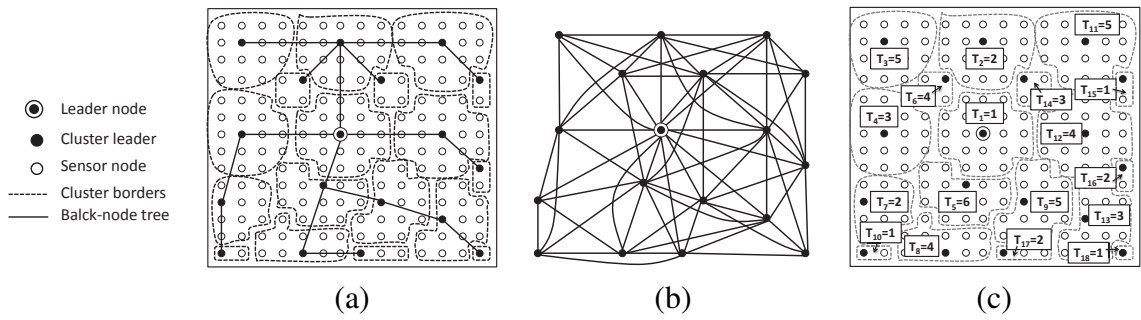
Figure 6.5: Cluster-based approach: (a) cluster formation and black-node tree (B) construction. $R_{co} = 5$ and we assume $r = R_{co}/2$. With the given virtual range r, 18 clusters are constructed; (b) cluster interfering graph G_i (with $d = 14$). This graph is used by the leader node to compute the activation timeslot for each cluster. Two clusters are assumed to be interfering if the distance between the cluster leaders is less than $3 \times r$; (c) timeslot assignments (the chromatic number for the interfering graph is 6).

6.5.1 The Cluster-based Approach

In the clustering approach, proposed in [APT07], a topology discovery algorithm is first executed to partition the network such that all nodes in each partition are in the same broadcast domain (*Setup phase*). Then, at runtime, nodes within the same cluster find the minimum sensor reading and communicate these values to their cluster leaders. The cluster leaders form a collection tree with root at the leader node where the query for computing `MIN` was initiated.

The high-level pseudo code of the cluster-based approach is given in Algorithm 11. A minimum virtual dominating set (MVDS), as introduced in [DBN03], has been considered during the setup phase. With MVDS it is possible to divide the network into several clusters where the nodes in each cluster form an SBD domain. The cluster leaders (known as black-nodes in MVDS) are responsible for collecting `MIN` in each cluster and forwarding it to the leader node through a collection tree graph known as black-node tree (B). The virtual range is used to guarantee that all nodes in a cluster are located in the same broadcast domain. In fact the MVDS is a distributed algorithm with two main phases. In the propagation phase, it forms the clusters; and in the response phase, the topology information is delivered to the leader node (the node initiating the aggregation query). Figure 6.5-(a) shows an example of cluster construction using MVDS.

The leader node uses this topology information to schedule the activation time of

---

Algorithm 11: *Cluster-based approach*

---

1 **begin**
2   **run** *MVDS(R_{co}, r)* [DBN03] to partition the network (setup phase) `// execute on`
    `each sensor node` n_i
3   **construct** cluster interfering graph $G_i(V, E)$ and black-node tree B (response
    phase) `// execute on leader node`
4      $\Delta \leftarrow$ *timeslot-assignment(G)* `// executed on leader node`
5   **for** $i = 1$ **to** Δ **do**
6   **execute** one dominance *round* according to assigned timeslot `// execute on`
        `nodes in each active cluster`
7   **end**
8   **collect data** from black-node tree B `// execute on leader node`
9   **disseminate** global MIN to the network `// execute on leader node`
10 **end**

---

each cluster to avoid any collision between neighboring nodes that reside in different clusters. To make this approach more efficient, we utilize a heuristic that was proposed for the register interfering graph (RIG) problem [KP87] to find the *chromatic number* Δ for concurrent active clusters. However, unlike the RIG problem, in our case the number of available colors is not known in advance. k is the number of registers in the RIG problem.

Function `timeslot-assignment(G)` is performed by the leader node to find the value of Δ as shown in Algorithm 12. From basic graph theory it is known that, for an *n*-node graph $G(V_n, E)$, if the maximum degree of nodes in the graph is d, then it is possible to color the graph with $d + 1$ different colors [JT11]. In our modified heuristic, the leader node initiates the process of finding Δ by setting k to $\lceil \frac{d+1}{2} \rceil$, and then restricts the search area $[k_{min}, k_{max}]$. If the current k is able to color the graph (line 6 in Algorithm 12), the algorithm will add k into the set of possible chromatic numbers $\{C\}$ and updates k_{max}, otherwise, it updates k_{min}. The algorithm terminates when the current k is larger than an element in the set $\{C\}$. For the example given in Figure 6.5, with $d = 14$, the algorithm finds $\Delta = 6$ after four assignments of k.

6.5.2   The Ripple-based Approach

The ripple-based approach aims at eliminating the setup overhead in the cluster-based approach and mitigating the initialization cost by using a distributed algorithm to compute
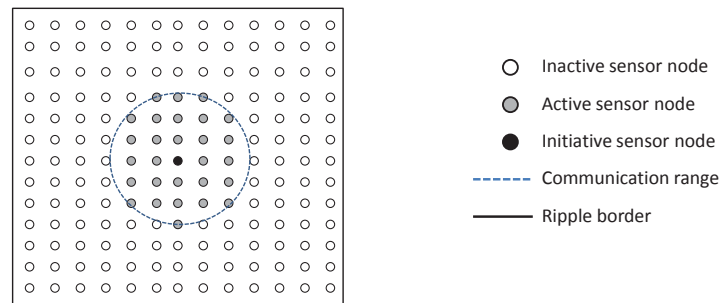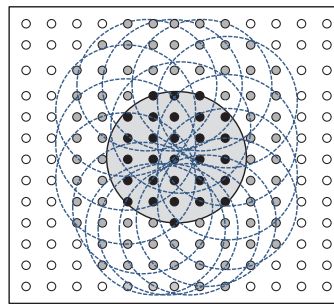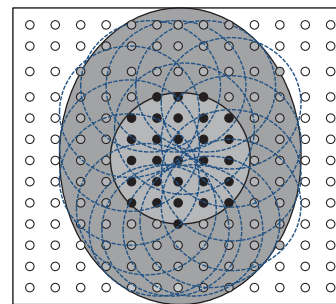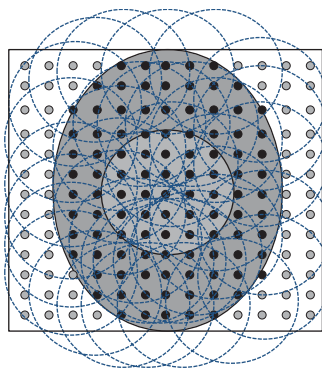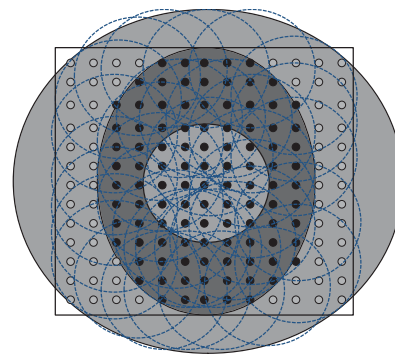
Figure 6.6: Ripple propagation throughout the network: (a) an initiator sensor node that signals start of a tournament. Sensor nodes within the communication range of this node then perform one tournament; (b) nodes participating in the previous tournament become initiator nodes in this round; (c) and (d) ripple moves toward the border of the network; and (e) all sensor nodes are activated.

Algorithm 12: *Function* `timeslot-assignment`*(G_i), executed on the leader node*

---

1 **begin**
2     $\{C\} \leftarrow \emptyset$ // possible chromatic numbers set
3     $k_{min} = 0, k_{max} = d + 1, continue = 1, k\text{-}colorable = 0$
4   **while** $\underline{continue == 1}$ **do**
5         $k = \lceil \frac{k_{max} - k_{min}}{2} \rceil + k_{min}$
6   **if** $\underline{k\text{-}colorable == 1}$ **then** // feasible to color the graph with k number based on the heuristic in [KP87]
7             $k_{max} = k$
8   **if** $\underline{\{C\} \neq \emptyset}$ **then**
9   **foreach** $\underline{k_i \in \{C\}}$ **do**
10   **if** $\underline{k \geq k_i}$ **then**
11                         $continue = 0$
12   **end**
13   **end**
14   **end**
15             $\{C\} \leftarrow k$
16   **else**
17             $k_{min} = k$
18   **end**
19   **end**
20     $\Delta \leftarrow min\{C\}$
21 **end**

---

the global extrema. It uses the concurrent transmission property of the dominance-based protocol to find the `MIN` in an MBD network. The details of the ripple-based approach are provided in Algorithm 13. A good analogy for this algorithm is a ripple's propagation on a water surface, and Figure 6.6 illustrates this approach with an example. Initially, all sensor nodes are inactive (n_i–*active* $= 0$); that is, they do not participate in any tournament. The process is initiated by a sensor node broadcasting a query for computing the global `MIN`. We assume that the query signal is a modulated wave, which is used both for synchronization and starting a new tournament. Sensor nodes that receive this signal (that is, in the initiator node's range), perform one tournament of the dominance protocol to find a `MIN` value. Since only a subset of all nodes are participating in this stage, the resulting value is a local `MIN`. Immediately after finishing the first tournament, all sensor nodes, that had participated in the last tournament, initiate another tournament of the dominance protocol by sending a new query signal (with the new `MIN` value). This tournament in turn activates those sensor nodes, which are situated within the communication range, to

---

Algorithm 13: *Ripple-based approach, executed on each sensor node n_i*

1 **begin**
2   n_i–active= 0, $i = 0$
3   **while** $i \leq 2 \times \lceil D/R_{co} \rceil$ **do**
4          $i{+}{+}$
5   **if** n_i–active== 1 **then** broadcast the query signal
6   **else if** n_i receives a query signal **then**
7   n_i–active= 1
8   **end**
9   execute one dominance *round*
10   **end**
11 **end**

---

change their status from idle to tournament state. This procedure continues until all nodes get activated.

To compute the global MIN in an MBD network, the tournament needs to be run in worst case $\mathcal{N} = 2 \times \lceil \frac{D}{R_{co}} \rceil$ times where, D is the network diameter in number of hops and R_{co} is the communication range of sensor nodes. Note that this is an upper-bound on the number of tournaments that needs to be performed till all nodes in the network become aware of MIN. Figure 6.7 reveals the rationale behind this process with an example. This bounding event occurs when the sensor node with the lowest value and the initiator node are located at opposite ends of the network (that is, initiator is D hops away from the sensor with the lowest value). Hence, it takes twice the length of $\frac{D}{R_{co}}$ to assure that the MIN value is propagated to all sensor nodes. The $\mathcal{N}$ times execution of the tournament is corresponding to one application of $\mathcal{M}$ function, or simply, one *round* in the MBD network. At the end of each *round*, the winner node broadcasts a packet which includes its location information and its identifier. This message is then flooded throughout the network, using the ripple-based approach, such that all nodes have the same knowledge about the properties of the winning node. Note that, in SBD, this information is broadcasted once by the winner.

Figure 6.8 shows an example of computing MIN in an MBD network, where the place of each node is represented by its measured value. In this example, we assume that the node located at the center of the network initiates the query for computing MIN (see Figure 6.8-a). Sensor nodes in the communication range of the initiator execute one
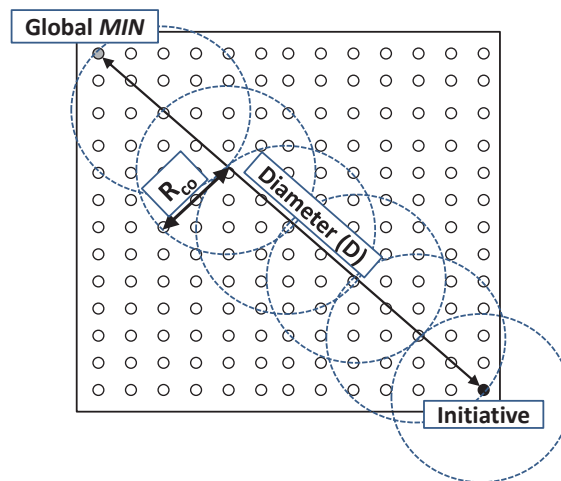
Figure 6.7: An example of the worst case scenario to determine the required number of tournament ($\mathcal{N}$). Assuming $D = 12\sqrt{2}$ and $R_{co} = 2\sqrt{2}$, the number of tournaments will be $\mathcal{N} = 2 \times \lceil \frac{D}{R_{co}} \rceil = 12$, i.e. two times the number of circles depicted in this figure. It takes six tournaments to activate the node with `MIN` and another six tournaments to receive back the global `MIN` by the initiative sensor node.

tournament. Since nodes that are located in the border of the communication range of the initiator are not reachable by each other, border sensor nodes find different `MIN` values according to their location.

Figure 6.8-b shows the result of finding `MIN` after execution of the first tournament. The two local `MIN` values (1 and 2) are propagated in the first tournament. In the next iteration, all activated nodes perform the tournament and update their `MIN` values (see Figure 6.8-c). Finally, after five tournaments, the global `MIN` is known throughout the network.

However, the multi-hop protocol described above can suffer from the hidden terminal problem. As dominance-based protocols allow nodes to listen to `MIN` value even from simultaneous receptions, hidden terminals in this case can cause a device in the middle, to learn a spurious `MIN` value.

To elaborate, consider three sensor nodes N_1, N_2 and N_3 (with measured values 1, 2 and 3, respectively) as depicted in Figure 6.9. According to dominance-based protocols, during the tournament a sensor node transmits its measured value bit-by-bit. Upon knowing the existence of other nodes with a smaller measured value, it stops sending the rest of the bits. Now consider the scenario given in Figure 6.9-b. Node N_3 loses the tourna-
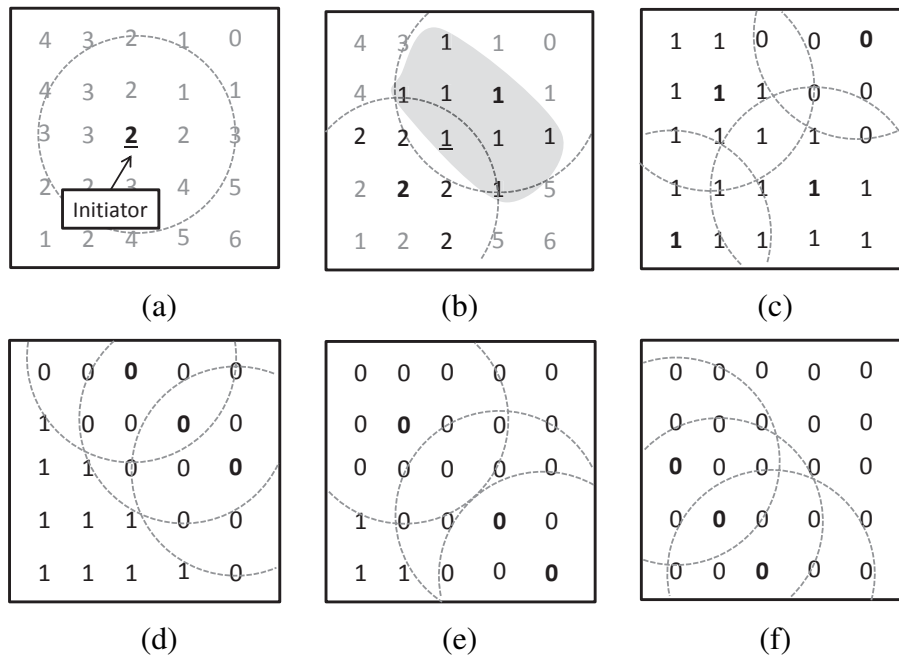
Figure 6.8: Compute MIN in the MBD network. The evolution of determining the MIN value is shown in (a)-(f). The network diameter $D = 5$ and communication range $R_{co} = 2$. Pale numbers show inactive sensor nodes; dotted circles show the communication range in an SBD; the effective sensor nodes are shown in bold.
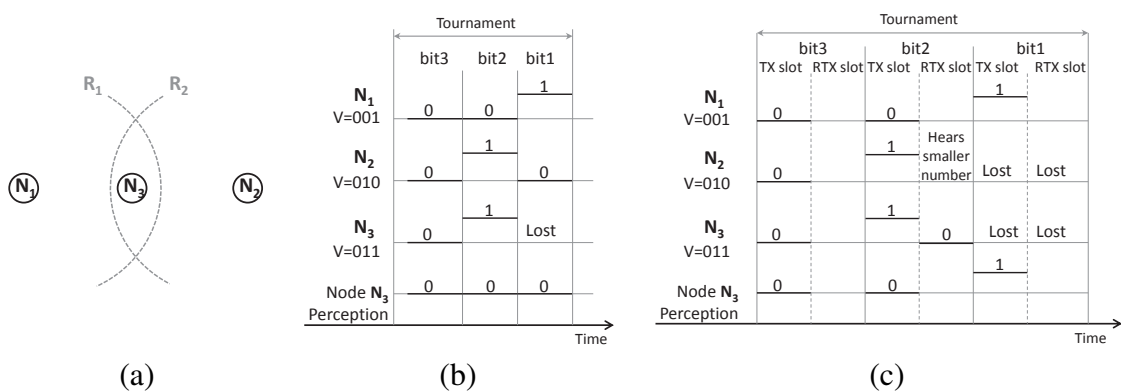
Figure 6.9: Example of hidden terminal problem during a tournament execution (we assume three priority bits) (a) network topology, (b) execution of tournament that leads to an error in node N_3, and (c) execution of tournament, including an extra time slot for bit retransmission.

ment after receiving the smallest value from node N_1. Since node N_1 and N_2 are not able to communicate directly, node N_2 proceeds sending its last bit, which is 0, and node N_3 mistakenly perceives `MIN` in the network as being 0.

To avoid this problem, we consider two slots for each bit transmission as proposed in [PATR07]. The first slot is dedicated to the bit transmission itself and the second slot is dedicated to the retransmission of the bit detected during the first slot. If the current bit of a sensor node is dominant, there is no need to retransmit this bit for the second time, but if the bit is recessive and the sensor node detects a dominant bit during the transmission slot, it retransmits a dominant bit in the following retransmission slot (see Figure 6.9-c). This bit-level redundancy solves the problem and leads to the correct perception of `MIN` in the network. Obviously, it will increase the tournament duration.

6.6   Evaluation

We evaluated our proposed approaches in different simulated scenarios by considering the following three metrics:

Number of Rounds. A sensor node gets channel-access permit to broadcast a message in one *round* of execution of the $\mathcal{M}$ function if its value is the global minimum. Hence, the number of *rounds* corresponds to the number of message broadcast or flooding.

Accuracy. It represents the fraction of sensor nodes that declare themselves to be located in the active region(s) N_{det} to the number of sensor nodes that truly lie in the active region(s) N_{true}:

$$\text{Accuracy} = \frac{N_{det}}{N_{true}} \times 100(\%). \tag{6.7}$$

In cases where the detected area is larger than the actual active region, ($N_{det} > N_{true}$), accuracy is more than 100%, which signifies the overestimation of the active region.

Execution Time. It is the time needed to extract the various features according to the proposed *augmenting functions* and is computed as follows:

$$\text{Execution Time} = \text{Number of Rounds} \times T_{\mathscr{M}} \tag{6.8}$$

where, $T_{\mathscr{M}}$ is the execution time of the $\mathscr{M}$ function. In SBD networks, $T_{\mathscr{M}}$ is equal to one tournament duration. However, in MBD networks, $T_{\mathscr{M}}$ depends on the approach used for computing the global extrema (as discussed in Section 6.5).

We first show the process of computing $T_{\mathscr{M}}$ in MBD networks, and then evaluate the feature extraction techniques for various exemplifying scenarios.

6.6.1 Computing the Execution Time of $\mathscr{M}$ Function, $T_{\mathscr{M}}$

As stated earlier, the application of $\mathscr{M}$ function results in identifying the global `MIN` over values of sensor nodes in a shared medium.

We consider a network of size 100×100 sensor nodes in a shared medium. We change the communication range of sensor nodes R_{co} to study the performance of the new ripple-based and the classical cluster-based approaches in scenarios where the communication range of the sensor nodes would divide the network into multiple broadcast domains. For the cluster-based approach, where clusters are built based on a virtual range, we set the range of virtual communication r, to be always half of the actual communication range (R_{co}) of the sensor nodes.

To have a precise computation of a tournament round, we consider the timeouts as given in Section 4.4.1, Table 4.4. As illustrated in Figure 6.9 to solve the hidden terminal problem in the ripple-based approach, it is needed to send each bit twice during the tournament. Considering $110\mu s$ as the length of one bit exchange, the tournament takes $110 \times n_{prio} + \eta \mu s$ for the cluster-based approach and $2 \times 110 \times n_{prio} + \eta \mu s$ for the ripple-based approach where, n_{prio} is the number of priority bits and η is the time overhead imposed by the MAC protocol during the tournament. This extra time overhead is mainly due to synchronization and hardware shortcomings. For $n_{prio} = 15$, the value of extra time overhead is $\eta = 3099\mu s$. Accordingly, the tournament takes $4749\mu s$ and $6399\mu s$ for the cluster-based and the ripple-based approaches, respectively.

Table 6.2: Computation time of the `MIN` value in the cluster-based and the ripple-based approaches

Communication	Cluster-based (R_{co}, r)		Ripple-based (R_{co})	
range	Tnmt[a]	Time(μs)	Tnmt[a]	Time(μs)
$R_{co} = 14, r = 7$	12	159388	8	96248
$R_{co} = 20, r = 10$	10	137602	5	64763
$R_{co} = 28, r = 14$	10	141698	4	50172
$R_{co} = 34, r = 17$	11	150543	3	39677
$R_{co} = 40, r = 20$	10	137602	3	35581

[a]Number of referenced tournaments.

Table 6.2 shows the number of referenced tournaments along with the time needed to find the global extremum in an MBD network. In this computation we took into account the time needed to aggregate data in the case of the cluster-based approach, as well as the time required for flooding the local information of the winner in the ripple-based approach. However, in both cases we assume the best case scenario. For data aggregation through the black-node tree, we first compute the maximum degree d of the cluster interfering graph (see Figure 6.5-a). To prevent any collision, it is considered that we need to have at least d time-slots to collect data in the leader node. The duration of the time-slot is considered to be the time needed to transmit a 128 byte-size packet. Assuming the IEEE 802.15.4-compliant MICAz's radio [CRO04] with data rate of 250 Kb/s, the time-slot duration (T_s) is then $4096 \mu s$.

For the ripple-based approach, we compute the flooding time according to the theoretical lower latency bound given in [FZTS11]. In that work, the authors simplify that given that nodes transmit concurrently, the theoretical lower latency bound in a network with size h hops is $h.(T_s + T_d)$. The number of hops is computed as $h = \lceil \frac{D}{R_{co}} \rceil$, where D is the network diameter and R_{co} is the communication range of sensor nodes. T_d is the radio processing delay, which is in the order of a few microseconds and is determined by the radio; for simplicity, we ignore T_d in our computation.

As expected, increasing the communication range results in a faster computation of `MIN` with the ripple-based approach. Also, this method needs a smaller number of tournaments as compared to the cluster-based approach. However, in the cluster-based approach,

we do not observe the same continuous descending trend in the number of referenced tournaments. The reason is that the placement of the clusters plays an important role in the construction of the black-node tree and the cluster interfering graph that affects the *d* value.

It should be mentioned that the given time for both approaches is slightly optimistic. In the cluster-based approach, we do not consider the extra overhead imposed by the setup phase for cluster formation and similarly in the ripple-based approach we have used the lower bound of the flooding delay as in [FZTS11]. Note that in the cluster-based approach, not all sensor nodes become aware of MIN, while, in the ripple-based approach, which is a fully distributed algorithm, all nodes would know MIN.

6.6.2 Identifying the Active Regions

We consider the same network settings as described in the previous subsection, with the size of 100×100 sensor nodes. First, we show the performance of *distance augmenting function* to identify circular active regions. For evaluating our approach, we generate various scenarios with several active regions. The active regions may or may not overlap resulting in complex *fields*. The details of the scenarios are provided in Figure 6.10.

In each *round* of execution, after finding the global maximum, all the sensor nodes compute local values of ϕ_β according to Equation 6.1. Figure 6.11 illustrates the number of circular active regions with different termination rules for scenario *sc1*. Increasing the threshold level helps the algorithm to converge faster in smaller number of *rounds*, but at the cost of reduced accuracy.

Figure 6.12 shows the number of *rounds* and the corresponding obtained accuracy for different threshold values. We believe that the property of the *field* plays an important role on the number of required *rounds* and on the accuracy of the detection. In some scenarios, increasing the termination threshold reduces the number of *rounds* as well as the overestimated area. This happens for scenarios *sc1*, *sc3* and *sc6*, where the active regions can overlap. However, for scenarios *sc2*, *sc4* and *sc5*, where either few active regions exist or active regions are far apart, the number of *rounds* and the accuracy remains almost the same for all termination conditions. The existence of isolated peaks in the *field*
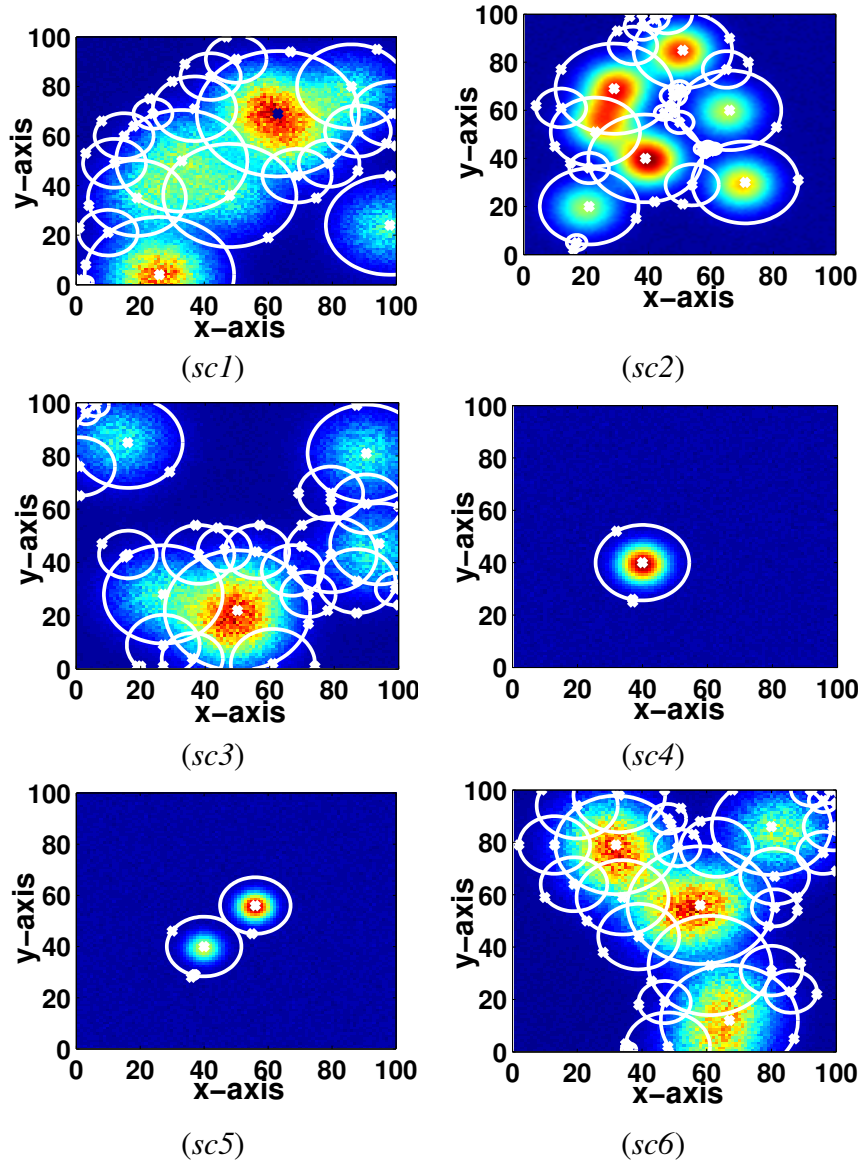
Figure 6.10: Six scenarios with different active regions; each sensor node sets the value of $\beta = 10$ to compute its priority —see Equation (6.1-6.3). Each circle represents one filtering zone that is computed by two readings from the sensor network and excludes sensor nodes located inside the circle from participation in the future iteration(s) of the algorithm. π_s is set to 10% of the global maximum value.

(a) (b)
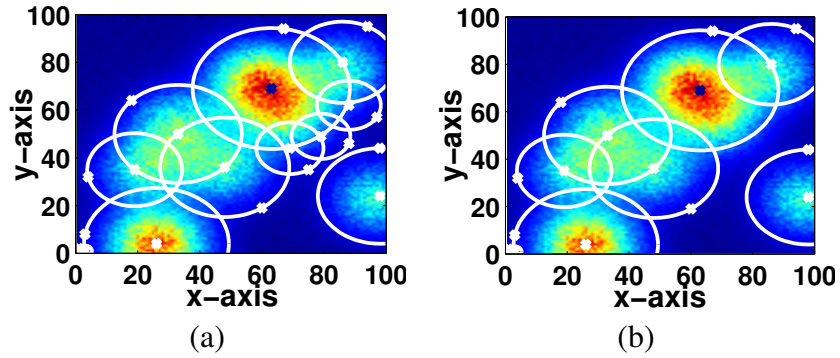
Figure 6.11: The effect of termination threshold, π_s on the detection of active regions. The algorithm terminates when a new detected peak is (a) 20% and (b) 30% of the global maximum value.
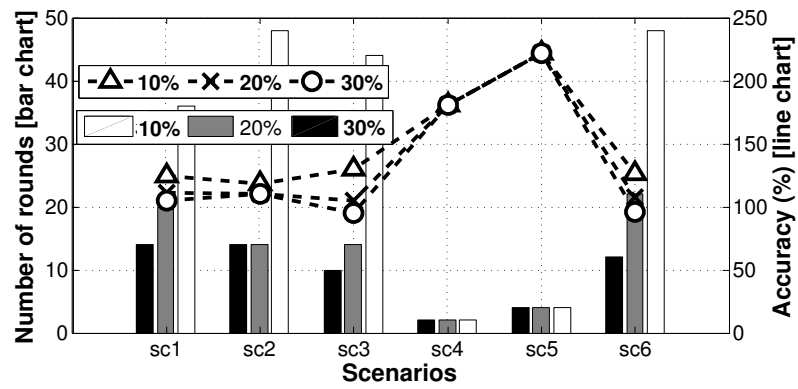
Figure 6.12: The number of *rounds* and the accuracy of active region estimation under the different scenarios for various $\pi_s = \{10\%, 20\%, 30\%\}$ of the global maximum.
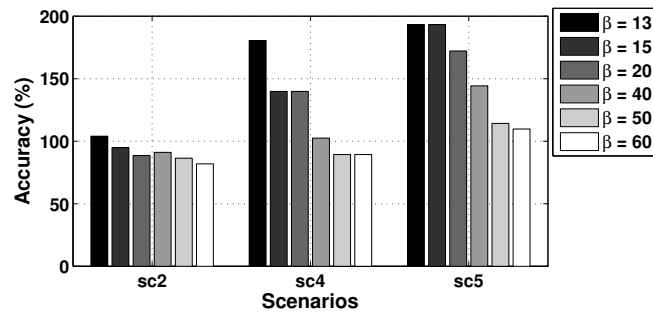
Figure 6.13: The effect of β on the accuracy.
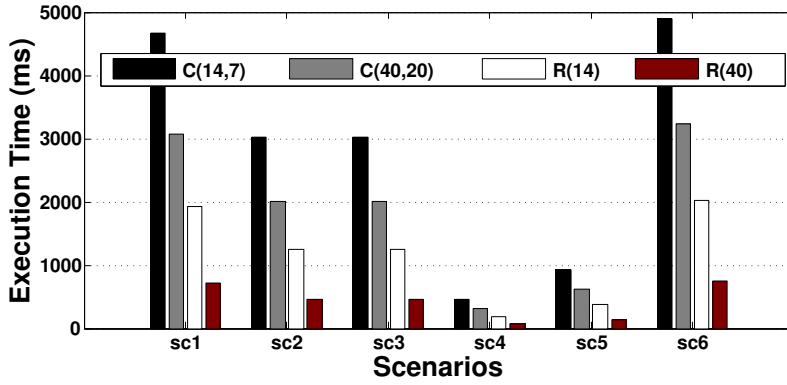
Figure 6.14: Execution time of $\mathscr{A}_\beta$ ($\beta = 10$, $\pi_s = 20\%$) in an MBD network with different communication ranges for the cluster-based approach: {C(14,7), C(40,20)} and the ripple-based approach: {R(14), R(40)}.

results in identifying all active regions by a fixed number of circular sections. The high value of overestimation in *sc4* and *sc5* is due to the steepness of the peak in the *field*. This steepness causes an overestimation in the filtering radius which in turn leads to a much larger (squared) overestimation of the circle's area.

We found that the choice of the exponential coefficient β in our given heuristic (Equation 6.3) affects the overestimation of active regions. In fact, the coefficient β impacts the relative weight of distance from the peak with respect to the value of the *field* at a given point. Choosing an optimal value of β is not possible without the prior knowledge of the *field*, but the order of β can be chosen based on the size of the *field* such that a proper trade-off between the sensor value at a given sensor node and its distance from the peak is maintained. Particularly, β should be chosen such that the impact of distance can be pronounced as compared to the distance normalization (d_{max} in Equation 6.3). For an area of 100×100, we found that suitable values of β are in the order of 10. Specific results on the accuracy for the scenarios *sc2*, *sc4* and *sc5* are shown in Figure 6.13. The main goal of this experiment is to investigate the level of overestimation given by $\mathscr{A}_\beta$. It is observed that for scenarios with isolated peaks, higher values of β improve the coverage estimation accuracy ($\beta = 40$ for scenario *sc4* and $\beta = 60$ for scenario *sc5*). But for scenarios where the spread of peaks overlap, the effect of changing β is less pronounced, as in the case of scenario *sc2*.

Figure 6.14 shows the time it takes to detect the location of active regions by $\mathscr{A}_\beta$.

We examined the performance of the cluster-based and the ripple-based approaches for different communication ranges $R_{co} = \{14, 40\}$, which are the extreme ranges (shortest and longest) in Table 6.2 . Interestingly, the execution time of $\mathscr{A}_\beta$ under the ripple-based approach is at least 58% faster than that for the cluster-based approach. Increasing the communication range from $R_{co} = 14$ to $R_{co} = 40$ leads the algorithm to be 63% faster under the ripple-based approach while it improves the cluster-based approach only by 34%.

6.6.3 Convex-hull Around Active Regions

For evaluating the convex-hull approach described in Section 6.4.2, we convert the *field* to a binary *field* by thresholding, such that a sensor node's value is 1 if the sensed value is greater than 10% of the maximum value, and 0 otherwise. The details of the scenarios are provided in Figure 6.15. We set the marginal extension angle to $\varepsilon = 1°$ and $\gamma = 1$. We compared our technique with a TDMA approach, where a fixed number of randomly chosen sensor nodes send their measurements. For the random approach, the number of readings was set to 150.

Figure 6.16 shows the accuracy of our second technique in terms of average percentage of coverage area by running the simulation over 100 iterations. As shown, our technique covers more than 97% of the area in all the scenarios through transmitting 26 to 33 broadcast messages compared to 36% to 72% coverage by 150 randomly chosen packets. Hence, we acquire a more accurate boundary estimation with 77% less broadcast messages.

Increasing the marginal extension angle, ε, still provides a satisfactory coverage area estimation, while reducing the number of messages. We tested the performance of our proposed algorithm with different marginal extension angles in all the mentioned scenarios. As shown in Figure 6.17, by increasing ε, the number of *rounds* decreases, since by enlarging the angle, more search space is filtered out and consequently less packets are needed to be broadcast.

However, increasing ε might diminish the performance of the algorithm in terms of estimated coverage area. Figure 6.18 shows the performance degradation by increasing
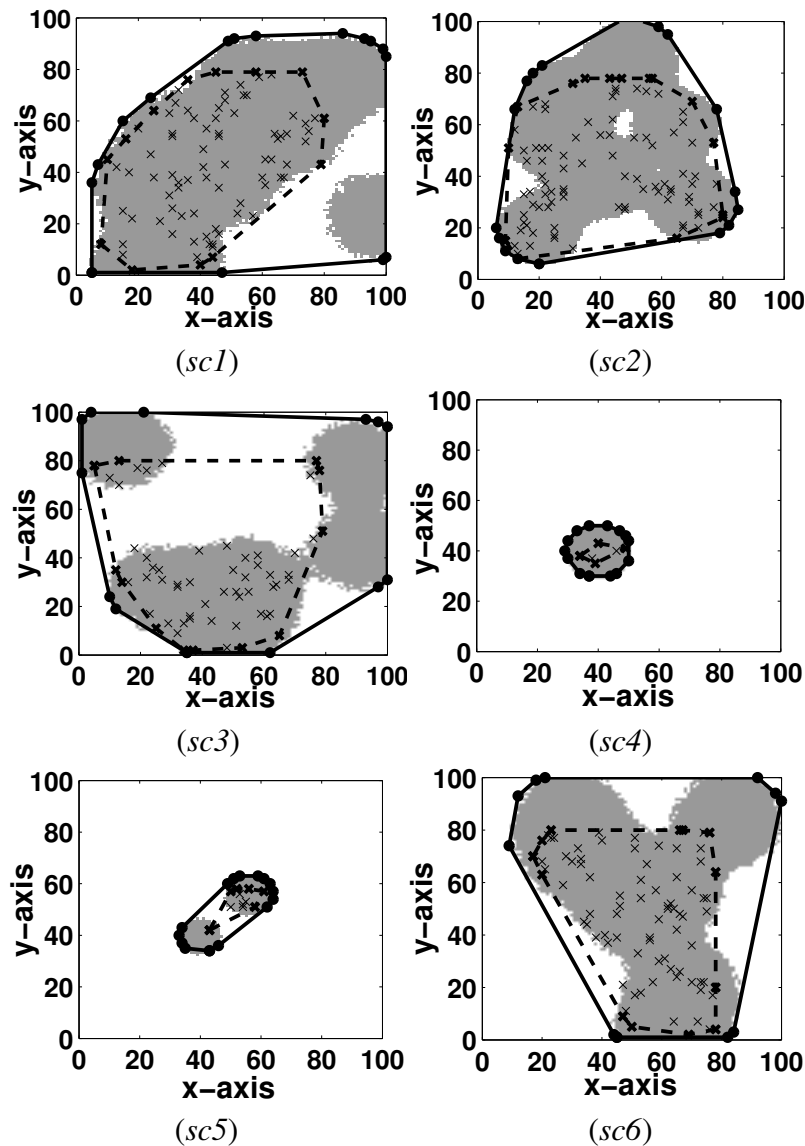
Figure 6.15: Six scenarios with different active regions; solid lines show the boundary computed by our algorithm with $\varepsilon = 1°$ and 40 iterations of the algorithm, and dash lines show the boundary computed by the random algorithm with 150 random readings.

the ε up to $90°$. Under the latter setting, the proposed algorithm is able to cover around 70% of the active region. In addition to the shown value of ε in the graph, we also ran the simulation for $\varepsilon = \{5°, 10°\}$ and took the standard deviation of the average coverage area for $\varepsilon = (1° : \varepsilon)$. Since the results for $\varepsilon = \{5°, 10°\}$ were very close to the case where $\varepsilon = 1°$, the coverage area computed by these values is not shown in the figure. As can be seen in Figure 6.18, $\varepsilon = 15°$ has the smallest standard deviation (smaller than 0.65), which suggests that the coverage area computed by $\varepsilon = 15°$ leads to the same coverage
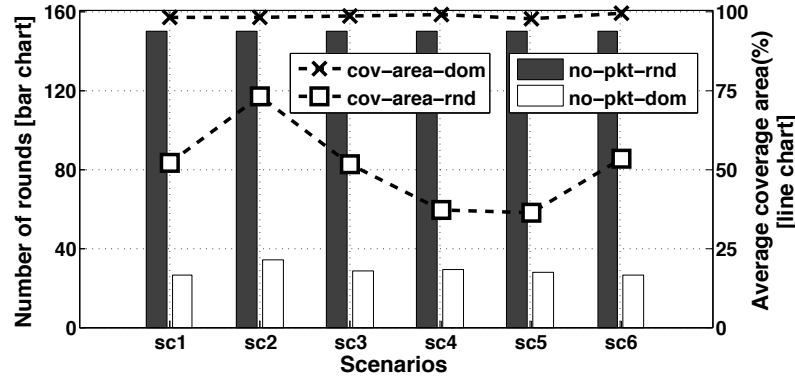
Figure 6.16: The number of *rounds* for $\mathscr{A}_\gamma$ (no-pkt-dom) and random approach (no-pkt-rnd) and the average coverage area estimation for $\mathscr{A}_\gamma$ (cov-area-dom) and random approach (cov-area-rnd) in different scenarios.

area as given by $\varepsilon = 1°$, while at the same time using $\varepsilon = 15°$ requires a much smaller number of *rounds* as compared with a $\varepsilon = 1°$ setting, as shown in Figure 6.17.

Figure 6.19 shows the execution time of *vector augmenting function* $\mathscr{A}_\gamma$ in an MBD network. In this experiment we set $\varepsilon = 15°$. As expected, the proposed ripple-based approach provides a faster detection than the cluster-based approach, independent of the communication range setting. Figures 6.14 and 6.19 show that while there are severe fluctuations in the execution time of $\mathscr{A}_\beta$ for the discussed scenarios, the execution time of $\mathscr{A}_\gamma$ is almost the same in all scenarios. The reason is that unlike $\mathscr{A}_\gamma$, the number of required *rounds* in $\mathscr{A}_\beta$ depends on the number and the location of active regions. The same reasoning is also applied to Figures 6.12 and 6.17.
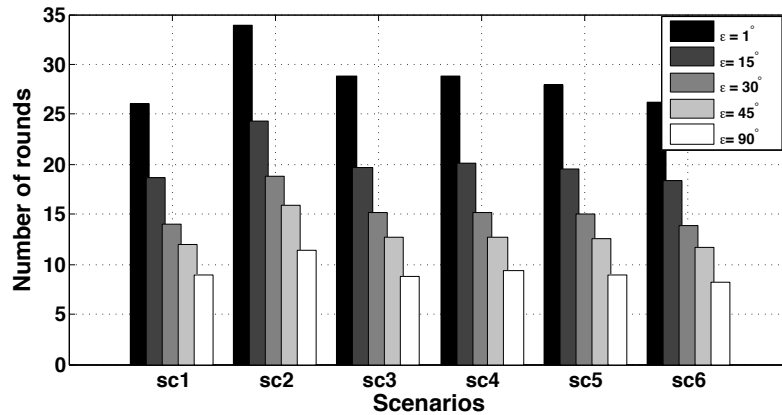
Figure 6.17: The number of *rounds* in $\mathscr{A}_\gamma$ with different marginal extension angle, ε.
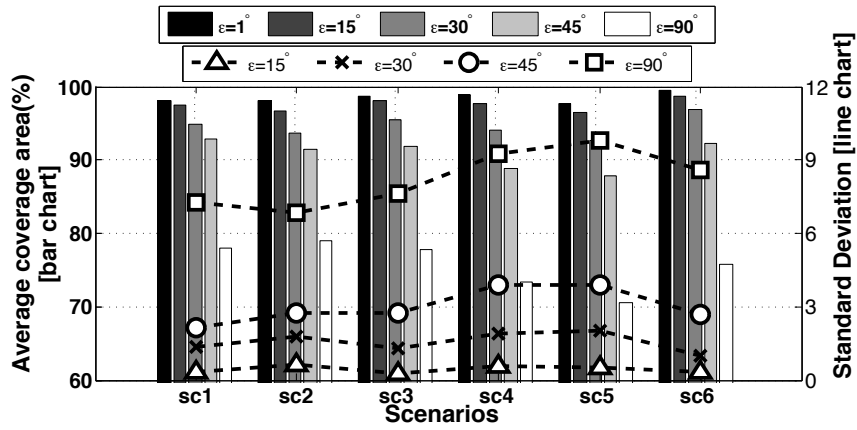
Figure 6.18: The average of estimated coverage area with different marginal extension angle, ε and its standard deviation.
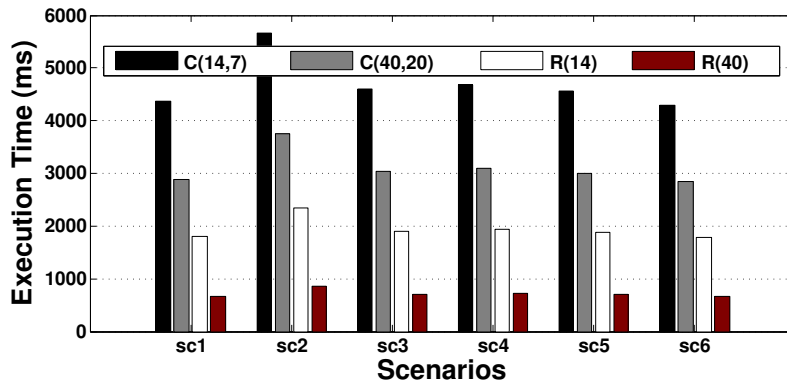
Figure 6.19: Execution time of $\mathscr{A}_\gamma$ ($\gamma = 1, \varepsilon = 15°$) in an MBD network with different communication ranges for the cluster-based approach: {C(14,7), C(40,20)} and the ripple-based approach: {R(14), R(40)}.
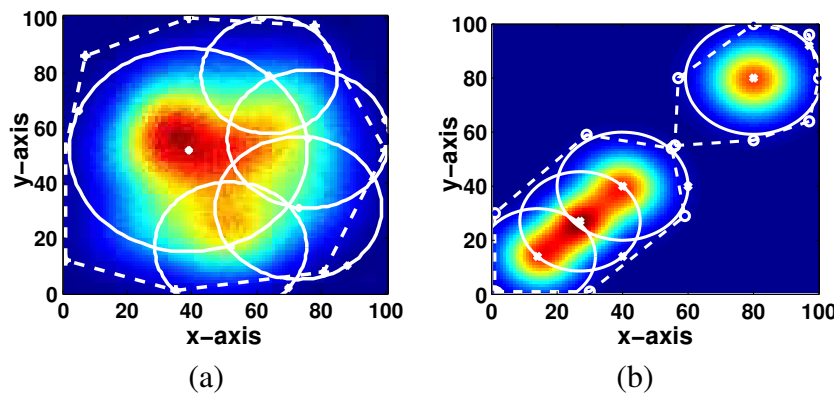
Figure 6.20: $\mathscr{A}_\beta$ versus $\mathscr{A}_\delta$, dash lines show the boundaries provided by $\mathscr{A}_\delta$, and solid lines refer to active regions detected by $\mathscr{A}_\beta$; (a) $\beta = 30$, $\gamma = 0.3$; (b) $\beta = 30$, $\gamma = 0.2$; with $\beta = 10$ for $\mathscr{A}_\beta$.

6.6.4 Non-circular Active Regions

As discussed in Section 6.4.3, $\mathscr{A}_\delta$ helps in finding the boundary of a non-circular active region, instead of identifying circular active regions from a complex shape.

Figure 6.20 shows the comparison of the performance of *distance augmenting function* with the *joint augmenting function*. For scenarios where a number of active regions lie very close to each other, the number of rounds required by $\mathscr{A}_\beta$ is 20% more than that for $\mathscr{A}_\delta$. For more sparse events, the number of rounds required by $\mathscr{A}_\beta$ is 50% less as compared to $\mathscr{A}_\delta$. This happens due to the higher number of iterations that are needed to be performed by $\mathscr{A}_\delta$ to find the boundary of more than one complex shape. It should be noted that $\mathscr{A}_\delta$ is able to find the boundary of a non-circular active region and to detect it as one region instead of a group of several close active regions.

The comparison of *vector augmenting function* and joint augmentation is shown in Figure 6.21. It is evident that the combined approach helps in demarcating different active regions, while $\mathscr{A}_\gamma$ detects the overall outer boundary. Figure 6.22 shows the execution time of the *augmenting functions $\mathscr{A}_\beta$, $\mathscr{A}_\gamma$ and $\mathscr{A}_\delta$* in an MBD network for the cluster-based and the ripple-based approaches with different communication range for the scenarios given in Figure 6.21(a) and (b). We observe that for scenarios with overlapping events, $\mathscr{A}_\delta$ converge faster, while $\mathscr{A}_\beta$ outperforms other *augmenting functions* for scenarios with sparse events.

We further examined the cluster-based and the ripple-based approaches to compare

(a)   (b)
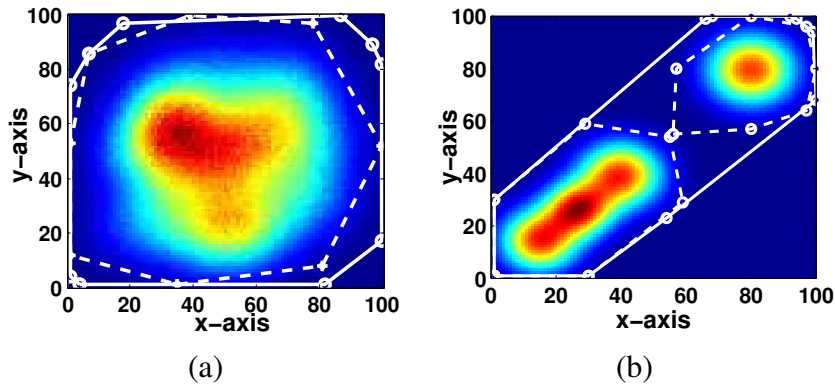
Figure 6.21: $\mathscr{A}_\gamma$ versus $\mathscr{A}_\delta$, dash lines show the boundaries provided by $\mathscr{A}_\delta$ and solid lines refer to that given by $\mathscr{A}_\gamma$ (a) $\beta = 30$, $\gamma = 0.3$; (b) $\beta = 30$, $\gamma = 0.2$; with $\varepsilon = 15°$ for $\mathscr{A}_\gamma$.

(a)   (b)
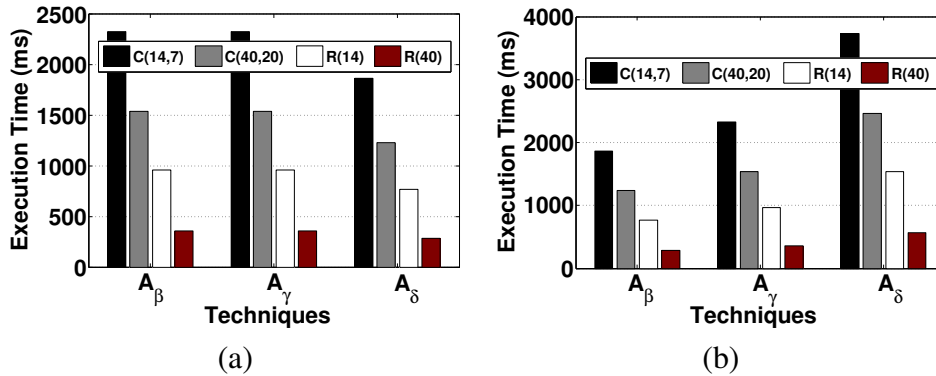
Figure 6.22: Execution time of different *augmenting functions* in an MBD network with different communication ranges for cluster-based approach {C(14,7), C(40,20)} and ripple-based approach {R(14), R(40)}: (a) considering scenarios depicted in (Figure 6.21-a) and (b) considering scenarios depicted in (Figure 6.21-b).
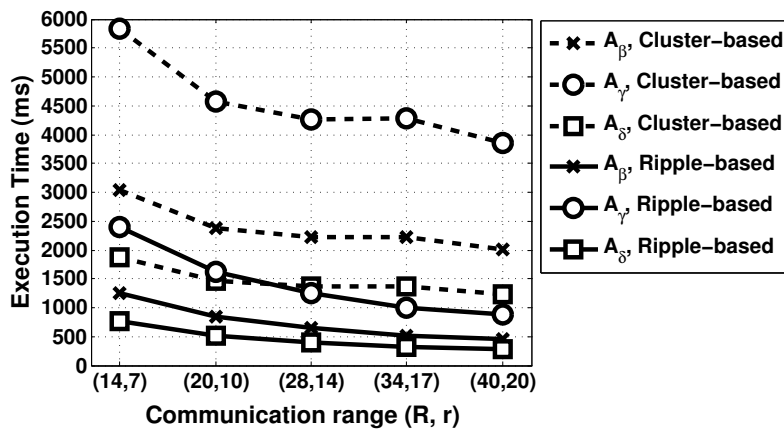
Figure 6.23: The computation time of various feature extraction techniques ($\mathscr{A}_\beta$, $\mathscr{A}_\gamma$ and $\mathscr{A}_\delta$) for scenario *sc2* with $\pi_s = 20\%$, $\varepsilon = 15°$, $\gamma = 1$, $\theta = \pi/4$.
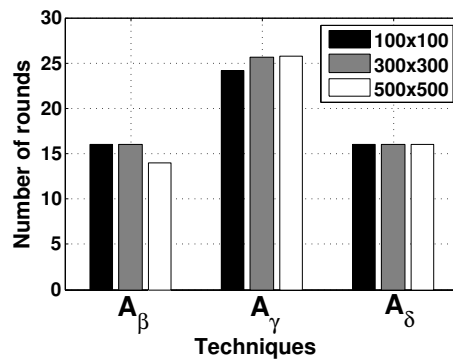
Figure 6.24: The impact of density on the performance of each technique for scenario *sc2*.

the time needed to extract different features according to the augmenting functions given in Section 6.4 for a single scenario. Figure 6.23 shows the elapsed time for different augmenting functions ($\mathscr{A}_\beta$, $\mathscr{A}_\gamma$, $\mathscr{A}_\delta$) for the sample scenario *sc2* over a 100×100 network. We chose this scenario because, according to the results in Section 6.6, this scenario includes the most complex *field*. It is evident that for all communication range settings, and for all augmenting functions, the proposed ripple-based approach outperforms the classical cluster-based approach.

6.6.5 The Impact of Network Density

Finally, we compare our techniques under various network densities. As our techniques only depend on collecting the global extrema of various *augmenting functions*, the results indicate that increasing the network density has almost no impact on the number of rounds. Figure 6.24 shows the number of *rounds* required in each technique with respect to the network size. The slight variation in the number of *rounds* is due to the effect of termination condition in $\mathscr{A}_\beta$ and the randomness in the choice of θ in $\mathscr{A}_\gamma$.

6.6.6 Alternative Flooding Approaches

Many emerging cyber physical systems need mechanisms to share and process data among all devices in the network. The ripple-based approach, proposed in this work, is one such mechanisms, in the sense that it computes an aggregate quantity over all the devices. Chaos [LFZ13] and Low-power Wireless Bus (LWB) [FZMT12] are two other examples

of such mechanisms that build their data collection or dissemination capabilities based on the Glossy protocol [FZTS11].

Since we aim at obtaining an efficient and scalable algorithm with low time-complexity, we compare the performance of different flooding approaches based on execution time and scalability. Chaos outperforms LWB in terms of completion time [LFZ13]. In fact Chaos is able to collect small amounts of data, such as a 1-byte payload, from a 100-node network within less than 100 *ms*. We believe that there are two main advantages of our proposed ripple-based approach over Chaos. Firstly it provides a faster execution time; considering the tournament duration 6399 μs (see Section 6.6.1), in the ripple-based approach, all nodes will know MIN in at most 52 *ms* within a seven-hop network deployment. Secondly, it offers better scalability; in fact while in Chaos the number of nodes is limited to 856 in a SBD (unless some data compression mechanism is applied), our ripple-based approach does not limit the number of involved devices.

6.7   Concluding Remarks

Low-power wireless sensor networks enable many emerging applications that need thousands of sensor nodes for control and monitoring. In this chapter, we presented a set of techniques that identify various *features* in the distribution of sensed physical quantities over a dense deployment of sensor nodes. With such simple yet effective modifications, we can obtain the location and shape of active regions with a number of messages proportional to the properties of the *field*. Our feature extraction techniques are efficient in the sense that they collect data from just the sensors that have more effective information for revealing the status of the monitored area.

We proposed a fully distributed approach to make our feature extraction scale with large dense networks, where sensor nodes lie in a multiple broadcast area.

Chapter 7

Conclusions, Perspective and Future Directions

This chapter reviews the research objectives of the Thesis and summaries its major results, highlighting how the research contributions fulfilled the original research objectives. Some guidelines for future research work in the area are also provided.

7.1 Summary of the Work

In this work we aimed at designing large-scale dense networked sensor systems where the sensing is performed at a very fine granularity, both in space and time. Previous research work [APE$^+$08, ETPA11, PGAT09] has proposed algorithms for obtaining an interpolation of sensor readings from different sensor nodes, and these algorithms are based on dominance protocols, presenting therefore excellent scalability properties for densely instrumented CPS. We believe however that it was possible to improve the performance of those algorithms not only by taking advantage of knowledge of often-occurring spatial correlation of sensor readings but also by embedding the dynamics of the physical phenomenon in the algorithms. We further proposed efficient novel mechanism able to extract meaningful features from the high spatial resolution of sensor readings utilizing the same building block as used for obtaining the interpolation: `MIN`.

123

7.1.1 Review of Research Objectives

To address the problem of reliable and timely data transmission and data aggregation in dense sensing networks, we defined the following three theoretical objectives:

1. Devising an error recovery scheme for WiDOM protocol in a noisy wireless channel.

2. Devising a mechanism that captures the dynamics of the physical quantities and self adapts according to the physical changes.

3. Devising a set of algorithms to identify various features in a distribution of a physical quantity.

7.1.2 Main Research Contributions

Next we briefly summarize the main research contributions.

Improving the reliability of the wireless communication infrastructure. Sensor nodes must communicate using a shared broadcast medium (such as a shared bus or a wireless channel), as it would be unfeasible (due to the number of nodes) to deploy dedicated communication channels for each sensor/actuator node. The WiDOM protocol is known as a MAC protocol suitable to be exploited to allow computation of aggregate quantities in wireless. In order to reduce the large overhead of the WiDOM protocol, the slotted WiDOM was proposed. However, none of these designs were considered to tolerate errors that may occur in data transmissions. One of the main contributions of this research work is the introduction of an error recovery scheme able to significantly improve the reliability of the WiDOM protocol and as such to increase the utility of the approach for computing complex aggregate quantities. We develop this scheme over slotted WiDOM since it offers lower overhead as compared to the original WiDOM design.

Developing scalable and efficient aggregate quantities that consider the physical dynamics. Previous works tackling densely deployed networked sensor systems have proposed algorithms that allow computing an approximate interpolation of sensor readings by exploiting dominance-based protocols. The second main contribution in this Thesis is a novel approach for computing approximate interpolations, where the algorithm is

self-adaptable to incorporate the physical dynamics and the trade-offs between accuracy and timeliness.

Extracting various features from the distribution of the physical quantity being monitored. Many CPS applications need to detect regions with specific level of *activities* immediately after the occurrence of an event. While computing the interpolation together with a centralized signal processing technique might be considered as an option, we devised a set of fully distributed algorithms that provide meaningful information from the distribution of the physical quantity without the need of having the interpolated image. We showed that similarly to the case of interpolation algorithm, the time complexity of the novel algorithms depends only on the property of the distribution of the physical quantity.

Extending the feature extraction algorithm to multi-hop networked infrastructures. To extend the devised algorithm to work in a multi-hop network, we devised a distributed approach that takes advantage of dominance-based protocol. We further examined the functionality of the proposed multi-hop approach against the traditional cluster-based approach and revealed that our novel approach outperforms the traditional approaches.

7.1.3 Validation of the Hypothesis

We have shown through extensive evaluations that it is possible to extract certain features of a physical phenomenon in a dense sensing network with a time complexity that is independent of the number of sensor nodes.

7.2 Future Directions

There are several opportunities that can be identified for further research:

– **Devising distributed algorithms for extracting other features or computing different aggregate quantities over a distribution of a physical quantity (related to Chapter 6).** It is shown that the efficient computation of MIN through exploiting dominance-based protocol can serve as the basic building block for extracting

different features from a physical signal. Leveraging `MIN` computation would eventually be considered to further develop other aggregation algorithms.

– **Implementing the feature extraction algorithms on a real dense sensor platform using WiDOM protocol (related to Chapter 6).** An experiment is required, using a test bed, to implement a dense sensor network to observe a phenomena and verify the results discussed in Chapter 6. Along this line, improvements to the proposed feature extraction algorithm would be required, by developing a proper synchronization algorithm for the MBD network, in order to increase its reliability. Furthermore, the limitations imposed by communication medium may also have to be considered. The current platform that exists for slotted WiDOM is a prototype developed from components commercially available at the time [PGAT09]. The development and research of better radios for the execution of slotted WiDOM and hardware miniaturization are two topics that would enable practical implementation of the proposed algorithm in a wireless domain.

– **Development of an adaptive interpolation algorithm for accommodating non-linear change patterns in an dynamic signal (related to Chapter 5).** Proposed interpolation algorithms consider fixed change rates of the signal [ETPA11]. In this Thesis we solve the problem of dynamic change pattern for linear change model. One interesting future work is to develop this scheme for non-linear change patterns.

– **Investigation of a more realistic noise pattern for wireless channel (related to Chapter 4).** To provide the RMA for hard real-time support in the slotted WiDOM under noisy channel environment, the considered noise model was based on the technique proposed in [BVT⁺10]. There is a need to have a better noise model for real-time data traffic over wireless channel.

– **Developement of a probabilistic end-to-end delay guarantee for the case that no valid noise patterns exist (related to Chapter 4).** In some scenarios, the RMA deemed to be hardly applicable to wireless networks due to high error probability

associated with such networks. However, it must be mentioned that this is a techno-
logical problem. The reliability of wireless networks has evolved noticeably over
the last few years and hence, it is safe to assume that this evolution will continue.
Nonetheless, computing a probabilistic delay guarantee can also be considered as
a way to mitigate the constraint of hard real-time system and makes the protocol
applicable in the context of soft real-time QoS guarantee.

Author's List of Publications

The following publications have been derived from work directly related to this dissertation:

Journals

- **M. Vahabi**, V. Gupta, M. Albano, R. Rangarajan and E. Tovar. Feature Extraction in Densely Sensed Environments: Extensions to Multiple Broadcast Domains. *International Journal of Distributed Sensor Networks (2015)*. (Accepted.)

- **M. Vahabi**, S. Tennina, E. Tovar and B. Andersson. Extended version of: Response Time Analysis of Slotted WiDOM in Noisy Wireless Channels. (Under submission.)

- **M. Vahabi**, E. Tovar. and M. Albano. Extended version of: A Self-Adaptive Approximate Interpolation Scheme for Dense Sensing. (Under submission.)

Conferences and Workshops

- **M. Vahabi**, E. Tovar. and M. Albano. A Self-Adaptive Approximate Interpolation Scheme for Dense Sensing. In *8th IEEE International Symposium on Industrial Embedded Systems (SIES 2013)*, pages 105–109, June 2013, Porto, Portugal. doi: 10.1109/SIES.2013.6601481.

- **M. Vahabi**, V. Gupta, M. Albano and E. Tovar. Feature Extraction in Densely Sensed Environments. In *27th IEEE International Conference on Distributed Computing in Sensor Systems (DCOSS 2014)*, pages 143-151, May 2014, Marina Del Rey, U.S.A.. doi:10.1109/DCOSS.2014.29.

- **M. Vahabi**, S. Tennina, E. Tovar and B. Andersson. Response Time Analysis of Slotted WiDOM in Noisy Wireless Channels. Accepted to be presented in *20th IEEE International Conference on Emerging Technologies and Factory Automation (ETFA 2015)*, September 2015, Luxembourg.

Posters and Demos

- **M. Vahabi**, B. Andersson. New Schedulability Analysis for WiDom. Work-In-Progress Session in conjunction with the *22nd EUROMICRO Conference on Real-Time Systems (ECRTS 2010)*, 6, July, 2010. Brussels, Belgium.

- J. Loureiro, N. Pereira, E. Tovar, F. Pacheco, **M. Vahabi**. The SmartSkin Project: Densely Instrumented Physical Infrastructures. In *1st Industrial Workshop on Real-Time and Embedded Systems (CiWork 2013)*, Porto, Portugal.

- J. Loureiro, N. Pereira, E. Tovar, F. Pacheco, **M. Vahabi**. Reducing Aircraft Fuel Consumption with WSAN-based Active Flow Control. In *1st Industrial Workshop on Real-Time and Embedded Systems (CiWork 2013)*, Porto, Portugal.

Bibliography

[80206]   IEEE Standard for local and metropolitan area networks - part
            15.4: Low-Rate Wireless Personal Area Networks (LR-WPANs),
            IEEE Std 802.15.4-2011 (Revision of IEEE Std 802.15.4-2006).
            http://standards.ieee.org/getieee802/802.15.html, 2006.

[80212]   IEEE Standard for Local and Metropolitan Area Networks–Part 15.4: Low-
            Rate Wireless Personal Area Networks (LR-WPANs)–Amendment 1: MAC
            Sublayer. https://standards.ieee.org/findstds/standard/802.15.4e-2012.html,
            2012.

[AC01]   Imad Aad and Claude Castelluccia. Differentiation Mechanisms for IEEE
            802.11. In 20th Annual Joint Conference of the IEEE Computer and
            Communications Societies (INFOCOM), volume 1, pages 209–218, 2001.

[AIM10]   Luigi Atzori, Antonio Iera, and Giacomo Morabito. The Internet of Things:
            A Survey. Computer networks, 54(15):2787–2805, 2010.

[APE+08]   Björn Andersson, Nuno Pereira, Wilfried Elmenreich, Eduardo Tovar, Fil-
            ipe Pacheco, and Nuno Cruz. A Scalable and Efficient Approach for Ob-
            taining Measurements in CAN-Based Control Systems. IEEE Transactions
            on Industrial Informatics (TII), 4(2):80–91, 2008.

[APT07]   Björn Andersson, Nuno Pereira, and Eduardo Tovar. Exploiting a Priori-
            tized MAC Protocol to Efficiently Compute Min and Max in Multihop Net-
            works. In 5th Workshop on Intelligent Solutions in Embedded Systems,
            pages 239–249. IEEE, 2007.

[APT08]   Björn Andersson, Nuno Pereira, and Eduardo Tovar. How a Cyber-Physical System can Efficiently Obtain a Snapshot of Physical Information even in the Presence of Sensor Faults. In International Workshop on Intelligent Solutions in Embedded Systems, pages 1–10. IEEE, 2008.

[APT09]   Björn Andersson, Nuno Pereira, and Eduardo Tovar. Estimating the Number of Nodes in Wireless Sensor Networks. 2009.

[AT06]   Björn Andersson and Eduardo Tovar. Static-Priority Scheduling of Sporadic Messages on a Wireless Channel. In Principles of Distributed Systems, pages 322–333. Springer, 2006.

[ATS14]   Besim Avci, Goce Trajcevski, and Peter Scheuermann. Managing Evolving Shapes in Sensor Networks. In 26th International Conference on Scientific and Statistical Database Management. ACM, 2014.

[BCV01]   Michael Barry, Andrew T Campbell, and Andras Veres. Distributed Control Algorithms for Service Differentiation in Wireless Packet Networks. In 20th Annual Joint Conference of the IEEE Computer and Communications Societies (INFOCOM), volume 1, pages 582–590, 2001.

[BGHS06]   Chiranjeeb Buragohain, Sorabh Gandhi, John Hershberger, and Subhash Suri. Contour Approximation in Sensor Networks. In Distributed Computing in Sensor Systems, pages 356–371. Springer, 2006.

[BLDB06]   Reinder J Bril, Johan J Lukkien, Rob I Davis, and Alan Burns. Message Response Time Analysis for Ideal Controller Area Network (CAN) Refuted. 5th Int. Work. on Real-Time Network (RTN), pages 5–10, 2006.

[Bos91]   Bosch. CAN Specification version 2.0. Robert Bosch GmbH, Stuttgart, pstfach 30 02 40, d-70442 edition, 1991.

[BVN+11]   C.A. Boano, T. Voigt, C. Noda, K. Romer, and M. Zuniga. JamLab: Augmenting Sensornet Testbeds with Realistic and Controlled Interference

Generation. In 10th International Conference on Information Processing in Sensor Networks (IPSN), pages 175 –186, 2011.

[BVT$^+$10]   C. Boano, T. Vigot, N. Tsiftes, L. Mottola, K. Romer, and M. Zuniga. Making Sensornet MAC Protocols Robust Against Interference. In 7th European Conference on Wireless Sensor Networks (EWSN), pages 272–288, 2010.

[CBBS03]   Thomas W Carley, Moussa A Ba, Rajeev Barua, and David B Stewart. Contention-Free Periodic Message Scheduler Medium Access Control in Wireless Sensor/Actuator Networks. In 24th IEEE Real-Time Systems Symposium (RTSS), pages 298–307, 2003.

[CG03]   Krishna Kant Chintalapudi and Ramesh Govindan. Localized Edge Detection in Sensor Fields. Ad Hoc Networks, 1(2):273–291, 2003.

[CGJ$^+$04]   John Caffrey, Ramesh Govindan, Erik Johnson, Bhaskar Krishnamachari, Sami Masri, Gaurav Sukhatme, Krishna Chintalapudi, Karthik Dantu, Sumit Rangwala, Avinash Sridharan, et al. Networked Sensing for Structural Health Monitoring. In 4th International Workshop on Structural Control, pages 57–66. Columbia University NY, 2004.

[CO05]   Martin Connolly and Fergus O'Reilly. Sensor Networks and the Food Industry. In 1st Workshop on Real-World Wireless Sensor (REAL WSN), pages 20–21. Citeseer, 2005.

[COM09]   EMBEDDED COMPUTING. Cyber-Physical Systems. 2009.

[CRO04]   CROSSBOW. Datasheet: MICAz. Crossbow Technology, Inc, San Jose, USA, 2004.

[CVV08]   Gianluca Cena, Adriano Valenzano, and Stefano Vitturi. Hybrid Wired/Wireless Networks for Real-Time Communications. IEEE Industrial Electronics Magazine, 2(1):8–20, 2008.

[CWKS97]   Brian P Crow, Indra Widjaja, Jeong Geun Kim, and Prescott T Sakai. IEEE
            802.11 Wireless Local Area Networks. IEEE Communications Magazine,
            35(9):116–126, 1997.

[CZSB02]   Marco Caccamo, Lynn Y Zhang, Lui Sha, and Giorgio Buttazzo.   An
            Implicit Prioritized Access Protocol for Wireless Sensor Networks.   In
            23rd Conference on Real-Time Systems Symposium (RTSS), pages 39–48.
            IEEE, 2002.

[DBBL07]   R. Davis, A. Burns, R. Bril, and J. Lukkien.   Controller Area Net-
            work (CAN) Schedulability Analysis: Refuted, Revisited and Revised.
            Real-Time Systems, 35:239–272, 2007.

[DBMC04]   Guido Di Bacco, Tommaso Melodia, and Francesca Cuomo. A MAC Pro-
            tocol for Delay-Bounded Applications in Wireless Sensor Networks.   In
            3rd Annual Mediterranean Ad Hoc Networking Workshop, pages 27–30.
            Citeseer, 2004.

[DBN03]   Budhaditya Deb, Sudeept Bhatnagar, and Badri Nath.   Multi-Resolution
            State Retrieval in Sensor Networks. In 1st IEEE Sensor Network Protocols
            and Applications, pages 19–29, 2003.

[DM10]   C Dickey and T MCNICOLL. The Flying Prius. Newsweek, July, 2010.

[DOBY14]   Xuewu Dai, Peter E Omiyi, Kaan Bür, and Yang Yang. Interference-Aware
            Convergecast Scheduling in Wireless Sensor/Actuator Networks for Ac-
            tive Airflow Control Applications. Wireless Communications and Mobile
            Computing, 14(3):396–408, 2014.

[DRK11]   Subhasri Duttagupta, Krithi Ramamritham, and Purushottam Kulkarni.
            Tracking Dynamic Boundaries using Sensor Network. IEEE Transactions
            on Parallel and Distributed Systems, 22(10):1766–1774, 2011.

[ECPS02]   D. Estrin, D. Culler, K. Pister, and G. Sukhatme. Connecting the Physical World with Pervasive Networks. <u>IEEE Pervasive Computing</u>, 1(1):59–69, Jan 2002.

[ERR05]   A. Eswaran, A. Rowe, and R. Rajkumar. Nano-rk: An energy-aware resource-centric rtos for sensor networks. In <u>26th IEEE International Real-Time Systems Symposium (RTSS)</u>, pages 256–265, December 2005.

[ETPA11]   Aida Ehyaei, Eduardo Tovar, Nuno Pereira, and Björn Andersson. Scalable Data Acquisition for Densely Instrumented Cyber-Physical Systems. In <u>IEEE/ACM International Conference on Cyber-Physical Systems (ICCPS)</u>, pages 174–183, 2011.

[FLE06]   Emad Felemban, Chang-Gun Lee, and Eylem Ekici. MMSPEED: Multi-path Multi-SPEED Protocol for QoS Guarantee of Reliability and Time-liness in Wireless Sensor Networks. <u>IEEE Transactions on Mobile Computing</u>, 5(6):738–754, 2006.

[FRWZ07]   Elena Fasolo, Michele Rossi, Jorg Widmer, and Michele Zorzi. In-Network Aggregation Techniques for Wireless Sensor Networks: A Survey. <u>IEEE Wireless Communications</u>, 14(2):70–87, 2007.

[Fun05]   Stefan Funke. Topological Hole Detection in Wireless Sensor Networks and its Applications. In <u>6th ACM SIGACT/SIGMOBILE International Workshop on FOUNDATIONS OF MOBILE COMPUTING (DIALM-POMC)</u>, pages 44–53. ACM, 2005.

[FZMT12]   Federico Ferrari, Marco Zimmerling, Luca Mottola, and Lothar Thiele. Low-power Wireless Bus. In <u>10th ACM Conference on Embedded Network Sensor Systems</u>, pages 1–14, 2012.

[FZTS11]   Federico Ferrari, Marco Zimmerling, Lothar Thiele, and Olga Saukh. Efficient Network Flooding and Time Synchronization with Glossy. In <u>10th International Conference on Information Processing in Sensor Networks (IPSN)</u>, pages 73–84. IEEE, 2011.

[GBT+04]   Carlos Guestrin, Peter Bodik, Romain Thibaux, Mark Paskin, and Samuel
             Madden. Distributed Regression: An Efficient Framework for Modeling
             Sensor Network Data. In 3rd International Symposium on Information
             Processing in Sensor Networks (IPSN), pages 1–10. IEEE, 2004.

[Gom08]   Ricardo Filipe Teixeira Gomes. Efficient Implementation of a Dominance
             Protocol for Wireless Medium Access. Master's thesis, School of Engi-
             neering, Instituto Politécnico do Porto. Instituto Superior de Engenharia do
             Porto, 2008.

[GSW09]   Sorabh Gandhi, Subhash Suri, and Emo Welzl. Catching Elephants
             with Mice: Sparse Sampling for Monitoring Sensor Networks. ACM
             Transaction on Sensor Networks, 6(1), 2009.

[Hei00]   Wendi Beth Heinzelman. Application-Specific Protocol Architectures for Wireless Networks.
             PhD thesis, Massachusetts Institute of Technology, 2000.

[HHMS03]   Joseph M Hellerstein, Wei Hong, Samuel Madden, and Kyle Stanek. Be-
             yond Average: Toward Sophisticated Sensing with Queries. In ACM/IEEE
             Conference on Information Processing in Sensor Networks (IPSN, pages
             63–79. Springer, 2003.

[HR10]   Michael I Ham and Marko A Rodriguez. A Boundary Approximation Al-
             gorithm for Distributed Sensor Networks. International Journal of Sensor
             Networks, 8(1):41–46, 2010.

[HZG09]   Heiko Hinkelmann, Peter Zipf, and Manfred Glesner. Design and
             Evaluation of an Energy-Efficient Dynamically Reconfigurable Architec-
             ture for Wireless Sensor Nodes. In International Conference on Field
             Programmable Logic and Applications (FPL), pages 359–366. IEEE, 2009.

[I. 04]   I. Crossbow Technology, San Jose, USA. CROSSBOW-Datasheet: MICAz,
             2004.

[IGE+03]   Chalermek Intanagonwiwat, Ramesh Govindan, Deborah Estrin, John Hei-
           demann, and Fabio Silva. Directed Diffusion for Wireless Sensor Network-
           ing. IEEE/ACM Transactions on Networking, 11(1):2–16, 2003.

[ISA09]   Wireless Systems for Industrial Automation: Process Control and Related
           Applications. ISA100.11a Standard, 2009.

[JC99]   DENG Jiunn and Ruay-Shiung Chang. A Priority Scheme for IEEE 802. 11
           DCF Access Method. IEICE Transactions on Communications, 82(1):96–
           102, 1999.

[JMMR97]   Philippe Jacquet, Pascale Minet, Paul Muhlethaler, and Nicolas Rivierre.
           Priority and Collision Detection with Active Signaling - The Channel Ac-
           cess Mechanism of Hiperlan. Wireless Personal Communications, 4(1):11–
           25, 1997.

[JT11]   Tommy R Jensen and Bjarne Toft. Graph Coloring Problems, volume 39.
           John Wiley & Sons, 2011.

[KCG+11]   A. Koubaa, S. Chaudhry, O. Gaddour, R. Chaari, N. Al-Elaiwi, H. Al-
           Soli, and H. Boujelben. Z-Monitor: Monitoring and Analyzing IEEE
           802.15.4-based Wireless Sensor Networks. In IEEE 36th Conference on
           Local Computer Networks (LCN), pages 939 –947, 2011.

[KEW02]   Bhaskar Krishnamachari, Deborah Estrin, and Stephen Wicker. Modeling
           Data-Centric Routing in Wireless Sensor Networks. In 21th Conference on
           Computer Communications (INFOCOM), volume 2, pages 39–44, 2002.

[KFPF06]   Alexander Kröller, Sándor P Fekete, Dennis Pfisterer, and Stefan Fischer.
           Deterministic Boundary Recognition and Topology Extraction for Large
           Sensor Networks. In ACM-SIAM Symposium on Discrete Algorithms
           (SODA), pages 1000–1009, 2006.

[KG93]   Hermann Kopetz and Günter Grunsteidl. TTP-A Time-Triggered Protocol
            for Fault-Tolerant Real-Time Systems. In 23rd International Symposium
            on Fault-Tolerant Computing (FTCS-23), pages 524–533. IEEE, 1993.

[KOK14]   S. Kumar, K. Ovsthus, and L.M. Kristensen. An Industrial Perspective
            on Wireless Sensor Networks—A Survey of Requirements, Protocols, and
            Challenges. IEEE Communications Surveys & Tutorials, 16(3):1391–1412,
            2014.

[Kop11]   Hermann Kopetz. Internet of things. In Real-Time Systems, pages 307–
            323. Springer, 2011.

[KP87]   Fadi J Kurdahi and Alice C Parker. REAL: a program for REgister ALloca-
            tion. In 24th ACM/IEEE Design Automation Conference, pages 210–215,
            1987.

[LBP03]   Joshua Lifton, Michael Broxton, and Joseph A Paradiso. Distributed Sensor
            Networks as Sensate Skin. In Proceedings of IEEE Sensors, volume 2,
            pages 743–747, 2003.

[LDB+09]   Michael Lehning, Nicholas Dawes, Mathias Bavay, Marc Parlange, Suman
            Nath, and Feng Zhao. Instrumenting the Earth: Next Generation Sensor
            Networks in Environmental Science. Technical report, Microsoft Research,
            2009.

[LFZ13]   Olaf Landsiedel, Federico Ferrari, and Marco Zimmerling. Chaos: Versatile
            and Efficient All-to-all Data Sharing and In-network Processing at Scale.
            In 11th ACM Conference on Embedded Networked Sensor Systems, pages
            1:1–1:14, 2013.

[LL10]   Mo Li and Yunhao Liu. Iso-Map: Energy-Efficient Contour Mapping in
            Wireless Sensor Networks. IEEE Transaction on Knowledge and Data
            Engineering, 22(5):699–710, 2010.

[LRS02]   Stephanie Lindsey, Cauligi Raghavendra, and Krishna M. Sivalingam. Data Gathering Algorithms in Sensor Networks Using Energy Metrics. IEEE Transactions on Parallel and Distributed Systems, 13(9):924–935, 2002.

[LRT15]   Joao Loureiro, Raghuraman Rangarajan, and Eduardo Tovar. Distributed Sensing of Fluid Dynamic Phenomena with the XDense Sensor Grid Network. In 3rd International Conference on Cyber-Physical Systems, Networks and Applications (CPSNA). IEEE, 2015.

[LRY$^+$12] Shuhui Li, Shangping Ren, Yue Yu, Xing Wang, Li Wang, and Gang Quan. Profit and Penalty Aware Scheduling for Real-Time Online Services. IEEE Transactions on Industrial Informatics, 8(1):78–89, 2012.

[LSBP02]   Joshua Lifton, Deva Seetharam, Michael Broxton, and Joseph Paradiso. Pushpin Computing System Overview: A Platform for Distributed, Embedded, Ubiquitous Sensor Networks. In Pervasive Computing, volume 2414 of Lecture Notes in Computer Science, pages 139–151. Springer Berlin Heidelberg, 2002.

[LSR04]   Huan Li, Prashant Shenoy, and Krithi Ramamritham. Scheduling Communication in Real-Time Sensor Applications. In 10th Real-Time and Embedded Technology and Applications Symposium (RTAS), pages 10–18. IEEE, 2004.

[LXH$^+$13] J.J. Liu, Wenyao Xu, Ming-Chun Huang, N. Alshurafa, M. Sarrafzadeh, N. Raut, and B. Yadegar. A Dense Pressure Sensitive Bedsheet Design for Unobtrusive Sleep Posture Monitoring. In IEEE International Conference on Pervasive Computing and Communications (PerCom), pages 207–215, 2013.

[MCG13]   Dorin Maxim and Liliana Cucu-Grosjean. Response Time Analysis for Fixed-Priority Tasks with Multiple Probabilistic Parameters. In 34th International Conference on Real-Time Systems Symposium (RTSS), pages 224–235. IEEE, 2013.

[MM09]   Pedro José Marrón and Daniel Minder. European Research on Cooper-
            ating Objects. In 6th Annual IEEE Communications Society Conference
            on Sensor, Mesh and Ad Hoc Communications and Networks Workshops
            (SECON), pages 1–3, 2009.

[MR04]   Ajay Mahimkar and Theodore S Rappaport. SecureDAV: A Secure Data
            Aggregation and Verification Protocol for Sensor Networks. In Global
            Telecommunications Conference (GLOBECOM), volume 4, pages 2175–
            2179. IEEE, 2004.

[MRR07]   Rahul Mangharam, Anthony Rowe, and Raj Rajkumar. FireFly: a Cross-
            Layer Platform for Real-Time Embedded Wireless Networks. Real-Time
            Systems, 37(3):183–231, 2007.

[MSFC02]   Samuel Madden, Robert Szewczyk, Michael J Franklin, and David Culler.
            Supporting Aggregate Queries Over Ad-Hoc Wireless Sensor Networks.
            In 4th IEEE Workshop on Mobile Computing Systems and Applications,
            pages 49–58, 2002.

[MW79]   Aloysiu K Mok and Stephen A Ward. Distributed Broadcast Channel Ac-
            cess. Computer Networks, 3(5):327–335, 1979.

[NM03]   Robert Nowak and Urbashi Mitra. Boundary Estimation in Sensor Net-
            works: Theory and Methods.   In Information Processing in Sensor
            Networks, volume 2634 of Lecture Notes in Computer Science, pages 80–
            95. Springer Berlin Heidelberg, 2003.

[ÖMV^{+}12] Fredrik Österlind, Luca Mottola, Thiemo Voigt, Nicolas Tsiftes, and Adam
            Dunkels. Strawman: Resolving Collisions in Bursty Low-Power Wireless
            Networks. In 11th international conference on Information Processing in
            Sensor Networks (IPSN), pages 161–172. ACM, 2012.

[PAT07]   N. Pereira, B. Andersson, and E. Tovar. WiDom: A Dominance Protocol
            for Wireless Medium Access. IEEE Transactions on Industrial Informatics,
            3(2):120 –130, 2007.

[PATR07]   Nuno Pereira, Björn Andersson, Eduardo Tovar, and Anthony Rowe. Static-Priority Scheduling over Wireless Networks with Multiple Broadcast Domains. In 28th IEEE International Real-Time Systems Symposium (RTSS), pages 447–458, 2007.

[PGAT09]   Nuno Pereira, Ricardo Gomes, Björn Andersson, and Eduardo Tovar. Efficient Aggregate Computations in Large-Scale Dense WSN. In 15th IEEE Conference on Real-Time and Embedded Technology and Applications Symposium (RTAS), pages 317–326, 2009.

[PLB04]   J. A. Paradiso, J. Lifton, and M. Broxton. Sensate Media-Multimodal Electronic Skins as Dense Sensor Networks. BT Technology Journal, 22(4):32–44, 2004.

[R+04]   J Reneaux et al. Overview on Drag Reduction Technologies for Civil Transport Aircraft. ONERA: Tire a Part, 153:1–18, 2004.

[SAL+03]   John A Stankovic, Tarek F Abdelzaher, Chenyang Lu, Lui Sha, and Jennifer C Hou. Real-Time Communication and Coordination in Embedded Sensor Networks. Proceedings of the IEEE, 91(7):1002–1022, 2003.

[SBP04]   Mitali Singh, Amol Bakshi, and Viktor K Prasanna. Constructing Topographic Maps in Networked Sensor Systems. In Workshop on Algorithms for Wireless and Mobile Networks (ASWAN). Citeseer, 2004.

[SBR10]   Petcharat Suriyachai, James Brown, and Utz Roedig. Time-Critical Data Delivery in Wireless Sensor Networks. In Distributed Computing in Sensor Systems, pages 216–229. Springer, 2010.

[SCMSJ11]   Sung-Han Sim, Juan Francisco Carbonell-Márquez, BF Spencer, and Hongki Jo. Decentralized Random Decrement Technique for Efficient Data Aggregation and System Identification in Wireless Smart Sensor Networks. Probabilistic Engineering Mechanics, 26(1):81–91, 2011.

[SGLW09]   Lui Sha, Sathish Gopalakrishnan, Xue Liu, and Qixin Wang. Cyber-Physical Systems: A New Frontier. In Machine Learning in Cyber Trust, pages 3–13. Springer, 2009.

[She]   Donald Shepard. A Two-Dimensional Interpolation Function for Irregularly-Spaced Data. In 23rd ACM national conference of the 1968, pages 517–524. ACM.

[SK96]   Joao L Sobrinho and Anjur Sundaresan Krishnakumar. Real-Time Traffic over the IEEE 802.11 Medium Access Control Layer. Bell Labs Technical Journal, 1(2):172–187, 1996.

[SK99]   Joao L Sobrinho and Anjur Sundaresan Krishnakumar. Quality-of-Service in Ad Hoc Carrier Sense Multiple Access Wireless Networks. IEEE Journal on Selected Areas in Communications, 17(8):1353–1368, 1999.

[SLMR05]   J.A. Stankovic, Insup Lee, A. Mok, and R. Rajkumar. Opportunities and Obligations for Physical Computing Systems. Computer, 38(11):23–31, Nov 2005.

[SRS12]   Petcharat Suriyachai, Utz Roedig, and Andrew Scott. A Survey of MAC Protocols for Mission-Critical Applications in Wireless Sensor Networks. IEEE Communications Surveys & Tutorials, 14(2):240–264, 2012.

[SS04]   Mehdi Sharifzadeh and Cyrus Shahabi. Supporting Spatial Aggregation in Sensor Network Databases. In 12th annual ACM international workshop on Geographic information systems, pages 166–175. ACM, 2004.

[SSH99]   John A Stankovic, Sang Hyuk Son, and Jörgen Hansson. Misconceptions about Real-Time Databases. Computer, 32(6):29–36, 1999.

[SZBG14]   Wei Shen, Tingting Zhang, Filip Barac, and Mikael Gidlund. Priority-MAC: A Priority-Enhanced MAC Protocol for Critical Traffic in Industrial Wireless Sensor and Actuator Networks. IEEE Transactions on Industrial Informatics, 10(1):824–835, 2014.

[T. 07]   T. Instruments. <u>CC2420 Datasheet</u>, 2007.

[TAP+08]   Eduardo Tovar, Björn Andersson, Nuno Pereira, Mário Alves, K Shashi
            Prabh, and Filipe Pacheco. Highly Scalable Aggregate Computations
            in Cyber-Physical Systems: Physical Environment Meets Communication
            Protocols. 2008.

[THW94]   KW Tindell, Hans Hansson, and Andy J Wellings. Analysing Real-Time
            Communications: Controller Area Network (CAN). In <u>Real-Time Systems</u>
            <u>Symposium</u>, pages 259–263. IEEE, 1994.

[TLB12]   Emanuele Toscano and Lucia Lo Bello. Multichannel Superframe Schedul-
            ing for IEEE 802.15. 4 Industrial Wireless Sensor Networks. <u>IEEE</u>
            <u>Transactions on Industrial Informatics</u>, 8(2):337–350, 2012.

[TOMO05]   Richard Tynan, GMP O'Hare, David Marsh, and Donal O'Kane. Interpo-
            lation for Wireless Sensor Network Coverage. In <u>2nd IEEE Workshop on</u>
            <u>Embedded Networked Sensors (EmNetS-II)</u>, pages 123–131. IEEE, 2005.

[TPB+12]   Eduardo Tovar, Nuno Pereira, Iain Bate, Leandro Indrusiak, Sérgio Penna,
            José Negrão, Júlio C Viana, François Philipp, Dirk Mayer, and José Heras.
            Networked Embedded Systems for Active Flow Control in Aircraft. In <u>11th</u>
            <u>International Workshop on Real-Time Networks (RTN)</u>, 2012.

[TRNA14]   Maryam Tabesh, Mustafa Rangwala, Ali M Niknejad, and Amin Arbabian.
            A Power-Harvesting Pad-Less mm-Sized 24/60GHz Passive Radio with on-
            chip Antennas. In <u>Symposium on VLSI Circuits Digest of Technical Papers</u>,
            pages 1–2. IEEE, 2014.

[TWTLB11]   Henning Trsek, Lukasz Wisniewski, Emanuele Toscano, and L Lo Bello.
            A Flexible Approach for Real-Time Wireless Communications in Adapt-
            able Industrial Automation Systems. In <u>IEEE Conference on Emerging</u>
            <u>Technologies & Factory Automation (ETFA)</u>, pages 1–4, 2011.

[VA10]   Maryam Vahabi and Björn Andersson. New Schedulability Analysis for
            WiDom. In 22nd Euromicro Conference on Real-Time Systems (ECRTS).
            IEEE, 2010.

[Vah15]   Maryam Vahabi. Implementation of Feature Extraction Functions in Dense
            Sensing Networks. https://goo.gl/HJzhNm, March 2015.

[VGA+15]   Maryam Vahabi, Vikram Gupta, Michele Albano, Raghuraman Rangara-
            jan, and Eduardo Tovar. Feature Extraction in Densely Sensed Environ-
            ments: Extensions to Multiple Broadcast Domains. International Journal of
            Distributed Sensor Networks (IJDSN), 2015.

[VGAT14]   Maryam Vahabi, Vikram Gupta, Michele Albano, and Eduardo Tovar. Fea-
            ture Extraction in Densely Sensed Environments. In 10th International
            Conference on Distributed Computing in Sensor Systems (DCOSS), pages
            143–151. IEEE, 2014.

[VLVS+03]   Kristof Van Laerhoven, Nicolas Villar, Albrecht Schmidt, Hans-Werner
            Gellersen, Maria Hakansson, and Lars Erik Holmquist. Pin&Play: The
            Surface as Network Medium. IEEE Communications Magazine, 41(4):90–
            95, 2003.

[VTA13]   Maryam Vahabi, Eduardo Tovar, and Michele Albano. A Self-Adaptive
            Approximate Interpolation Scheme for Dense Sensing. In 8th International
            Symposium on Industrial Embedded Systems (SIES), pages 105–109.
            IEEE, 2013.

[VTTA15]   Maryam Vahabi, Stefano Tenina, Eduardo Tovar, and Björn Andersson.
            Response Time Analysis of Slotted WiDOM in Noisy Wireless Channels.
            In 20th International Conference on Emerging Technologies and Factory
            Automation (ETFA). IEEE, 2015.

[WFS08] Yan Wu, Sonia Fahmy, and Ness B Shroff. On the Construction of a Maximum-Lifetime Data Gathering Tree in Sensor Networks: NP-Completeness and Approximation Algorithm. In 27th Conference on Computer Communications (INFOCOM). IEEE, 2008.

[WGM06] Yue Wang, Jie Gao, and Joseph SB Mitchell. Boundary Recognition in Sensor Networks by Topological Methods. In 12th annual international conference on Mobile computing and networking, pages 122–133. ACM, 2006.

[WIA11] Industrial Communication Networks–Fieldbus Specifications–WIA-PA Communication Network and Communication Profile. International Electrotechnical Commission (IEC) Standard, 2011.

[wir10] Industrial Communication Networks–Wireless Communication Network and Communication Profiles–WirelessHART. International Electrotechnical Commission (IEC) Standard, 62591, 2010.

[WUT05] Hongyi Wu, Anant Utgikar, and Nian-Feng Tzeng. SYN-MAC: A Distributed Medium Access Control Protocol for Synchronized Wireless Networks. Mobile Networks and Applications, 10(5):627–637, 2005.

[XHE01] Ya Xu, John Heidemann, and Deborah Estrin. Geography-Informed Energy Conservation for Ad Hoc Routing. In 7th annual international conference on Mobile computing and networking, pages 70–84. ACM, 2001.

[XLCL06] Wenwei Xue, Qiong Luo, Lei Chen, and Yunhao Liu. Contour Map Matching for Event Detection in Sensor Networks. In SIGMOD international conference on Management of data, pages 145–156. ACM, 2006.

[YG02] Yong Yao and Johannes Gehrke. The Cougar Approach to in-Network Query Processing in Sensor Networks. ACM Sigmod Record, 31(3):9–18, 2002.

[YV06]   Xue Yang and Nitin Vaidya. Priority Scheduling in Wireless Ad Hoc Networks. Wireless networks, 12(3):273–286, 2006.

[ZJX10]   Jun Zhang, Xiaohua Jia, and Guoliang Xing. Real-Time Data Aggregation in Contention-Based Wireless Sensor Networks. ACM Transactions on Sensor Networks (TOSN), 7(1):2, 2010.

[ZKI10]   Teng Zheng and Kim Ki-Il. A Survey on Real-Time MAC Protocols in Wireless Sensor Networks. Communications and Network, 2(2), 2010.

[ZNLF04]   Bin Zhou, Lek Heng Ngoh, Bu Sung Lee, and Cheng Peng Fu. A Hierarchical Scheme for Data Aggregation in Sensor Network. In 12th IEEE International Conference on Networks (ICON), volume 2, pages 525–529, 2004.